SYNTHESIS, SORPTION AND SENSING CAPABILITY OF

CARBON NANOTUBE BASED MATERIALS

FOR GAS-PHASE CHLORINATED PHENOLS

Mr. Ekkachai Kanchanatip

A Dissertation Submitted in Partial Fulfillment of the Requirements

for the Degree of Doctor of Philosophy Program in Environmental Management

(Interdisciplinary Program)

Graduate School

Chulalongkorn University

Academic Year 2016

Copyright of Chulalongkorn University

การสังเคราะห์วัสดุคาร์บอนนาโนทิวบ์เพื่อใช้ในการดูดซับและตรวจวัดสารประกอบคลอรีเนทเต็ดฟีนอลในแก๊สเฟส

นายเอกชัย กัญจนาทิพย์

Thesis Title	SYNTHESIS, SORPTION AND SENSING CAPABILITY OF CARBON NANOTUBE BASED MATERIALS FOR GAS-PHASE CHLORINATED PHENOLS
By	Mr. Ekkachai Kanchanatip
Field of Study	Environmental Management
Thesis Advisor	Associate Professor Nurak Grisdanurak, Ph.D.
Thesis Co-Advisor	Professor Walter Den, Ph.D.

Accepted by the Graduate School, Chulalongkorn University in Partial Fulfillment of the Requirements for the Doctoral Degree

‒‒‒‒‒‒‒‒‒‒‒‒‒‒‒‒‒‒‒‒‒‒‒‒‒‒‒‒ Dean of the Graduate School

(Associate Professor Sunait Chutintaranond, Ph.D.)

THESIS COMMITTEE

‒‒‒‒‒‒‒‒‒‒‒‒‒‒‒‒‒‒‒‒‒‒‒‒‒‒‒‒ Chairman

(Assistant Professor Chantra Tongcumpou, Ph.D.)

‒‒‒‒‒‒‒‒‒‒‒‒‒‒‒‒‒‒‒‒‒‒‒‒‒‒‒‒ Thesis Advisor

(Associate Professor Nurak Grisdanurak, Ph.D.)

‒‒‒‒‒‒‒‒‒‒‒‒‒‒‒‒‒‒‒‒‒‒‒‒‒‒‒‒ Thesis Co-Advisor

(Professor Walter Den, Ph.D.)

‒‒‒‒‒‒‒‒‒‒‒‒‒‒‒‒‒‒‒‒‒‒‒‒‒‒‒‒ Examiner

(Associate Professor Patiparn Punyapalakul, Ph.D.)

‒‒‒‒‒‒‒‒‒‒‒‒‒‒‒‒‒‒‒‒‒‒‒‒‒‒‒‒ Examiner

(Assistant Professor On-anong Larpparisudthi, Ph.D.)

‒‒‒‒‒‒‒‒‒‒‒‒‒‒‒‒‒‒‒‒‒‒‒‒‒‒‒‒ Examiner

(Assistant Professor Tassanee Prueksasit, Ph.D.)

‒‒‒‒‒‒‒‒‒‒‒‒‒‒‒‒‒‒‒‒‒‒‒‒‒‒‒‒ External Examiner

(Panida Prompinit, Ph.D.)

เอกชัย กัญจนาทิพย์ : การสังเคราะห์วัสดุคาร์บอนนาโนทิวบ์เพื่อใช้ในการดูดซับและตรวจวัดสารประกอบคลอรีเนทเต็ดฟีนอลในแก๊สเฟส (SYNTHESIS, SORPTION AND SENSING CAPABILITY OF CARBON NANOTUBE BASED MATERIALS FOR GAS-PHASE CHLORINATED PHENOLS) อ.ที่ปรึกษาวิทยานิพนธ์หลัก: รศ. ดร. นุรักษ์ กฤษดานุรักษ์, อ.ที่ปรึกษาวิทยานิพนธ์ร่วม: ศ. ดร. Walter Den, 106 หน้า.

ในวิทยานิพนธ์นี้ได้ทำการศึกษาการดูดซับไอโซเทอมและการตรวจจับแก๊สสามชนิดได้แก่ ฟีนอล, 2-คลอโรฟีนอล และ 2,4-ไดคลอโรฟีนอลโดยใช้วัสดุคาร์บอนนาโนทิวบ์ที่ถูกปรับแต่งด้วยหมู่ฟังก์ชั่นกรด คาร์บอนนาโนทิวบ์ถูกสังเคราะห์ขึ้นโดยใช้วิธีการตกเคลือบด้วยไอเคมี (CVD) ที่อุณหภูมิ 800 องศาเซลเซียส จากนั้นทำการปรับแต่งด้วยหมู่ฟังก์ชั่นกรดโดยใช้กรดไนตริกผสมกับกรดซัลฟิวริก คาร์บอนนาโนทิวบ์ที่ถูกปรับแต่งแล้วถูกนำไปกรองโดยสูญญากาศเพื่อขึ้นรูปเป็นแผ่นบาง (Buckypaper) และใช้ในการทดลองดูดซับและตรวจจับสารคลอโรฟีนอล จากการทดลองดูดซับพบว่าการดูดซับเกิดขึ้นคล้ายกับการโมเดลการดูดซับแบบแลงเมียร์ไอโซเทอม (Lungmuir isotherm) และวัดค่าประสิทธิภาพการดูดซับได้ 61.35, 93.46 และ 104.17 มิลลิกรัมต่อกรัม สำหรับ ฟีนอล, 2-คลอโรฟีนอล และ 2,4-ไดคลอโรฟีนอล ตามลำดับ จากการศึกษาพลังงานในการคายซับด้วยเทคนิควิเคราะห์สมบัติทางความร้อนของวัสดุพบว่า การดูดซับของสารคลอโรฟีนอลบนคาร์บอนนาโนทิวบ์เกิดขึ้นแบบการดูดซับทางเคมี ในส่วนของการทดลองตรวจจับแก๊สคลอโรฟีนอลพบว่า Buckypaper สามารถตรวจจับแก๊สได้อย่างรวดเร็วและยังมีความเสถียรสูงสามารถใช้งานซ้ำได้หลายครั้งโดยประสิทธิภาพไม่ลดลง ค่าความไวต่อการตรวจจับสารพบว่ามีค่าเป็น 13.778×10^{-4}, 8.835×10^{-4} และ 7.122×10^{-4} สำหรับ ฟีนอล, 2-คลอโรฟีนอล และ 2,4-ไดคลอโรฟีนอล ตามลำดับ เป็นที่น่าสังเกตว่าความสามารถในการดูดซับและการตรวจจับสารของวัสดุคาร์บอนนาโนทิวบ์เพิ่มขึ้นตามจำนวนอะตอมของคลอรีนที่อยู่ในสารคลอโรฟีนอล

จุฬาลงกรณ์มหาวิทยาลัย
CHULALONGKORN UNIVERSITY

สาขาวิชา การจัดการสิ่งแวดล้อม	ลายมือชื่อนิสิต ....
ปีการศึกษา 2559	ลายมือชื่อ อ.ที่ปรึกษาหลัก ....
	ลายมือชื่อ อ.ที่ปรึกษาร่วม ....

5387876520 : MAJOR ENVIRONMENTAL MANAGEMENT

KEYWORDS: CARBON NANOTUBES / CHLOROPHENOL / GAS SENSOR / ADSORPTION

EKKACHAI KANCHANATIP: SYNTHESIS, SORPTION AND SENSING CAPABILITY OF CARBON NANOTUBE BASED MATERIALS FOR GAS-PHASE CHLORINATED PHENOLS. ADVISOR: ASSOC. PROF. NURAK GRISDANURAK, Ph.D., CO-ADVISOR: PROF. WALTER DEN, Ph.D., 106 pp.

The adsorption equilibrium isotherms as well as gas sensing of three chlorinated phenolic compounds (CPCs) including phenol, 2-chlorophenol, and 2,4-dichlorophenol by acid-functionalized carbon nanotubes (CNT) were studied. CNTs were synthesized via floating catalyst chemical vapor deposition method at $800^{\circ}C$ and then functionalized with a mixture of HNO_3 and H_2SO_4. The functionalized CNTs were vacuum filtered to form CNT buckypaper. The adsorption isotherm followed the Langmuir adsorption model better than the Freundlich and Redlich-Peterson models. The maximum adsorption capacities were found to be 61.35, 93.46 and 104.17 mg/g for phenol, 2-chlorophenol and 2,4-dichlorophenol, respectively. The desorption activation energy determined via thermogravimetric analysis indicates that adsorption of all three CPCs onto the CNTs belonged to chemisorption type. For the gas sensing test, the CNT buckypaper showed fast response to the tested CPCs with good stability and repeatability. The sensitivity values obtained were 13.778×10^{-4}, 8.835×10^{-4} and 7.122×10^{-4} for 2,4-dichlorophenol, 2-chlorophenol and phenol, respectively. It is noteworthy that the adsorption capacity and sensitivity of the CNT based materials to the target gases increased with the increase in the number of chlorine atoms in the phenolic compounds.

Field of Study: Environmental Management   Student's Signature _____

Academic Year: 2016   Advisor's Signature _____

Co-Advisor's Signature _____

ACKNOWLEDGEMENTS

CONTENTS

List of Tables

List of Figures

Figure   **Page**

Figure   Page

Figure   **Page**

Chapter 1

Introduction

1.1 Research motivation

Gas sensors are attracting great interest in various fields such as manufacturing (e.g. to increase productivity and safety (de Vargas-Sansalvador et al., 2011, Cui et al., 2016)), medical diagnosis (e.g. to monitor disease via breath analysis (Ryabtsev et al., 1999, Karmaoui et al., 2016)) and environmental monitoring (to ensure environmental safety and health (Fine et al., 2010, Gardner et al., 2015)). Gas sensors with high sensitivity and selectivity are imperative for real-time and leakage detections of toxic gases. Carbon nanotubes (CNTs) have gained substantial attention as an active element of gas sensing because of their distinct properties such as high specific surface area, high chemical stability and outstanding electrical properties (Schuerle et al., 2011). Additionally, CNT is very sensitive to the adsorption of gas molecules, leading to the electrical conductivity changes caused by electron transfer between the nanotubes and the adsorbed gas molecules (Akbari et al., 2016, Li et al., 2016). The electrical conductance of CNTs sensitively changes at room temperature on exposure to several gases (Dube et al., 2015). Consequently, the development of CNT-based gas sensor has received an increasing interest in the last several years. For example, Kong and co-workers used pristine CNT gas sensor to detect NO_2 and NH_3. The conductivity of CNTs changed significantly upon exposure to the gas molecules. The response time was in a scale of seconds for 200 ppm NO_2 and of a few minutes for 1% NH_3. The recovery was approximately 12 hours at room temperature but decreased to 1 hour upon heating (Kong et al., 2000). Li and co-workers fabricated a gas sensor for NO_2 with a detection limit of 44 ppb and 262 ppb for nitrotoluene. The detection response time was on the order of seconds and minutes for the recovery (Li et al., 2003). Jung and co-workers synthesized multi-walled carbon nanotube (MWCNT) sheet for H_2 detection. The resistivity of the gas sensor increased on exposure to H_2 with response time of 20s. The gas sensor became saturated when the concentration of H_2 exceeded 30%. They also found that the recovery response was improved with an increased carrier gas flow (Jung et al., 2014).

For environmental monitoring purposes, the effects of environmentally hazardous gases on the electronic properties of carbon nanotubes as gas sensor have recently been investigated by several research groups. The CNT gas sensor is able to detect some gas species at very low concentration with excellent performance in terms of rapid response, high sensitivity, and good repeatability (Lucci et al., 2006, Park et al., 2009, Xie et al., 2012). Moreover, the interfacial interaction between the CNT surface and the adsorbed molecules can be improved by the functionalization of CNTs, which plays a critical role in its electrochemical performance. The polar groups attached on the CNT surface improve the adsorption affinity of the electron-donor or acceptor gases, and subsequently give enhanced responses (Xu et al., 2009). Dhall and co-workers reported the use of acid functionalized MWCNT gas sensor to detect 0.05% H_2 gas at room temperature. The functionalized sensor performed faster response to H_2 as compared to the pristine one. Moreover, the sensitivity increased with the acid functionalized sensor and recovery time decreased from 190 to 100 s (Dhall et al., 2013). Dong and co-workers used acid functionalized CNTs to detect CO and NH_3 gas mixture at 150°C. Their results showed that the sensor was more sensitive to these gases after acid functionalization (Dong et al., 2013).

Chlorinated phenolic compounds (CPCs) present an important family of environment pollutants. CPCs are widely used in many industrial manufacturing processes as intermediates for pesticide, herbicide, wood preservatives, paint, plastic and pharmaceuticals. They are highly stable and can withstand conventional biodegradation (Kılıç and Çınar, 2008), therefore their emissions to the atmosphere cause serious environmental concerns due to the adverse and toxic effect on ecosystems. CPCs in the gas phase have also been known as precursors to form polychlorinated dibenzo-p-dioxins and polychlorinated dibenzofurans (PCDD/PCDF) through the proposed pathways involving the recombination of chlorophenoxy radical–radical, radical–molecule, and molecule–molecule reactions between chlorophenols (Milligan and Altwicker, 1996, Okamoto and Tomonari, 1999, Gerasimov, 2007). Among the family of CPCs, the monochlorophenols (CP) and dichlorophenols (DCP) are most likely to be released into the air because they have the greatest tendency of being gases or vapors (as indicated by their large Henry's law constant). Furthermore, chlorophenols are also released to the atmosphere through the chlorinated wastes incineration. For instance, 2,4-dichlorophenol has been founded in air from the combustion of chlorophenol-based herbicides as well

as municipal solid waste and hazardous waste inceneration (Gomez et al., 1988, Öberg et al., 1989). To control the emission of the CPCs effectively, the use of accurate and reliable methods which are capable to detect their presence is necessary. Conventional techniques for detecting CPCs in air comprise of spectrometric and chromatographic techniques that require precision instrumentational analyses (Plümacher and Renner, 1993). These analytical methods generally give accurate quantitative measurements, but entail long lag time and can be cost prohibitive for frequent measurements. Hence, simple to operate and cost-effective alternative techniques for routine detection of CPC contaminants are highly desirable. Negash and co-workers reported the use of SWCNTs and poly(3,4-ethylenedioxythiophene (PEDOT) composite modified glassy carbon electrode to detect phenol and chlorophenols in water. The sensor exhibited a good performance for the detection of phenolic compounds in a flowing system. The sensor was found to be highly stable and reproducible after 20 repetitive injections (Negash et al., 2014).

At present, application of CNTs for the sensing of gaseous CPCs has not been sufficiently studied. Therefore, the aims of this reasearch are to investigate the adsorption characteristics of selected CPCs (i.e., phenol, 2-chlorophenol and 2,4-dichlorophenol) on the CNTs synthesized in this research, and to evaluate the sensing performance of the CNT gas sensor on the exposure of the gaseous CPCs. The results of the morphological and chemical properties of the as-synthesized and the functionalized CNTs using electron microscopy, thermal gravimetric analysis, infrared spectroscopy, and Raman spectroscopy were presented in this study. The sensing patterns of the CNT membranes on the tested CPCs were collected through measuring the change in membrane resistivity, and were associated with the gaseous adsorption properties.

1.2 Objectives

Main objectives of this study is to synthesize highly sensitive and selective carbon nanotubes (CNTs) for low concentration gaseous chlorinated phenols (CPs) detection. The sub-objectives consisted of:

1. To study CNTs growth by thermal chemical vapor deposition (TCVD) and floating catalyst chemical vapor deposition (FCCVD) methods

2. To evaluate adsorption capacity of CPs on the synthesized CNTs

3. To investigate the effect of CNTs surface modification on the adsorption and sensing characteristics of the selected CPs

4. To develop a sensing prototype using four-point probe to measure the electronic properties of the synthesized CNTs

1.3 Hypotheses

1. The synthesized CNTs have a favorable chlorinated phenols adsorption.

2. The adsorption and sensing behaviors are influenced by the number of chlorine in the target compounds.

3. Surface functionalization can enhance the gas selectivity and sensitivity of the CNTs.

1.4 Scope of the research

1. The catalytic growths of CNTs on Si wafer were carried out using two methods namely Thermal CVD and Floating Catalyst CVD. The reaction parameters such as flow rate of carbon precursors, reaction temperature were varied individually in order to optimize the growth of CNTs.

2. The catalysts were used in the experiment include Ni for TCVD, and Ferrocene for FCCVD. The catalyst, loading will be varied in order to optimize the growth of CNTs.

3. The synthesized CNTs were characterized by a variety of physical and chemical techniques such as FE-SEM, TEM, TGA, Raman and FTIR spectroscopy.

4. The gases used in adsorption and sensing test included phenol, 2-chlorophenol, and 2,4-dichlorophenol.

Chapter 2

Theoretical backgrounds and literature review

2.1 Chlorinated phenols

Chlorinated phenols (CPs) are a group of 19 chemicals produced by adding chlorine atom to phenol (1-hydroxybenzene) in different number of chlorine atom and where the chlorine atom are positioned in the atomic structure. The isomers of chlorophenols include mono, di, tri, tetra, and one pentachlorophenol. The information involving physical and chemical properties of the chlorophenols is shown in **Table 2.1**. Most chlorinated phenol compounds are solids at room temperature. Melting temperatures increase with the number of chlorine atoms. They have a strong medicinal smell and taste. They are industrial chemicals with wide applications, such as pesticides, herbicides, disinfectants, biocides and wood preservatives (Arcand et al., 1995, Keane, 2005). 2-chlorophenol is a commercial chemical normally used as an intermediate to produce higher chlorinated phenols.

Chlorophenols can go into the environment during production process or being used as pesticides. Most of them transport into the water, with little going to the air. Human is often exposed to these compounds via air and food chains pathways. Among the chlorophenols, Mono- and dichlorophenols have high vapor pressures, they are most likely to be found in air rather than the particulate phase because they are the most volatile. (Eisenreich et al., 1981). Chlorinated phenols have been detected in water, air and soils as a result from inappropriate disposal, landfills leaching, and the chlorinated wastes combustion (ATSDR). Chlorinated organic by-products are generally produced from the burning of chlorine-containing materials. Industrial processes such as waste incineration, cement kiln combustion, nonferrous metal smelting are recognized as sources of polychlorinated dibenzodioxins (PCDD) and polychlorinated dibenzofurans (PCDF) (Muna et al., 2005).
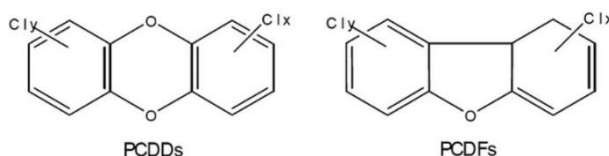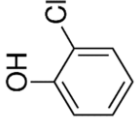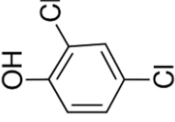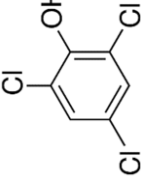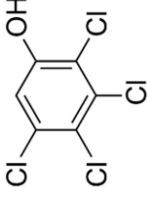
Figure 2.1 Chemical structures of PCDD and PCDF

Table 2.1 Physical and chemical properties of chlorinated phenolic compounds (Mackay et al., 2006)

	2-Chlorophenol	2,4-dichlorophenol	2,4,6-Trichlorophenol	2,3,4,5-Tetrachlorophenol
Synonym	2-CP	2,4-DCP	2,4,6-TCP	2,3,4,5-TTCP
Chemical formula	C_6H_5ClO	$C_6H_4Cl_2O$	$C_6H_3Cl_3O$	$C_6H_2Cl_4O$
Chemical structure				
CAS registry	95-57-8	120-83-2	88-06-2	4901-51-3
Molecular weight	128.556	163.001	197.446	231.891
Physical state	Liquid	Solid	Solid	Solid
Melting point	9.4°C	45°C	69°C	116.5°C
Boiling point	174.9°C	210°C	246°C	Sublimation
Density	1.257	1.383	1.4901	No data
Vapor pressure at 25°C	0.99 mmHg	0.14 mmHg	0.03 mmHg	0.0059 mmHg
Henry's law constant at 25°C (Pa m^3/mol)	0.688	0.435	0.5687	0.140

Chlorinated phenols are the most direct precursors of PCDD and PCDFs found in exhaust gases emitted from municipal solid waste incinerators (MSWIs). They are highly carcinogenic and classified as persistent organic pollutants (POPs). Therefore, their emissions are an important environmental issue. Kishi found that 2,4,6-trichlorophenol formed 1,3,6,8-TCDD or 1,3,7,9-TCDD (Kishi et al., 2009). With poor combustion conditions, chlorophenols form toxic organic contaminants such as PCDD, PCDFs, polychlorinated biphenyls (PCBs) and polycyclic aromatic hydrocarbons (PAHs). All of which can have serious effects on humans and environment.
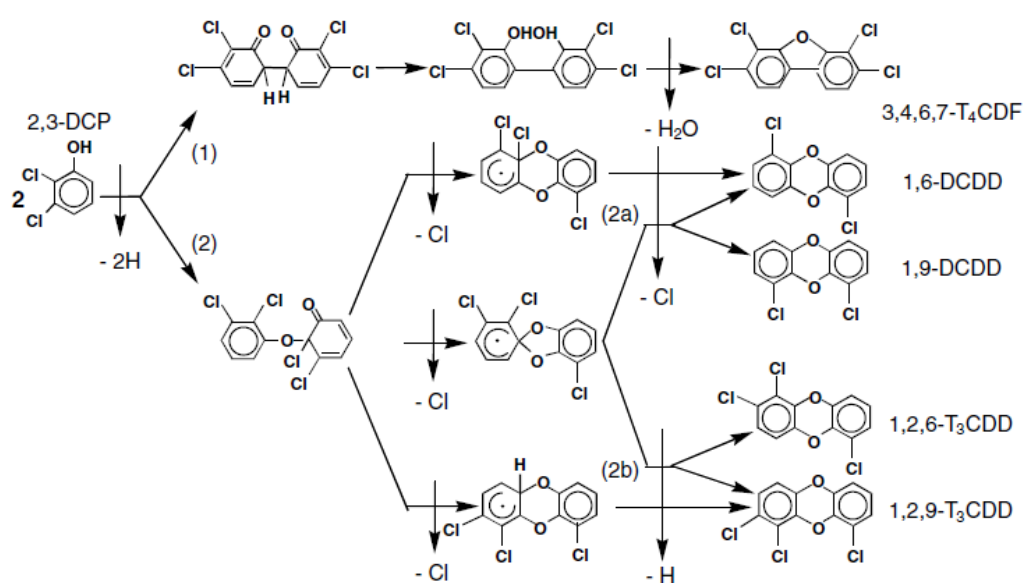
Figure 2.2 PCDD/PCDF formation pathways from 2,3-dichlorophenol (DCP) (Ryu, 2008)

2.1.1 Adverse effect of chlorinated phenols and PCDD/PCDF

People who exposed to chlorinated phenols for a long time may have slightly higher chances of cancer. The EPA has derived RfDs for individual compounds as follows: The oral RfD for 2-CP is 0.005 mg/kg/day based on a decrease (p<0.1) in litter size observed at 50 but not 5 mg/kg/day. The oral RfDs for 2,4-DCP and 2,4,5-TCP are 0.003 mg/kg/day and 0.1 mg/kg/day, respectively (IRIS 1998). 2,4,6-TCP has been classified as a group B2 carcinogen (probably human carcinogen) based on leukemias in male rats and hepatocellular adenomas or carcinomas in male mice (NCI 1979). Exposure to high levels of chlorophenols can cause damage to the liver and immune system.

Exposure to PCDD and PCDF can increase risk of severe skin injuries in human (chloracne and hyperpigmentation), weakness, severe weight loss, alter in liver function and enzymes activities, lipid metabolism as well as the abnormalities of immune system, and endocrine and nervous system. Chronic effects of acute exposure can increase frequency of certain kinds of cancers (Procaccini et al., 2003). 2,3,7,8-TCDD is a strong teratogenic and fetotoxic chemical and also causes cancers of the liver and other organs in animals.

2.1.2 Existing methods for detecting chlorinated phenols

The principal methods for detecting CPs in environmental samples are based on spectrometric and chromatographic techniques (e.g. gas chromatography equipped with different detectors such as electron capture, flame ionization, mass spectrometry, and high pressure liquid chromatography). Highly sensitive and specific analytical techniques are necessary for measurements. The preferred analytical measurement for CPs typically involves the use of high resolution gas chromatography equipped with high resolution mass spectrometry for congener-specific determination of CPs in environmental matrices, depending on the commercial availability of labeled congener standards.

Typical gas chromatography with electron capture detector (ECD) have also been used for the quantification of organo-chlorines. However, the direct measurement by GC for chlorophenols is difficult because of their highly polarity with relatively low vapor pressures. Therefore, they are usually derivatized to less polar form before analysis. Although GC and HPLC provide reliable results at trace levels, these methods also have some disadvantages. require high-priced and sophisticated equipment (Ayude et al., 2009). Sample extraction and cleanup is required to achieve correct separation and quantitation. HPLC required extraction steps and long run times in analysis (Lokhnauth and Snow, 2005).

2.2 Carbon nanotubes

Carbon nanotube (CNT) is a cylindrical graphitic tube made of graphene sheet rolled up into a cylinder with diameters of nanometers and macroscopic size length. Nanotubes made of one graphene sheet are called single-walled carbon nanotubes (SWCNTs). While, nanotubes with two or more shells are called multi-walled carbon nanotubes (MWCNTs). SWCNTs typically have a range of external diameter of only 0.4~3 nm, whereas that of MWCNTs is typically less than 50 nm.
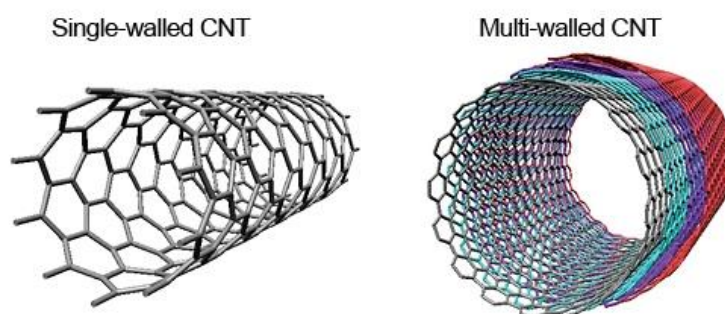
Figure 2.3 Structural models of a SWCNT (left) and an MWCNT (right)

Table 2.2 Allotropes of graphene and their properties.

Dimension	0D	1D	2D	3D
Allotrope	C_{60} buckyball	Carbon nanotubes	Graphene	Graphite
Structure	Spherical	Cylindrical	Planar	Stacked planar
Hybridization	sp^2	sp^2	sp^2	sp^2
Electronic properties	Semiconductor	Metal or semiconductor	Semi-metal	Metal

An isolated carbon atom has four valances electrons in atomic orbitals ($2s$, $2p_x$, $2p_y$ and $2p_z$). In graphene, carbon atoms are bonded by the interaction of the $2s$, $2p_x$, and $2p_y$, and hybridized into sp^2 orbitals making three σ bonds with neighboring carbon atoms in the same plane. They have electrons localized along the plane connecting carbon atoms which make it the strongest type of covalent bonds. These bonds offer graphene and carbon nanotubes the outstanding strength and

excellent mechanical properties. The $2p_z$ electrons, where the electron cloud is distributed perpendicular to the plane connecting carbon atoms, are loosely bound to the nuclei and are relatively delocalized. They either form covalent bonds called π bonds out of the plane of graphene or participate in interactions between two different planes of carbon atoms via a "π-π stacking" mechanism. These π orbitals are responsible for the electronic properties of graphene and carbon nanotubes by delocalized states (Javey and Kong, 2009).

SWCNTs can have electronic properties of either metallic or semiconducting depending on the way the graphene sheet is rolled into a cylinder. The design of SWCNTs is represented by the chiral vector (a pair of indices (n,m)). The chiral vector is explained in **Figure 2.4**. For instance, rolling a graphene sheet from its corner (Armchair, m = n), and a different design (Zigzag, m = 0) are formed by rolling from its edge. The design of structure has a direct effect on the electrical properties. The Armchair design is always metallic which have a band degeneracy between the highest π valence band and the lowest π conduction band, where these bands meet the Fermi level. While Zigzag or Chiral (m ≠ n), the major part of CNTs, are semiconducting in nature and have a smaller band gap (Dai, 2001). They exhibit field effect transistor (FET) behavior and are applied in many devices like transistors and sensors. MWCNTs have different orientations of the lattice (chiral vectors and angles) and defect concentration. However, the electron transport in the MWCNTs is found to be similar to that of SWCNTs because most of the current which passes through the tube is limited to the outermost layer of the CNTs (Kanoun et al., 2014).
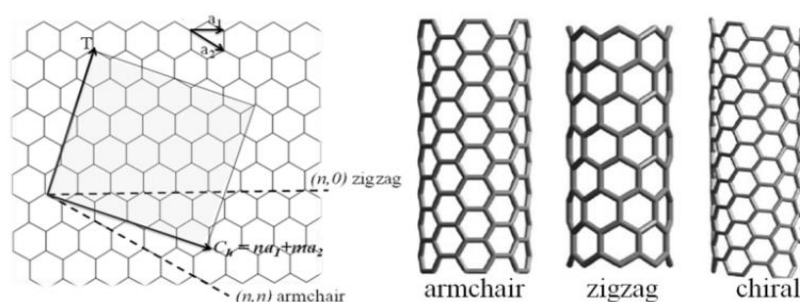
Figure 2.4 Different types of single-walled carbon nanotube

Electrical behavior of CNTs stimulates the continuous research and application of CNT based materials. Nanotube synthesized by different methods show completely different electrical conductivities, metallic, quasi-metallic and semiconducting. Such properties are reported to be sensitive to the nanotubes' diameter, wrapping vector angle as well as defects. Slight differences in these parameter can turn quite similar carbon materials from metallic to semiconducting states.

Carbon nanotubes possess many unique properties which had not been observed previously, and thus the application of CNTs and their derived structures have been under intense research studies. Since their discovery by Iijima (Iijima, 1991), CNTs have gained a great interest for their unique nanostructures with enchanting mechanical, chemical, and electronic properties. Its one-dimensional quantum effects lead to the outstanding electronic properties. Due to its nano-scale size, CNTs inherently contain fairly large specific surface area with highly ordered structure. Its porous components include not only of the interstitial and interlayer micropores, but also of those intra-tubular pores existed in a bundle of CNTs. The well distributed pore sizes thus make the CNTs a potent sorbent which may be applied to atomic storage (e.g., H_2) and molecular storage (e.g., CH_4, CO_2) which are of great interest for the future generation of energy supply, as well as surface interaction with larger organic molecules which are of interest of environmental pollution control. In addition, CNTs are also a very promising material for sensor applications because of their high electrical conductance and electrochemical properties.

2.2.1 Methods for carbon nanotube synthesis

CNTs are generally synthesized by three methods, namely arc discharge, laser ablation, and chemical vapor deposition (CVD) methods. Arc discharge is the earliest method for CNTs synthesis. CVD is a new, controllable and economic technique compared to the other two methods. It provides considerably high yield as well as purity.

(a) Arc discharge

Arc discharge is the most common method to produce carbon nanostructures (Ando and Iijima, 1993). It was first used for the production of fullerene (Kratschmer et al., 1990). The system consists of two graphite rods (cathode and anode) placed in an inert atmosphere (such as He). Metal catalyst particles (such as Co, Ni, Fe) are contained in the chamber. Direct current (50 to 100 A, driven

by 20 V potential) is applied between the rods. This will cause high current density producing high temperature discharge (3,000-4,000^{o}C) between the two rods. The surface of the carbon electrode is vaporized by the discharge and then condenses upon cooling, forming a rod-shaped carbon deposit on the chamber wall and the electrode. The deposits contain CNTs with fullerene and amorphous carbon particles as by-products.

(b) Laser ablation

The laser ablation method was developed in 1995 by Smalley's group. A block of graphite contained in a quartz tube is heated in a furnace with a continuous flow of Ar gas. A laser beam is introduced through the window and focused onto the graphite target containing catalyst materials (usually Ni or Co) in the furnace at 1200°C. The target is vaporized, carried by argon gas and forms SWNTs on the cooler surfaces of the reactor (Arepalli, 2004). The product from method appear as a CNT bundle with 10-20 nm diameter and the length up to 100 μm or more. The laser ablation method is more suitable to grow SWNTs. However, MWNTs can also be produced with special reaction conditions.

(c) Chemical vapor deposition

Chemical vapor deposition (CVD), a simple and economic technique, becomes the most favorable method for synthesizing high quality CNTs at large scale. It can produce CNTs at low temperature and ambient pressure. It offers using of hydrocarbons in any state (solid, liquid or gas), allows CNTs to grow on various materials in various forms, such as powder, films (Kukovitsky et al., 2003), aligned (Lee et al., 2001), entangled, coiled nanotubes (Fejes and Hernádi, 2010), or a preferred architecture of CNT with a predefined pattern (Kuljanishvili et al., 2009). This method has advantages of the very high yield, the consistent alignment of the nanotubes as well as better control on the growth parameters. The schematic diagram of a simple CVD setup is illustrated in **Figure 2.5**.

The typical mechanism of CNT growth in CVD process relates to the hydrocarbon decomposition at elevated temperature catalyzed by the metal catalyst nanoparticles. Then the dissociated carbon precipitates on the saturated metal nanoparticle and form tubular carbon solids in sp^2 structure. The diameter of the synthesized CNT is generally governed by the catalyst nanoparticle

size. Most commonly used precursors in CVD process are methane (CH_4), ethylene (C_2H_4), acetylene (C_2H_2), benzene (C_6H_6), xylene ($C_6H_4(CH_3)_2$) and carbon monoxide (CO). Typically, MWCNTs are produced at low temperature CVD (600-900°C), while high temperature (900-1200°C) reaction is required to grow SWCNTs because SWCNTs have a higher formation energy. Moreover, MWCNTs can be grown from most kinds of the hydrocarbon but SWCNTs require selected hydrocarbons.
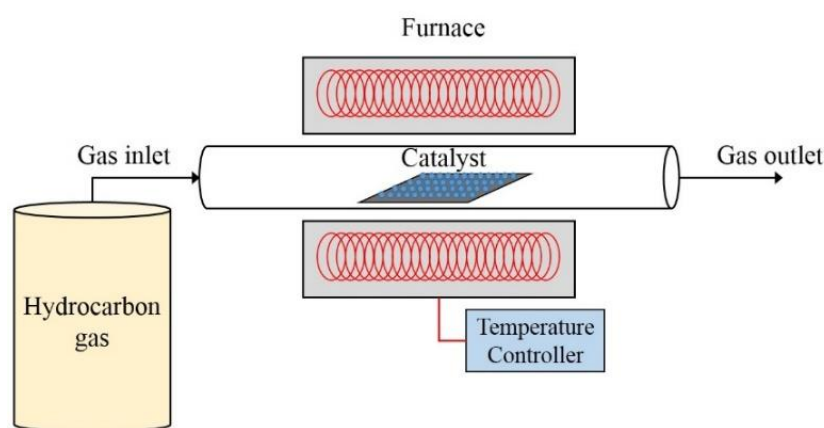
Figure 2.5 Schematic diagram of a CVD setup

Thermal CVD is the simplest CVD technique that only heat to activate hydrocarbon decomposition. It is obviously suitable for large quantity CNT synthesis. The yield, size, and morphology of the synthesized CNT are crucially affected by the type of catalyst (Dong et al., 2004, Qi et al., 2010). The catalyst particle size dictates the nanotube diameter. Therefore, metal catalyst particles with well-ordered size could be employed to grow controlled diameter CNTs (Fan et al., 1999). CNT synthesis typically requires metal catalyst particles in nanometer size to allow hydrocarbon to decompose of at lower temperatures. Transition metals often used to catalyze CNT formation include Fe, Co and Ni, because of the high solubility and diffusion rate of carbon in these kinds of metals at high temperatures (Dupuis, 2005). The non-filled "d" shells of these transition metals enable them to interact with hydrocarbons and show the catalytic activity. High melting point and low equilibrium vapor pressure of these metals offer a wide range of carbon precursors used in CVD. In addition, Fe, Co and Ni catalysts are efficient to form CNTs with low diameter because they have strong adhesion with the growing CNTs (Ding et al., 2008). Solid organometallocenes (such as ferrocene, cobaltocene, nickelocene) are also widely used catalysts because they in-situ discharge metal nanoparticles to catalyze the decomposition of hydrocarbon more effectively.

CNT growth consists of two growth modes. The base-growth mode occurs when strong interactions between metal-support exist, the catalyst particle remains on the substrate surface and the nanotube grows with a closed-end. On the other hand, in the tip-growth mechanism, where interaction of metal-support is weak, the catalyst particle were raised from the substrate and lifted at the tube end during the nanotube growth (Cassell et al., 1999).

2.2.2 Purification of as-synthesized carbon nanotubes

The main impurities usually found in as-synthesized CNTs can be divided into (1) metal catalyst particles from the synthesis and (2) carbonaceous impurities such as amorphous and other forms of carbon. Acid treatment is an effective method to remove the impurities from the carbon nanotubes. The acid is usually heated to its boiling point during acid treatment with cold water running through the system helps in refluxing the acid and preventing it from vaporizing. The important parameters to be considered during acid treatment are type of acid, acid concentration, amount of nanotubes to acid ratio, duration of acid treatment and temperature used in acid treatment. At the end of the acid treatment, the acid is neutralized using de-ionized water and the nanotubes are filtered. The filtered nanotubes are then dried in an oven because all the moisture must be removed to obtain a pure sample of carbon nanotubes.

In contrasts, gas phase oxidation is a milder purification technique than acid treatment. Carbon impurities are burnt out selectively at elevated temperature in the presence of oxygen or air. This method is based on the assumption that CNTs are more resistant to oxidation than impurities. Therefore, the impurities (mainly amorphous carbon) can be eliminated at a temperature below the oxidation temperature of CNTs without damaging the nanotubes (Dementev et al., 2009).

2.2.3 Functionalization of carbon nanotubes

There are two types of functionalization relying on the attaching of the functional groups onto the CNT sidewall: (a) covalent functionalization and (b) non-covalent functionalization. Covalent functionalization of CNTs is often carried out by acid treatment. This process generates defect sites and results in a loss of conductivity. In contrast, non-covalent functionalization, based on Van der Waals interactions and π-stacking. The structure of CNTs and their physical properties of are preserved (Eder, 2010, Karousis et al., 2010).

(a) Covalent methods

The covalent method is the most common method for the functionalization of CNTs which involves the adding of carbonyl and carboxyl groups through a treatment with a mixture of HNO_3/H_2SO_4. The solubility and reactivity of CNTs could be significantly improved via introducing these functional groups (Pavese et al., 2008). Acid-oxidized proved versatile for further elaboration, because the end caps of the nanotubes are opened and acidic functionalities in the oxidation, which is suitable for further derivatization by fluoroalkanes, silanes and polymers to CNTs. However, this method creates structural defects and interrupts the delocalized electron system in the CNT surface, and lead to change of the electronic and mechanical properties which may influence the performance (Yuca et al., 2011).

(b) Noncovalent methods

Noncovalent adsorption of polymer gained much attraction because It can possibly introduce various functional groups on the nanotube surface without affecting the π system of the graphite sheets (Thostenson et al., 2001). Noncovalent adsorption of polymer has been indicated as one of the most effective treatment for functionalization of CNTs without detrimental effect on the original CNT structure, maintaining and reinforcing their electronic properties.

2.3 Carbon nanotube membrane (Buckypaper)

Buckypaper, invented by Dr. Smalley and his research group (Sreekumar et al., 2003), is a thin sheet formed with carbon nanotubes. It can be serve as an ideal freestanding flexible and versatile electrode for electrochemical devices. CNT Buckypaper shows a wide range of potential applications, such as water purification, desalination (Yang et al., 2013, Das et al., 2014), gas separation (Gilani et al., 2013, Holt et al., 2006), drug delivery (Wu et al., 2010b), super-capacitor electrodes (Futaba et al., 2006), and gas sensor (Slobodian et al., 2011). A buckypaper was originally a thin carbon nanotube mesh, with relatively uniform nanotube rope size and porous structure, peeled from the membrane after filtration process. The thickness, density, and porosity of buckypapers can be controlled in manufacturing by adjusting main parameters, such as concentration of suspension, sonication time, surfactant type and vacuum pump pressure.

2.3.1 Methods for CNT buckypaper fabrication

CNT buckypaper can be prepared by many techniques and the widely used fabrication techniques includes spray coating (Schindler et al., 2007), dip coating (Li et al., 2011), spin coating (Meitl et al., 2004) and vacuum filtration (Luo et al., 2008).

Among them, vacuum filtration method is the most promising and widely used because the homogeneity of the buckypaper can be adjusted by the filtration process itself (Wu et al., 2004). The method is based on separating CNTs composites from solvents and compress into films by the different pressures between two sides Buchner funnel. A pump is attached to the vacuum port of the filtration flask. The solution is then vacuum-filtered through a filter resulting in the CNT film to collect on the filter and subjected to drying process. The film thickness can be precisely controlled by the volume and concentration of the CNT solution. It can be applied with various types of materials e.g. CNTs, carbon nanofiber and graphene, or even mixed types of material (Memon et al., 2011).

2.4 Characterization of carbon nanotubes

2.4.1 Morphology analysis

There is a robust interrelationship between the properties and the structure of the carbon nanotubes. The structure and morphology of the CNTs is formed during the synthesis step. It can be presented in uniformly dispersed, agglomerated, entangled or aligned patterns. The shape, size, and distribution of CNTs influence its properties. Therefore, the morphology observation of CNTs is an important thing for the material characterization. Scanning electron microscopy (SEM) and transmission electron microscopy (TEM) are commonly used techniques to analyze material morphology. They provide good depth of field images with high magnification.

SEM is a fundamental technique for observing the surface morphology of materials. Normally, SEM operates at a high vacuum condition. Electron beam is generated and accelerated by a high voltage (e.g. 20 kV) and then the beam scans the surface of the specimen and the emitted electrons from the specimen are collected by a suitably-positioned detector. The schematic layout of SEM instrument is shown in **Figure 2.6**
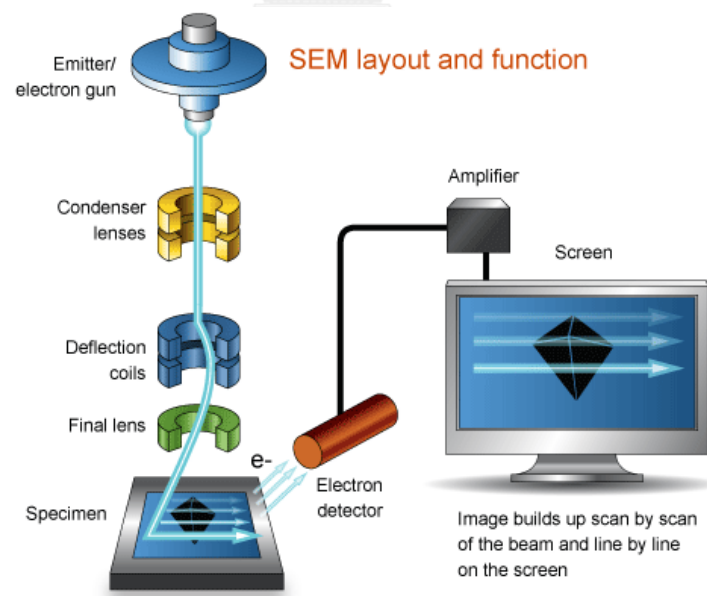
Figure 2.6 Schematic layout of SEM

TEM is a powerful imaging technique for material science. It is used to characterize atomic features found in nanostructures. A high energy beam of electrons is transmitted through a very thin specimen. The image is formed from the interaction between electrons and the specimen atoms. TEM can be used to observed crystal structure, quality, shape, size of the specimens as well as feature structures such as grain boundaries and dislocation. TEM typically gives more detailed structural information than SEM, it can achieve a resolution down to 0.1 nm. The schematic layout of TEM instrument is shown in **Figure 2.7**
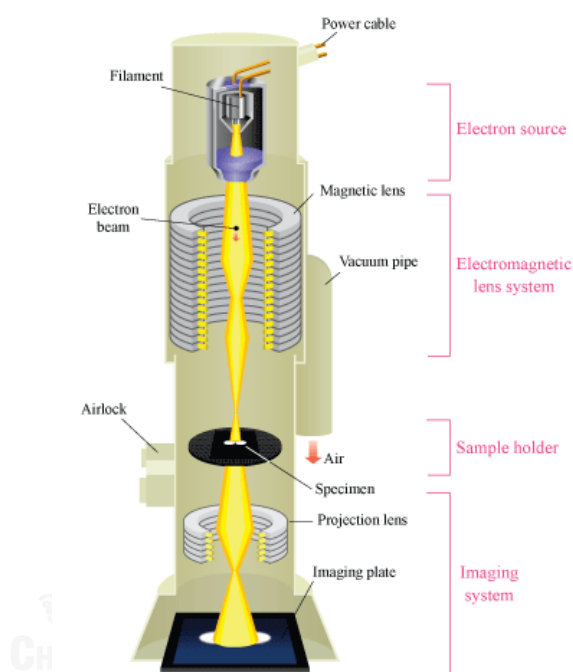
Figure 2.7 Schematic layout of TEM

2.4.2 Spectroscopic characterization

Spectroscopic techniques are effective methods to examine the chemical compositions in the materials and identify the surface modification of CNTs. Raman spectroscopy and Fourier-transform infrared spectroscopy (FTIR) are forms of vibrational spectroscopic techniques for characterizing CNT based materials. Adsorption of infrared radiation results in vibrations within molecules and the bond vibrate arises the adsorption bands.

Raman spectroscopy is used to investigate the vibrational, rotational, and other low frequency modes of a material based on the change in the polarizability of the molecule. A specimen is irradiated with a monochromatic laser beam. The laser interacts with the molecules and generates a scattered light with different frequencies from that of incident light, and is then used to create a Raman spectrum (Bumbrah and Sharma, 2015). The schematic diagram of Raman spectroscopy (Biswas et al., 2010) is shown in **Figure 2.8**.

All allotropic of carbon are active in Raman spectroscopy. However, the different forms of carbon have the difference in of absorption bands in term of position, width, and relative intensity. The features of CNTs in Raman spectra consist of the radial breathing mode (RBM), D-band, and G-band. The degree of graphitization can be inferred by the intensity ratio of D band (I_D) to G band (I_G). A lower in I_D/I_G ratio implied a better graphite structure. The change in intensity of absorption bands have been detected for functionalized CNTs. In addition, exposure to target gases was observed to reduce G-band intensity of CNTs gas sensor in Raman spectra (Ghaddab et al., 2012).
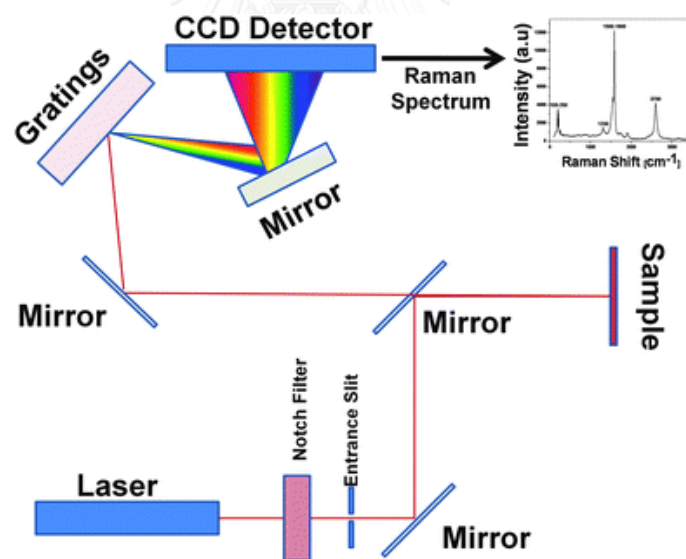
Figure 2.8 Schematic diagram of Raman spectroscopy

FTIR is a very useful technique for identifying the presence of certain functional groups of organic molecules compounds that attached on CNTs. Functional groups, side chains and cross-links will have the unique vibrational frequencies in the infrared range. The adsorption bands, specifically corresponding to the bonds in the molecule, confirm the property change of materials after surface modification and also identify the presence of specific impurities. The schematic diagram of a Michelson interferometer, configured for FTIR is shown in **Figure 2.9**.
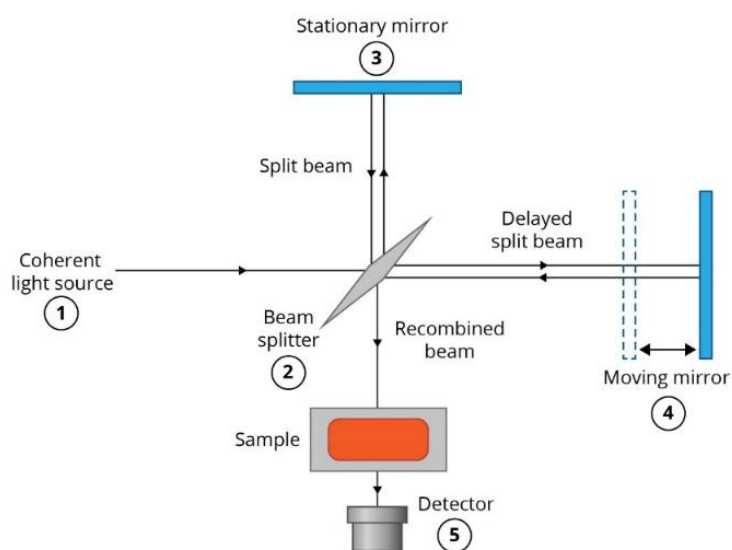
Figure 2.9 Schematic diagram of FTIR

2.4.3 Thermal analysis

The thermal limitation is an important characteristic of the CNTs materials because some applications require high temperature working condition. The thermal stability is determined by the tolerance temperature which the structure of CNTs begins to change. Thermal gravimetric and derivative thermal gravimetric (TG-DTG) analyses are typically utilized for evaluating the thermal stability of the materials. The schematic diagram of TGA instrument is shown in **Figure 2.10**. TGA is based on the mass loss of sample as a function of temperature. Meanwhile, DTG performs the mass change as a function of temperature (dm/dt). Both measurement data are obtained when a material is heated at a constant rate.
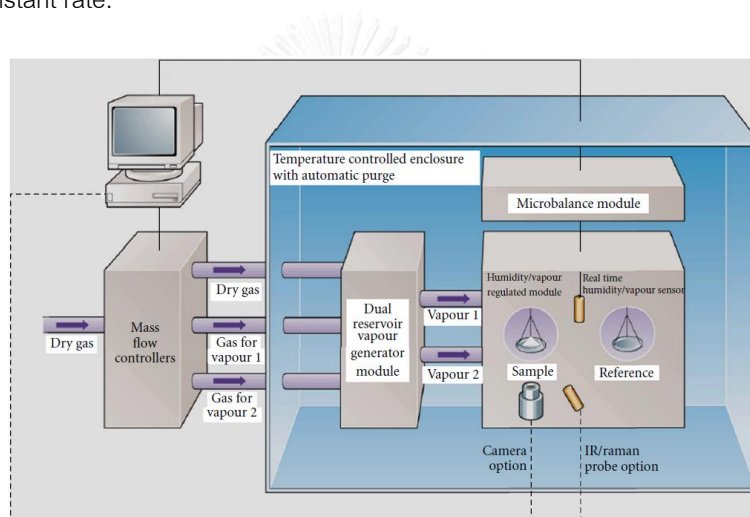
Figure 2.10 Schematic diagram of TGA instrument (White, 2012)

2.5 Adsorption

Adsorption is the process in which a gas molecules or vapor is brought into contact with a solid by unbalanced residual force, and adhere at the surface of the solid. Adsorption process involves two components namely adsorbent and adsorbate. The solid that adsorb the gas is called "adsorbent" and the gas molecules or vapor being adsorbed on the surface is called "adsorbate". Adsorption is essentially a surface-based process where adsorbates accumulate on the surface of the adsorbent. The adsorption forces between adsorbates and adsorbent define the type of adsorption whether it is physical or chemical. Adsorption and desorption processes of gases on solids are often quite complex. It is seldom unclear to indicate the type of adsorption in a certain situation. Adsorption sometimes occurs as a combination of chemisorption and physisorption.

Physisorption is fast and reversible. It generally predominates at low temperatures. Molecules are typically binding to the surface of porous material by the attraction of van der Waals forces without chemical reaction with the adsorbent. Molecular interactions with permanent dipole changes, heats of adsorption ranging from 10 to 40 kJ/mole. The important parameters for physisorption include the surface area, pore structure, pore size, and pore volume.

In contrast, the chemisorption of a gas-phase adsorbate to a solid occurs through an overlap between the electronic orbitals of the molecule and the surface. This overlap could induce a weakening of the internal bindings of the molecule and end up in a dissociation of the molecule. Electron transfer between an adsorbate a solid surface is required for the formation of chemisorptive bonds. Normally the energies of chemisorption are greater than 40 kJ/mol. The main advantage of chemisorption is the ability to effectively handle low concentrations of gas molecules.

2.5.1 Adsorption isotherm

The adsorption isotherms characterize the dependency of the amount of adsorbate on the adsorbent as a function of concentration or relative vapor pressure at constant temperature. Gas adsorption on solid surfaces involves the mass and energy interaction between adsorptive molecules and adsorbent surface which resulted from pore texture and surface structure. Adsorption isotherm offers information for the active surface of a material, cavity structures and adsorption affinity of molecules.

Figure 2.11, Type I isotherms describe microporous adsorbents (e.g. activated carbons). It indicates the single monolayer of adsorbate at the adsorbent surface. Type II describe the formation of indefinite multi-layer after the monolayer completion and III describe amount of gas adsorption increase without limit on mesoporous adsorbents. Type IV isotherm is a variation of Type II, but with hysteresis loop associated with a finite multi-layer formation due to capillary condensation in mesopores. The Type V isotherm is obtained with certain porous adsorbents. It is related to the Type III isotherm in which the interaction between adsorbent and adsorbate is weak. The Type VI isotherm describes multilayer adsorption occurred on a uniform non-porous surface.
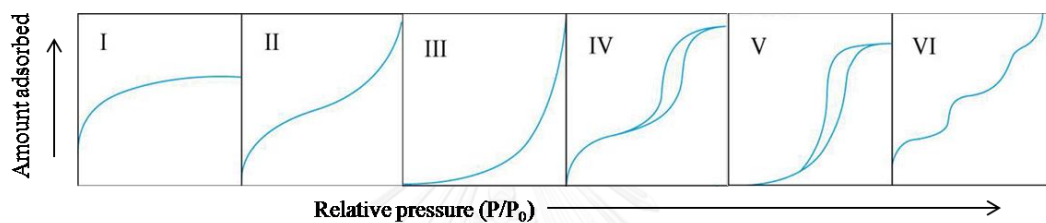
Figure 2.11 The IUPAC classification of adsorption isotherms.

2.5.2 Adsorption isotherm models

Modeling of the experimental data form adsorption isotherm is necessary to predict the adsorption mechanisms and estimate the adsorption capacity of the adsorbent.

(a) Langmuir isotherm model

Langmuir isotherm was initially developed by Irving Langmuir in 1916 to describe the adsorption between gas-solid phases on activated carbon. The model is based on the assumption that the adsorbed layer is one molecule in thickness (monolayer adsorption). The adsorption can only occur at a fixed number of identical and equivalent sites, with no side interaction and steric interferent between the adsorbed molecules.

(b) Freundlich isotherm model

Freundlich isotherm describes the non-ideal, reversible and not restricted to the formation of monolayer adsorption. This isotherm provides empirical equation which can be applied to multilayer adsorption, with non-uniformly distributed adsorption affinities over the heterogeneous surface. The

model assumes that the stronger binding sites are taken up first, until energy of adsorption decreased exponentially upon the adsorption end. The amount adsorbed is the summation of adsorption on all sites.

(c) Redlich–Peterson isotherm model

Redlich–Peterson isotherm (Redlich and Peterson, 1959) is a hybrid isotherm containing three parameters and involves the features of both Langmuir and Freundlich isotherms. The Redlich–Peterson model can be applied either in homogeneous or heterogeneous systems due to the equation versatility. Normally, the procedure for solving equations involves maximizing the correlation coefficient (R^2) between the theoretical model predictions and the experimental data with solver function of the Microsoft excel (Wu et al., 2010a). At high concentration (as the exponent β tends to zero), it approaches the Freundlich isotherm model and is in accordance with the Langmuir isotherm at low adsorbate concentrations (as the β values are all close to one).

2.5.3 CNT adsorption of chlorinated aromatic compounds

The adsorption of various aromatic compounds on CNTs has been expansively studied, but relatively little results have been published on the adsorption of chlorinated aromatics. CNTs have a highly graphitic surface structure and contain cylindrical pores that allow CNT interacts with an adsorbing molecule more substantially than slit-shape pores materials, such as activated carbon (Rege and Yang, 2000). Moreover, CNTs are highly aromatic, a high density of π electrons contained on the surface of a CNT could involve in charge transfer with an adsorbate molecule, especially one that also contains π electrons (Sumanasekera et al., 2002). These unique properties of CNTs make it adsorbs molecules with aromatic rings much stronger than other kinds of adsorbents.

For instance, Long and Yang have demonstrated that the bond energy between dioxin molecules and CNTs was nearly three times that between dioxins and activated carbon used for removing dioxin from incineration off-gases. The stronger bond energy stems from the overlapping potentials when the two benzene rings of dioxin molecules are optimally aligned with the graphitic ring of the CNT walls (Long and Yang, 2001). A number of other studies showed that CNTs have strong adsorption of molecules with aromatic rings, such as benzene and chlorobenzenes (Eswaramoorthy

et al., 1999, Peng et al., 2003). For example, Lin and Xing studied the adsorption of several polar aromatic compounds, and observed that the adsorption affinity of these compounds by CNTs increased with increasing number of aromatic rings (cyclohexanol < phenol < 2-phenylphenol < 1-naphthol), and was greatly improved by the substitution of -OH (phenol (1-OH) < catechol (2 -OH) < pyrogallol (3 -OH)). They concluded that the substitution of electron-donating on the aromatic rings enhanced the π-π interaction between the CNTs and aromatics, and accordingly the adsorption affinity (Lin and Xing, 2008).

Den and co-workers also reported that the adsorption capacity of the nanotubes was substantially greater than that of activated carbon due to the π-π interaction between the benzene ring of the phthalates and the graphitic surface of the nanotubes. Between the nanotubes with different outer diameters, the adsorption capacity appeared to be controlled by their specific surface areas, although the abundance of oxygenated surface functional groups may also facilitate adsorption of the phthalate esters (Den et al., 2006). Also, the adsorption process of the carbon nanotubes was an endothermic one, as the adsorption capacity was enhanced under higher temperatures. Yang and co-workers studied the adsorptivity of polycyclic aromatic hydrocarbons (PAHs), including pyrene, phenanthrene, and naphthalene on MWCNTs, and successfully described the experimental results using the Polanyi-Manes model. They proposed that the molecular size of the adsorbate may determine the adsorption capacity, because larger molecules tend to be physisorbed on graphite surface, whereas smaller molecules penetrate into the interior pores, but are limited by the diffusion rate. The observed results exhibiting better adsorption for PAH molecules with planar structure are consistent with those involving π-π bonding (Yang et al., 2006).

Similarly, Zhang and co-workers found that the pore volume occupancies of three aromatic compounds followed the order of activated carbon fiber (ACF) > granular activated carbon (GAC) > SWNT > MWNT, implying that the adsorption site availability was related to the pore size distributions of the adsorbents (Zhang et al., 2010). ACF and GAC with higher microporous volumes showed higher adsorption affinities to aromatic compounds with low molecular weight than SWNT and MWNT with higher mesopore and macropore volumes. In contrast, SWNTs and MWNTs are expected to be more

efficient in adsorption of larger size molecules. Elimination of oxygen-containing functional groups from the surface of SWNT enhanced adsorption of these aromatic compounds.

In recent years, Toth's group has published a number of results focusing on the CNT adsorption of multi-component phenols and chlorophenols, among other compounds. In one study, they reported that the surface coverage for the two aromatic probe molecules (21–33% for dopamine and 8–12% for phenol) is significantly lower than the performance of porous carbons, but the free energy change (ΔG) values show that the adsorption potential is stronger (Tóth et al., 2011). In another study involving co-adsorption of phenol and m-chlorophenol on the two purified commercial CNTs, they reported that the chemical nature of the aromatic compound, the surface chemistry of the CNT, as well as their relative and total concentration all play an important role in the performance. The uptake of phenol was restrained in comparison to its single solute behavior on both nanotubes, independently of the initial pollutant concentration. The uptake of m-chlorophenol, in contrast, was more sensitive to the surface chemistry of the nanotube and the concentration. CP was preferentially adsorbed in about 95% of the relative concentration range (Tóth et al., 2012).

In summary, the consensus in the scientific community is that both the adsorption capacity and the affinity were found to increase with the number of aromatic rings as π-π bonds play a significant role in the interaction with such molecular structures. Also, the number of -OH groups attached either on the aromatic compounds or the CNT surface enhances the uptake of aromatic compounds. A number of studies have been done to modify chemically both SWNTs and MWNTs. A mixture of sulfuric acid and nitric acid was used to form carboxylic acid groups on the surface (Liu et al., 1998). The addition of carboxylic acid groups on the CNTs surface is convenient because a variety of chemical reactions can be carried out with this group. Furthermore, the chlorinated aromatics appeared to be favorably adsorbed as compared to their non-chlorinated counterparts. Vast majority of these studies, however, pertains to aromatic and chlorinated aromatic compounds in aqueous phase. Those in gaseous phase are still very limited. Also, while theoretical computation concerning CNT adsorption of CPs with different number of chlorines exists, there has not been any systematic experimental investigation on the effect of chlorine position and number on the adsorption of these chlorinated aromatics. Through Density functional theory (DFT) calculations, Jiang and co-workers

observed that 2-chlorophenol and 2-chlorophenoxy radical naturally interact with the pristine CNT by the van der Waals force; in contrast, they exhibit much higher reactivity towards the Si-doped CNT. Doped CNTs, thus, can be considered as promising material for adsorbing (concentrating) and/or detecting these PCDD/PCDF precursors (Jiang et al., 2009).

2.6 Gas sensor

Traditional solutions for chemical gas sensing have been dominated by conventional laboratory analytical instruments such as mass spectroscopy, gas chromatography and ion mobility spectroscopy. Although these methods are accurate for detecting chemicals in low concentration, they are costly and require complex instruments to run analysis. Their high cost, time consumption and the prerequisite of trained operators often prohibit practical use for routine detection in residential sensing of toxic chemicals. Since 1970s, microelectronic gas sensors have been investigated to be an alternative to laboratory chemical sensing methods for lower cost, faster response times and greater accessibility (Neri, 2015). Typical gas sensors have advantages in its smaller size (micrometers to centimeters) and simpler to operate. These advantages make gas sensors feasible for real time use in environments.

Chemical gas sensor is a physical device that can change the properties upon exposure to gas molecules. The change in their properties generates electrical signal and are then used to detect the gas molecules. The sensors are based on the chemical reaction between the sensor and the analyte molecules. The resistance of the gas sensor is typically proportional to the concentration of a target chemical in the atmosphere. In addition, changes in the operating conditions such as temperature can affect the sensor response. These temperature-dependent sensor responses may be helpful to get a characteristic response for different chemicals, thus improving the selectivity of the sensors without changing their physical properties.

Several important parameters for evaluating the gas sensor performance include: (1) Sensitivity: a change of signal over target gas concentration unit, i.e., the slope of a calibration graph; (2) Selectivity: the ability to recognize a specific gas among a gas mixture; (3) Response time: the time required for sensor to respond to a concentration change; (4) Recovery time: the time for the sensor signal to return to its initial value; (5) Reversibility: whether the sensor could return to its original state

after detection (6) Stability: the ability of a sensor to provide reproducible results for a certain period of time. This includes retaining the sensitivity, selectivity, response, and recovery time; (7) Working temperature: the temperature that corresponds to maximum sensitivity; (8) Life cycle: the period of time which the sensor can operate continuously; (9) Energy consumption; (10) fabrication cost (Liu et al., 2012, Kumar et al., 2015).

2.6.1 CNT gas sensors

Due to the high surface area and the ability to change electrical properties at room temperature upon exposure to gas molecules, carbon nanotubes (CNT) have been a promising gas sensing material. Gas sensors made from carbon nanotubes have good sensitivity at room temperature (Kong et al., 2000), in comparison with the commercially available semiconductor sensors which have operating temperature at above 200°C. In multi-walled carbon nanotube (MWCNT), the electrical resistance is mainly determined by the atom at the surface. This means that no diffusion is required, which in turn has impact on the response time of the gas sensor. These factors make MWCNT to be potential material for gas sensing applications. However, the high binding energy between gas molecules and CNT makes gas molecule desorption process difficult, thus causing long recovery time.

The adsorption of gas molecules onto the surface of CNT, results in donation or withdrawal of electrons to or from the CNT. As molecules adsorb on CNT surface, charges transfer causing its Fermi level, carrier density, and electrical resistance to change and production of a sensor signal. Jijun and co-workers used Density Functional Theory (DFT) to measure the SWCNT/gas molecules interaction by evaluating the binding energy, the distance between SWCNT and gas molecule, and the charge transfer between SWCNT and the molecule. High binding energy corresponds to the chemisorption of analytes, while low binding energy indicates a physisorption mechanism. Physisorption allows the sensor to be easily reset , in contrast, chemisorption brings a larger charge transfer resulting in higher sensitivity (Jijun et al., 2002).

Semiconducting CNT is usually p-type, which is different from that of the other metal oxide nanowire (n-type). Comparing to metal oxide nanowires, such as In_2O_3, SnO_2 and ZnO, the difference in semiconductor type of CNTs can be utilized for gas molecule discrimination because CNTs appear to give inverse electrical response when exposed to target gases (Chen et al., 2009).

Table 2.3 The changes in the electrical resistance of gas sensor in gas atmosphere (Fine et al., 2010)

Classification	Majority charge	Oxidizing gases	Reducing gases
n-type	Negative (electron)	Resistance increase	Resistance decrease
p-type	Positive (Hole)	Resistance decrease	Resistance increase

2.6.2 Application of CNTs for detection of organic air contaminants

In the quickly emerging field of environmental monitoring, the development of progressively sophisticated instrumentation has arisen in areas with little changes before the 1990s. Applications include a broad range of activities, but mainly the potentially polluting industrial installations such as those of the energy, defense, chemical, paper, food, agriculture and waste processing (e.g., landfill sites and wastewater treatment plants) industries. Carbon nanotube (CNT) presents a promising one-dimensional nanostructure for various nanoscale electronic applications because of its high environment stability. Additionally, the nanostructure of CNTs would provide a significant high surface-to-volume ratio which is an advantage for high-responsive gas sensors. The absorption of gas on the CNT surface at room temperature varies its electrical properties with fast response, which enables them to be a potential candidate for gas sensing applications.

For example, Chopra and co-workers developed a method using wired SWNTs to study the resonant frequency shift phenomenon for several polar and nonpolar gaseous compounds (He, Ar, N_2, O_2, CO, NH_3), and found that there existed a correlation between the dielectric constant of SWNT in contact with these gaseous compounds and the responding resonant frequency shift, and that these correlations may be used for gas detection in the parts-per-million (ppm) level (Chopra et al., 2003). Qi and co-workers fabricated arrays of electrical devices comprising multiple SWCNTs bridging metal electrodes by CVD of nanotubes across prefabricated electrode arrays. They demonstrated the great changes in electrical conductance under electrostatic gating, thanks to the high percentage of semiconducting nanotubes. They also showed that, by coating polyethyleneimine, the n-type nanotube devices was capable of detecting NO_2 at less than 1 ppb while being insensitive to NH_3; whereas coating Nafion on nanotubes allowed for selective sensing of NH_3 (Qi et al., 2003).

For detection of organic vapors, Consales and co-workers applied Langmuir-Blodgett method to prepare SWNT on standard silica optical fibers (SOFs) and quartz crystal microbalance (QCM) elements. They tested the changes in frequency shift and optoelectronic signals during adsorption of volatile organic compounds (VOCs) such as toluene and xylene, and estimated sensitivity could reach parts-per-billion levels (Consales et al., 2007). The same group of researchers also attempted to use cadmium arachidate (CdA) as the substrate and the SWNTs-enhanced optical fibers for detecting VOC including toluene, xylene and ethanol. They reported that composite sensor CdA/SWNTs was more sensitive than SWNTs sensor along, with sensitivities in the ppb-level (120~560 ppb) (Consales et al., 2009). Li and co-workers casted SWCNTs on an inter-digitated electrode (IDE) for detecting gas and organic vapor at room temperature. The responses of the sensor were linear for concentrations of sub ppm to hundreds of ppm with detection limits of 44 ppb for NO_2 and 262 ppb for nitrotoluene. They proposed that the detection of the gas to organic vapors was related to direct charge transfer on individual semiconducting SWCNT with additional electron hopping effects on intertube conductivity. (Li et al., 2003).

The conductivity of CNTs can be significantly changed while absorbing gas molecules by withdrawing and donating electrons. For instance, Someya and co-workers fabricated SWNTs by evaporating Au with metal shadow masks, the results showed good reversibility and reproducibility while exposed to different alcohol vapors (such as methanol, ethanol, 1-propanol and 2-propanol) (Someya et al., 2003). Novak and co-workers also reported dimethyl methylphosphonate (DMMP) detection on a SWNT network based chemical field effect transistor at sub-ppb concentration levels (Novak et al., 2003).

2.6.3 Functionalization of carbon Nanotube-based gas sensors

Some potential disadvantages of using sole CNTs as sensors are the lack of selectivity and the low sensitivity to different gaseous analytes. As has been pointed out by Cantalini and co-workers, the cross-sensitivity of SWCNT gas sensors can result in incorrect alarms in a complicated atmosphere (Cantalini et al., 2003). To develop the sensitivity and selectivity CNT-based devices, the common approach is functionalization the CNT sidewall to modify the chemical activity and enhance their sensitivity to a specific gas.

Recent studies have extended the gas sensing applications to functionalized CNT gas sensors, which include nanoparticle functionalized CNTs as the metal nanoparticles can act as reactive sites to target gas molecules (Zhang et al., 2008), and organic polymer functionalized CNTs by delocalizing bonds to increase conductivity (Janata and Josowicz, 2003). For example, elemental Pd and Pt are catalysts with high H_2 diffusivity and solubility, thus, they are widely applied in hydrogen-related sensors. Randeniya and co-workers used Pd/MWCNTs and Pt-Pd/MWCNTs composites for the H_2 detection with a concentration range of 20 ppm - 2% in N_2 and 200 ppm - 2% in air (Randeniya et al., 2012). Pd nanoparticle is applied to CNTs to reduce the hole-carrier concentration by forming a Schottky contact localizing the depletion region which results in enhancing the response of the Pd-CNTs sensor for NO_2 gases (Yun et al., 2009). Pd nanoparticles can also be applied to CNTs sensors in detecting organic matters. Lu and co-workers developed a chemiresistive sensor for CH_4 detection using Pd-CNTs drop-coasted on interdigitated electrodes (Lu et al., 2004). The fabricated sensors are able to detect low CH_4 concentrations (6-100 ppm). The same group further produced a gas sensor array composted of 32 sensing elements with pristine, metal-doped and polymer coated SWNTs for sensing discriminated gases such as NO_2, acetone, HCN, and benzene at ppm concentration levels (Lu et al., 2006). Lu and co-workers also used Rh/SWCNTs for the detection of formaldehyde (HCOH) at room temperature. The sensors presented the estimated detection limit of 10 ppb with very quick response (~18 sec) and recovery time of ca. 1 min (Lu et al., 2011).

Chapter 3

Methodology: Synthesis and characterization of CNTs

The synthesis of carbon nanotubes by thermal CVD and floating catalyst CVD, the purification and functionalization of carbon nanotubes, the preparation of carbon nanotube buckypaper were explained. The characterization of the synthesized materials were also described in this chapter.

3.1 Substrate preparation

Silicon wafer was used as support substrate in CNTs growth. Before the CNTs can be grown on a substrate using thermal CVD system, a thin film needs to be formed on the substrate to form nanoparticles. However, Cobalt (Co), iron (Fe) and nickel (Ni) can diffuse into silicon at high temperatures. Minimal nanotube growth occurred when acetylene reacted with Ni catalyst deposited directly on a clean silicon substrate at $700^{o}C$ because Ni diffused into the substrate and form $NiSi_x$ at temperature above $450^{o}C$ (Sze, 1988). Thermally oxidization of silicon wafer prior to the catalysis deposition is expected to help achieve high yield and uniform growth of carbon nanotube on the substrate.
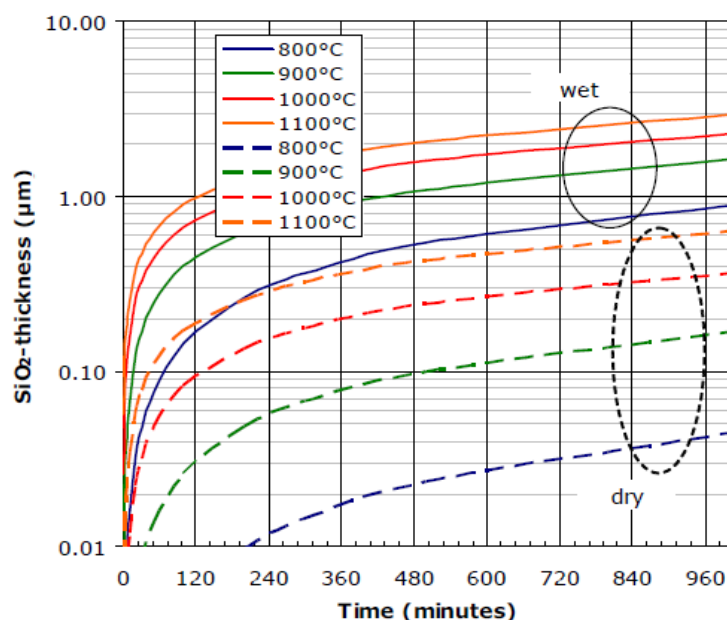
Figure 3.1 The attained SiO_2 film thickness as a function of time and temperature.

In this study, the substrate preparation consisted of two processes namely thermal oxidation of silicon substrate and catalyst deposition on the substrate. The procedure is shown in **Figure 3.2**
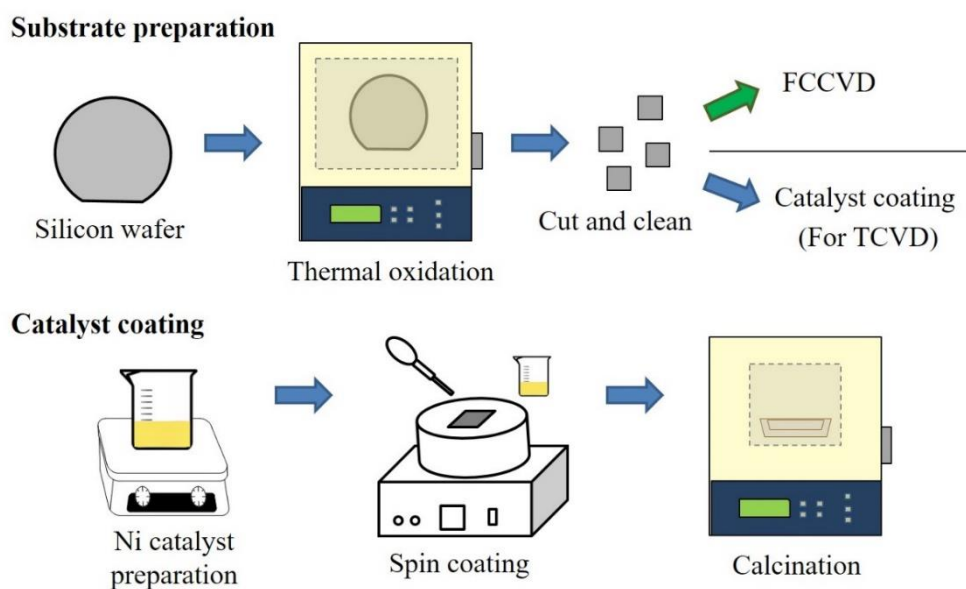
Figure 3.2 Flow diagram of substrate preparation

3.1.1 Thermal oxidation of silicon substrate

Silicon wafer was thermally oxidized at 900°C in air for 6 hours. It was expected to form approximately 80 nm-thick SiO_2 layer on the surface (**Figure 3.1**). This thin insulating layer of SiO_2 acts as a diffusion barrier which can prevent the diffusion of catalyst into the silicon substrate. (Rao et al., 2000, Teo et al., 2002). The oxidized wafer was cut into small square pieces in the size of 3×3 cm^2 and cleaned with acetone (3 min), methanol (3 min) and DI water (3 min) in ultrasonic bath, and then N_2 blow-dry (**Figure 3.3**). These substrates were subject to catalyst deposition before CNTs growth by thermal CVD process.
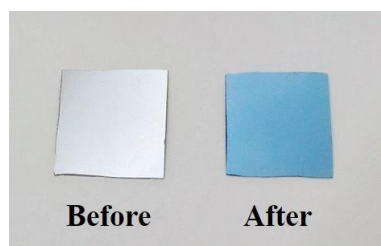
Figure 3.3 Silicon substrate before and after thermal oxidation at 900°C

3.1.2 Catalyst deposition on silicon substrate

The use of spin coating is a promising process due to its simplicity and cost effectiveness. Nickel catalyst was prepared by dissolving nickel chloride ($NiCl_2$) in ethanol water by magnetically stirred at $60^{o}C$. Triton X-100 was then added into the solution and kept stirring for 3 hours to achieve good dispersion. Then Ni catalyst was deposited onto Si substrate in a form of thin film by spin coating technique. Silicon substrate was fixed on the spin head of the spin coating machine by vacuum suction (**Figure 3.4**). Two milliliters of the prepared Ni catalyst mixture was dropped on the Si substrate. Then the substrate was spun at different revolution speeds (1500-5000 rpm) for 1 min. Finally, the Ni coated Si wafer was calcined at $550^{o}C$ in air for 4 h with the heating rate of $5^{o}C/min$ to form NiO nanoparticles.

Figure 3.4 Spin coating machine **Inset:** spin head

3.2 Carbon nanotube synthesis

Chemical vapor deposition (CVD) system was used for the growth of CNTs. The system includes a set of concentric quartz tubes (inner diameter: 35 mm, length: 120 cm) that was placed horizontally in a tubular furnace (Olink OT-T040, maximum temperature $1200^{o}C$), and a set of chiller. The mass flow meters rated with 2×300 sccm (Olink FCSA300C, calibrated with H_2 and CH_4) and 1×1000 sccm (Olink FCSA1000C, calibrated with Ar) linked to multichannel gas flow controller units (Olink GC400) were used to control the flow of hydrogen, argon and methane individually (**Figure 3.5**).
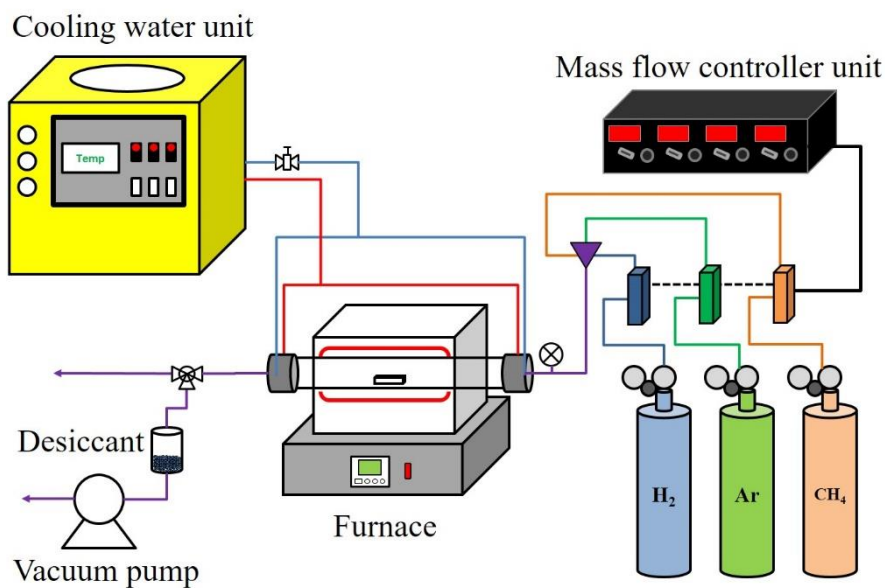
Figure 3.5 Schematic diagram of CVD system

3.2.1 Thermal CVD (TCVD) method

Nickel catalyst coated silicon substrates were placed at the middle of the quartz tube in the furnace. First, oxygen and moisture were eliminated from the reactor by vacuum suction for 5 min. The vacuum suction pressure was fixed at 1 atm. The cooling system was maintained at 15°C to protect the vacuum sealing part of CVD throughout the CNT growth process. After that, Ar was then fed into the reactor at a flow rate of 200 sccm (standard cubic centimeters per minute) until the pressure gauge returned to 0 and kept feeding for 5 min before starting CNT growth to ensure the absence of O_2 in the system. The system was heated up to 800°C at a rate of 5°C/min. At the same time, hydrogen gas was fed into the system at a flow rate of 100 sccm with a constant Ar flow rate. At temperature of 500°C, Ar was switched off and the flow rate of H_2 was increased to 200 sccm until the temperature reached 800°C.

Hydrogen acted as a reducing gas which activate Ni catalyst before CNT growth by reducing NiO to metallic Ni catalyst particles at temperature above 450°C (Manukyan et al., 2015). When the temperature reached 800°C, CH_4 was introduced into the system with a flow rate of 100 sccm to initiate CNT growth. The temperature was held at 800°C for 30 minutes which was the reaction time for CNTs growth. After that, CH_4 and H_2 feeds were switched off and system was cooled down to room

temperature under Ar atmosphere to prevent oxidation at high temperature. The samples were collected and kept in a desiccator until use. The temporal diagram of TCVD is shown in **Figure 3.6**.

Figure 3.6 The temporal diagram of TCVD CNT growth processes

Table 3.1 TCVD parameters corresponding to the processes in **Figure 3.6**

Step	Duration (min)	Gas composition	Flow rate (sccm)
(1)	5	Ar	200
(2)	95	Ar	100
		H_2	100
(3)	60	H_2	200
(4)	30	H_2	200
		CH_4	100
(5)	Cool down	Ar	200

3.2.2 Floating catalyst CVD (FCCVD) method

Compared with other CVD method, FCCVD avoid extra time consumed for catalyst preparation (Khavarian et al., 2009). In this research, CNT production by FCCVD was carried out with the same system as thermal CVD which is described in the previous section. In contrast, a heating zone at the entrance of the reactor was added. The FCCVD system consisted of two zones. The first zone was wrapped with a heating tape to control the temperature of 200°C for vaporizing catalyst and then the catalyst vapor was carried into the second zone (reaction zone) operating at 800°C (**Figure 3.6**). Lim and co-workers reported that temperature of 800°C and 850°C are suitable for CNTs growth by FCCVD. However, bigger diameter CNTs were produced with the temperature of 850°C (Lim et al., 2012). Ferrocene was used as a catalyst precursor for CNT growth.
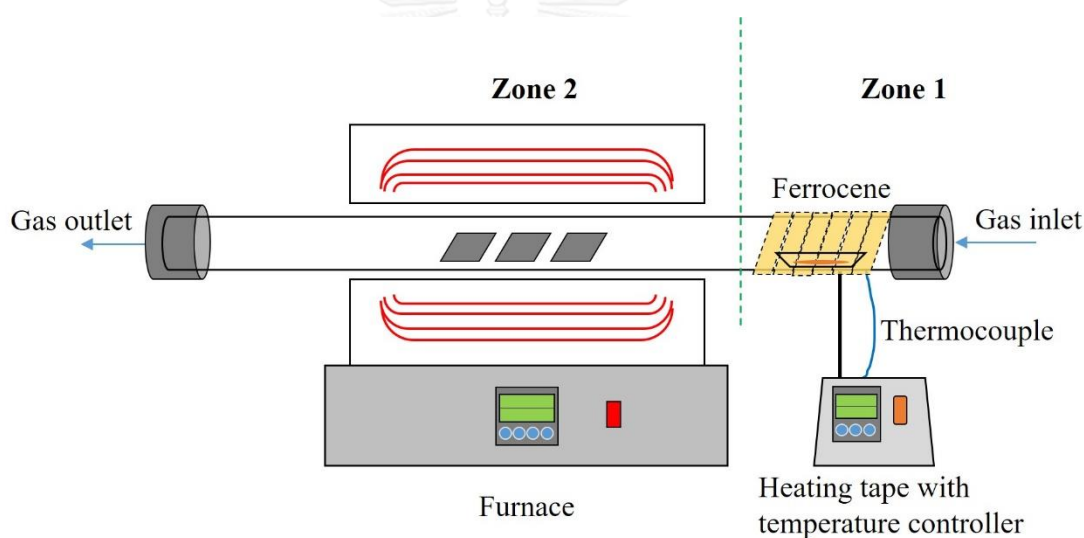
Figure 3.7 Schematic diagram of FCCVD system

Cleaned Si substrates were inserted at the reaction zone. Prior to CNT growth, the system was vacuumed to removed moisture and oxygen and Ar was fed into the system at a flow rate of 150 sccm for 10 min. Then the second stage was heated to 800°C with 20°C/min temperature ramp. At the same time hydrogen gas was introduced into the system at a flow rate of 50 sccm with a constant Ar flow rate. Ferrocene was vaporized at 200°C and then the ferrocene vapor was carried into the reaction zone by an Ar-H_2 gas flow with a total flow rate of 200 sccm. When the temperature of the reaction zone reached 800°C, methane was fed into the system with a flow rate of 50 sccm. The temperature

was held at 800°C for 30 min as well as CH$_4$ feed. After that, CH$_4$ and H$_2$ feeds were switched off and system was cooled down to room temperature under Ar atmosphere to prevent oxidation. The CNTs grown on Si substrates as well as the CNTs grown on the wall of the quartz tube were collected and kept in a desiccator. The temporal diagram of FCCVD is shown in **Figure 3.8**.
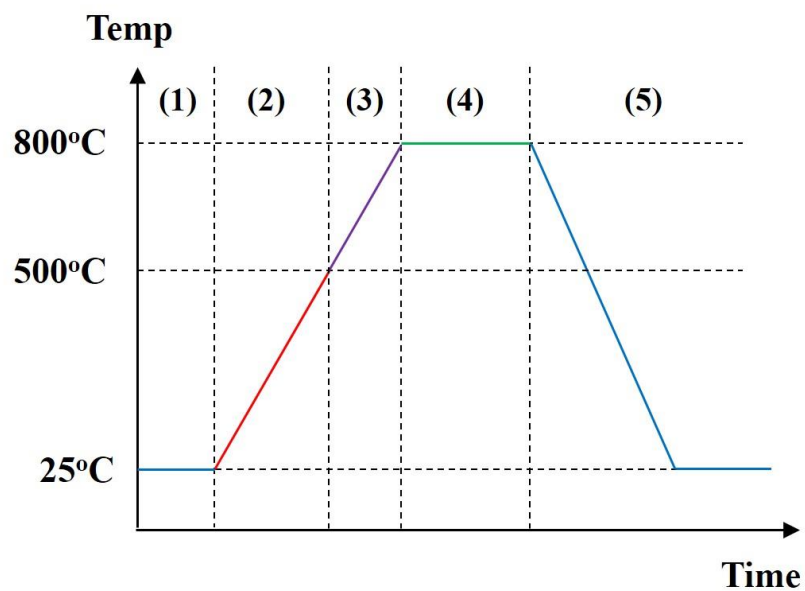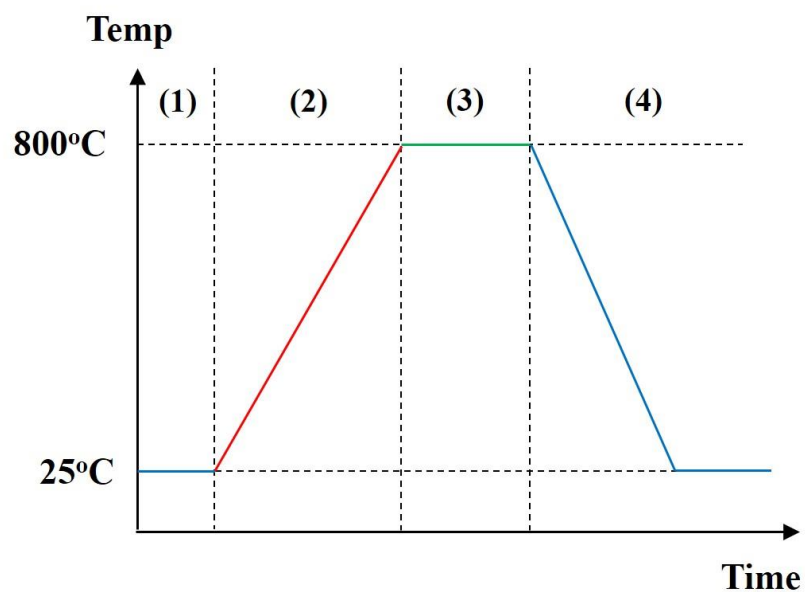

Figure 3.8 The temporal diagram of FCCVD CNT growth processes

Table 3.2 FCCVD parameters corresponding to the processes in **Figure 3.8**

Step	Duration (min)	Gas composition	Flow rate (sccm)
(1)	5	Ar	200
(2)	39	Ar	150
		H$_2$	50
(3)	30	Ar	150
		H$_2$	50
		CH$_4$	50
(4)	Cool down	Ar	200

3.3 Purification and functionalization of CNTs

3.3.1 Purification

The synthesized CNTs were purified with 5N hydrochloric acid (HCl) at 80°C for 1 h to remove iron nanoparticles. The samples were subsequently washed with distilled water to eliminate the acid. The samples were dried in an oven at 100°C. The acid-purified CNTs were then oxidized at 350°C for 4 h in air to remove amorphous carbon.

3.3.2 Preparation of acid-functionalized CNTs (CNTs-COOH)

Five hundred mg of CNTs were added into a flask containing 120 ml of 69% Nitric acid (HNO$_3$) and 95% Sulfuric acid (H$_2$SO$_4$) mixture. The (HNO$_3$/H$_2$SO$_4$) acid mixture was in the ratio of 1:3 by volume. The CNTs were refluxed in the acid mixture at 70°C for 12 h to attach carboxylic functional group (COOH) on the surface of the CNTs (**Figure 3.9**). Then the acid functionalized CNTs were filtered through a 0.45 µm pore-sized PVDF membrane and washed with DI water repeatedly until the pH reached neutral. The functionalized CNTs were dried in a vacuum oven at 60°C for 12 h.
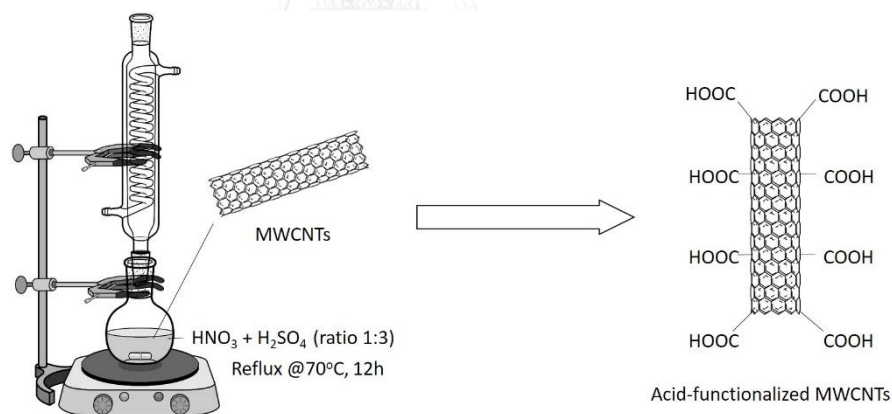
Figure 3.9 Acid functionalization of CNTs

3.4 CNT buckypaper preparation

Fifty mg of functionalized CNTs were dispersed in 150 ml deionized water using 30 W ultrasonic for 15 min. Then 1 ml of a surfactant (Triton X-100), and 100 ml DI water was added into the above suspension of CNTs. Triton X-100 is one of the most commonly used surfactants and is known to effectively disperse carbon nanotubes (Fatemi and Foroutan, 2015). The mixture was further sonicated at 30 W for 15 min. The suspension of well-dispersed CNTs was filtered by a vacuum pump through a 0.45 μm Durapore PVDF membrane filter. The filter was placed in air at room temperature for 1 h and then dried in a vacuum oven at 60°C for 3 h. The CNT buckypaper was peeled off from the filter and kept in a desiccator until application (**Figure 3.10**).

Figure 3.10 CNT Buckypaper preparation via vacuum filtration

3.5 Characterization of CNTs

The physical and chemical properties of the synthesized materials were characterized by various instruments such as SEM, TEM, TG/DTA, FTIR and Raman.

3.5.1 Microscopic examinations

The surface morphology of CNTs was observed by a field-emission scanning electron microscope (FESEM) (JOEL, JSM 7000F, Japan). The samples were placed in sample holder and sputtered with platinum (Pt) prior to SEM imaging. Sputter coating prevents charging of the sample occurred from the accumulation of electrostatic fields and also improve the signal to noise ratio.

High-resolution transmission electron microscope (HRTEM) (JOEL, JEM-2100, Japan) operating at 80 kV was used to observe the interior structure of the CNTs. The CNTs sample was suspended in isopropyl alcohol by ultrasonic to ensure separation of particles. The suspension of CNTs in isopropyl alcohol was dropped on a copper grid with carbon film. The sample was thoroughly dried before TEM imaging.

3.5.2 Thermal Gravimetric and Differential Thermal Analysis (TG/DTA)

The thermal stability and weight loss of the CNTs were analyzed by SII Exstar TG/DTA 6000 (Japan). The sample with known weight was loaded on a platinum pan, equipped inside the instrument. The flow rate of air through the pan during the experiment was 20 ml/min. The temperature was raised from 25 to 800°C with a heating rate of 5°C/min and the mass loss was recorded as a function of temperature.

3.5.3 Raman spectroscopy

Raman spectroscopy was used to investigate graphitic structures and structural defects of the CNTs. The measurement was carried out using NT-MDT, NTEGRA SPECTRA (Germany). The samples were excited with 514 nm (green) Ar ion laser. The Raman spectra were recorded in the range of 2000 to 1000 cm^{-1} with a scanning rate of 50 cm^{-1}/min.

3.5.4 Fourier-transform infrared spectroscopy (FTIR)

FTIR spectroscopy was used to identify surface functional groups of the CNTs. The sample were analyzed by potassium bromide (KBr) pellet method. To prepare a pellet, small amount of powder sample was added into a mortar containing KBr powder, mixed and crushed to a fine powder. The amount of the sample in KBr should be in the range of 0.2 to 1% since too high concentration of sample usually causes difficulties in obtaining clear pellets. The finely ground mixture was pressed in a 10 ton hydraulic press to make a KBr pellet, The characterization was performed using Jasco FT/IR-4100 (Japan) with a scanning range between 1000 and 4000 cm^{-1} at a rate of 10 cm^{-1}/s.

Chapter 4

Results and discussion: Synthesis and characterization of CNTs

4.1 Carbon nanotube synthesis

4.1.1 Thermal CVD

After spin coating with the catalyst, the wafer was annealed at 550°C in air for 4 h. This annealing step at over 500°C was carried out to decompose the deposited nickel salt and form NiO nanoparticles (Chang et al., 2004, Rahdar et al., 2015). The surface of the prepared Ni-coated silicon wafer was examined by SEM and are shown in **Figure 4.1 (a)** and **(b)**. It can be observed that catalyst particles were distributed thoroughly on silicon wafer surface. However, Ni catalyst appeared to connect together in a form of cluster rather than individual particles. This was due to the excess thickness of the Ni catalyst film in spin coating process.
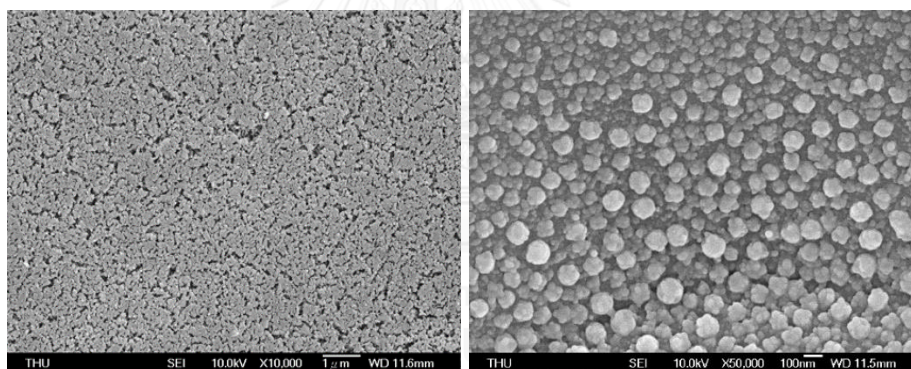
Figure 4.1 SEM images of Ni catalyst coated on silicon wafer after calcination **(a)** 10000x and **(b)** 50000x magnification

The thickness of films are proportional inversely to the rotational speed. The rotational speed of spin coating was varied between 1500, 3000, 4000 and 5000 rpm to study the effect on CNT growth. The SEM images of the grown CNTs on Ni catalyst spin-coated on Si wafer at different rotational speeds are shown in **Figure 4.2**. The results show that at 1500 rpm the Ni catalyst film was too thick due to slow spin speed. This resulted in the formation of particle groups sticking together after calcination. There was almost none of nanotube growth. It can be found that CNTs could not grow well on large catalyst particles. When the spin speed increased to 3000, 4000 and 5000 rpm, CNTs were observed

to grow better. The increase in density of CNTs grown on Si wafer was found with increasing spin speed as higher rotational speed can create smaller catalyst dots which effectively catalyze CNTs growth.

1500 rpm

3000 rpm
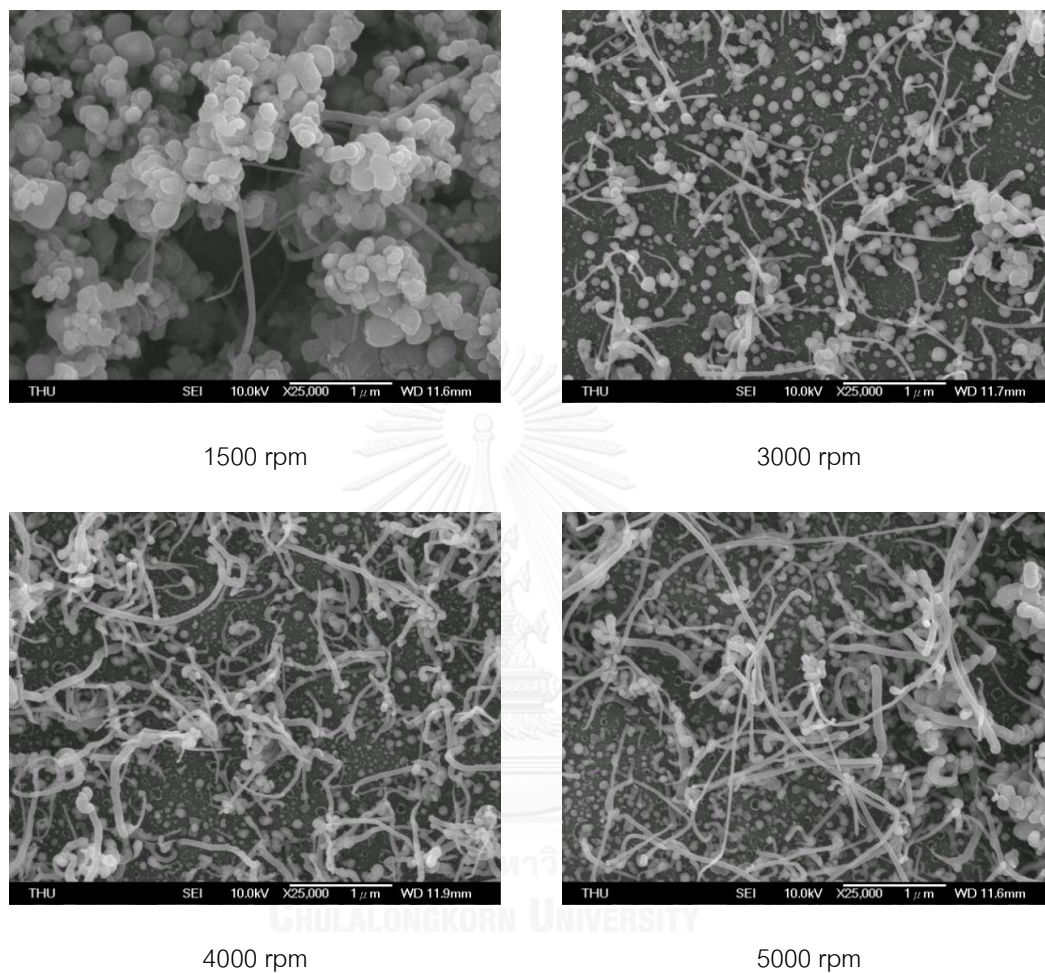
4000 rpm

5000 rpm

Figure 4.2 SEM images of CNTs grown on Ni coated silicon wafer at different rotational speed (1500, 3000, 4000 and 5000 rpm)

The results showed that although Thermal CVD could grow CNTs on the substrate using Ni as a catalyst, the yield of the CNT growth and the density were relatively low. Moreover, difference in nanotubes' size could be observed. The results suggested that, in this study, Thermal CVD process may not be suitable for producing a highly uniform and satisfactory quality CNTs for further use in adsorption and gas sensor applications.

4.1.2 Floating catalyst CVD

Methane (CH_4) flow rates were varied (25, 50, 100 and 150 sccm, accounted to CH_4-H_2 ratio of 0.5, 1, 2 and 3) to study its effect on the yield of CNTs. The parameters were set as follows:

- Ferrocene 150 mg

- Argon flow rate 150 sccm

- Hydrogen flow rate 50 sccm

- Reaction temperature 800°C

- Reaction time of 30 min
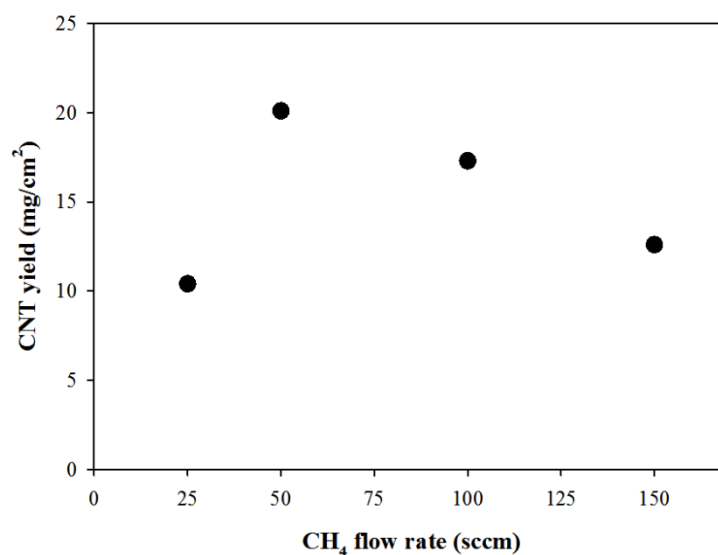
Figure 4.3 Effect of CH_4 flow rate on CNT yield

TGA analysis was performed to determine the yield of CNTs growth with different CH4 flow rates by FCCVD and is shown in **Figure 4.3**. The results showed that CNTs grown on a silicon substrate significantly increased when increased CH_4 flow rate from 25 to 50 sccm. The yield of CNTs increased almost twice (10.4 to 20.1 mg/cm^2). However, the CNT growth appeared to decrease when CH_4 flow rate exceeded 50 sccm (CH_4-H_2 ratio 1:1). This may be caused by the high CH_4 content decomposed to excessive amount of C atoms and coated around the catalysts. In addition, H_2 gas is required to activate catalyst, CNTs did not grow well due to inactive catalyst by insufficient H_2 gas. The results showed that the optimum CH_4 flow rate for CNT growth by FCCVD was 50 sccm with the yield of 20.1 mg/cm^2.

In the study, 50 sccm of CH_4 flow rate was used to synthesize CNTs. The other parameters were described earlier in **Chapter 3**. The as-synthesized CNTs on Si substrate by FCCVD method is shown in **Figure 4.4**.
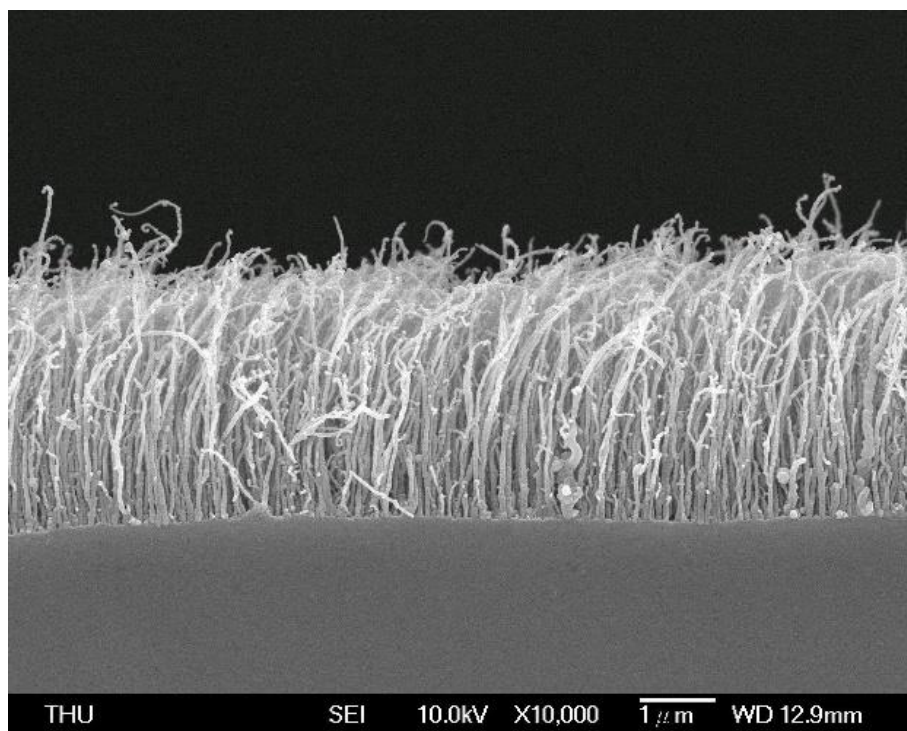
Figure 4.4 Cross-section SEM image of the synthesized CNTs via FCCVD

The result reveals a high density of CNTs growth in a forest-like form and vertically aligned to the substrate surface. The high density of the carbon nanotubes confirms the high catalytic activity of the iron catalyst in the growth process. The as-grown CNTs had a diameter range of 20 - 50 nm and a length range of 3 - 5 μm. In addition to the bundle of CNTs, white spots which are carbonaceous particles, mainly amorphous carbons, and the metal catalyst (Fe) particles on the surfaces of the CNTs were also observed on the top of the synthesized nanotubes **(Figure 4.5)**. These impurities were eliminated by acid treatment and thermal oxidation.
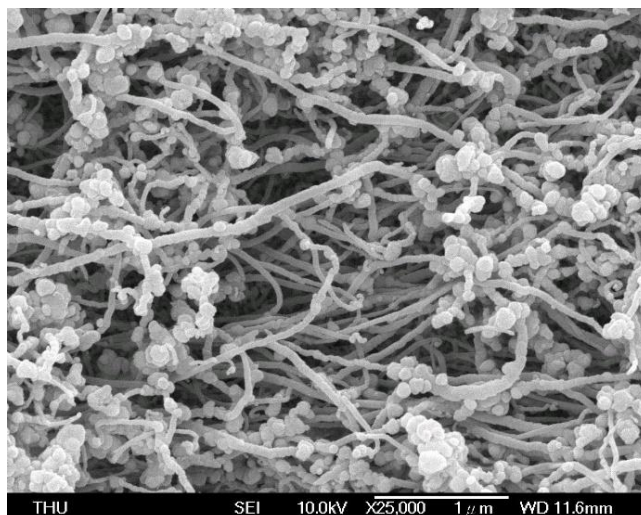
Figure 4.5 SEM image of the synthesized CNTs via FCCVD

HRTEM examination verified the tubular structure of the as-grown MWCNTs possessing 16 walls and the inter-wall spacing around 0.18 nm (**Figure 4.7**). The inter-wall spacing is not large enough for phenol molecules (0.46 nm) and other CPCs with greater molecular sizes to access (Lorenc-Grabowska, 2016). The results suggested that only the inner cavity and the external nanotube surface are available for CPCs adsorption on the synthesized MWCNTs (Yang and Xing, 2007).
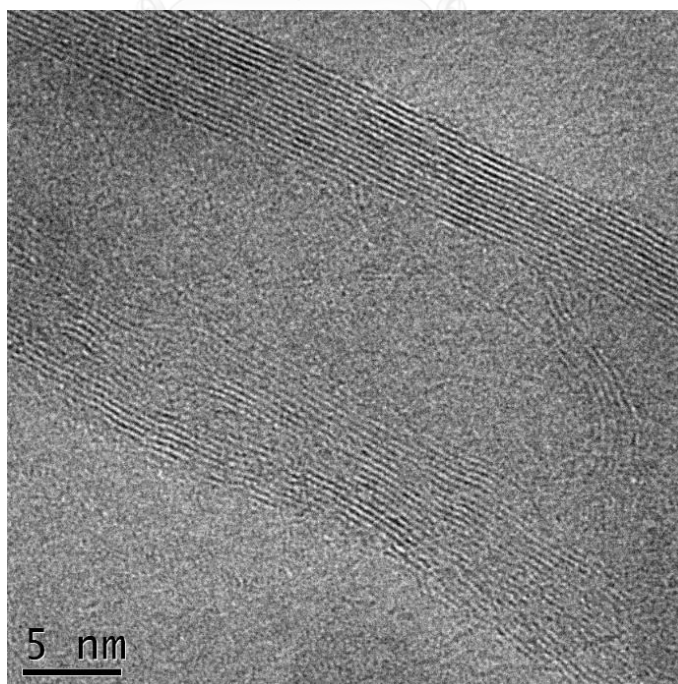
Figure 4.6 HR-TEM image of as-synthesized MWCNT.

4.2 Purification of carbon nanotubes

The as-synthesized CNTs was purified by HCl acid and followed by thermal oxidation to remove the amorphous carbons and residual metal catalyst particles. The SEM images of the CNTs before and after purification processes are shown in **Figure 4.7 (a)** and **(b)**. Clusters of metal catalyst particles were observed in the as-synthesized CNTs while very clean nanotubes were observed in the acid-purified CNTs. It can be clearly seen that metal particles resided on the CNTs were effectively removed by acid-treatment.
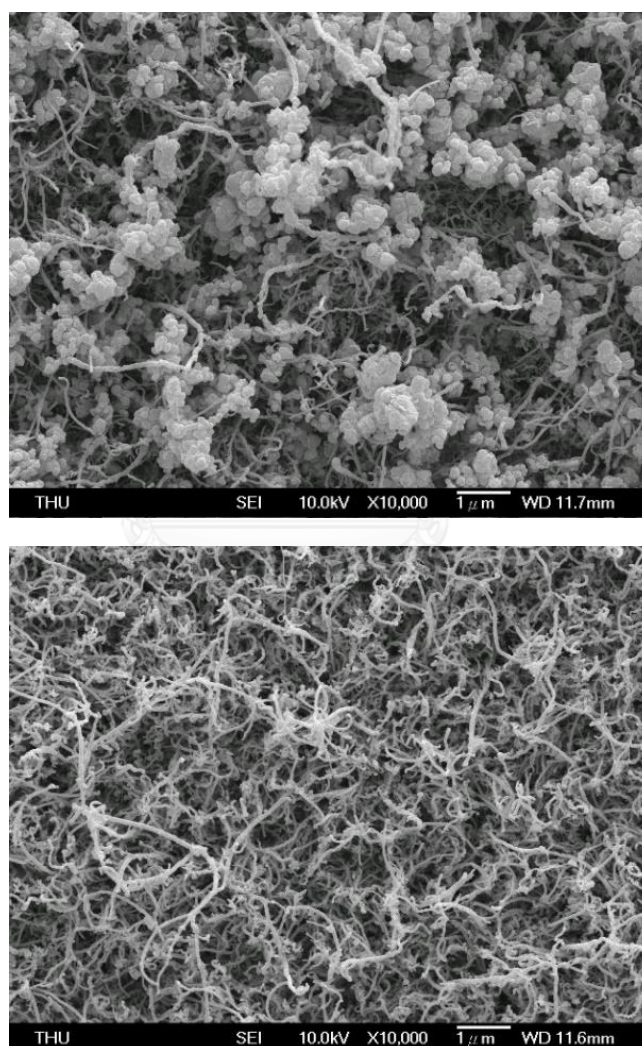
Figure 4.7 SEM images of the CNTs (a) before and (b) after purification

Beside the visual observation, the thermogravimetric analysis was carried out. TGA revealed the weight loss of the materials under air atmosphere was recorded from $30^{\circ}C$ to $800^{\circ}C$ with a heating temperature of $5^{\circ}C/min$. The weight loss was due to the combustion of carbon atoms in the sample by O_2. **Figure 4.8** shows TGA profiles of as-synthesized and acid-purified CNTs. The TGA profiles showed similar patterns as both CNT samples are thermally stable up to $550^{\circ}C$. However, the onset temperature of the acid-purified CNTs combustion was slightly lower than that of as-synthesized CNTs. This might be due to the more oxygenated groups on the purified CNT surface which were generated during the acid treatment process (Titus et al., 2006). These oxygenated groups were more reactive to oxygen, resulting in combustion at lower temperature. There was no weight loss after $650^{\circ}C$. The as-synthesized CNTs contained residual metal particles around 7% while the amount of residue in the acid-purified CNTs was reduced to less than 1%. These results are in good agreement with SEM results that the resided metal catalyst particles were effectively removed from the CNTs after acid treatment.
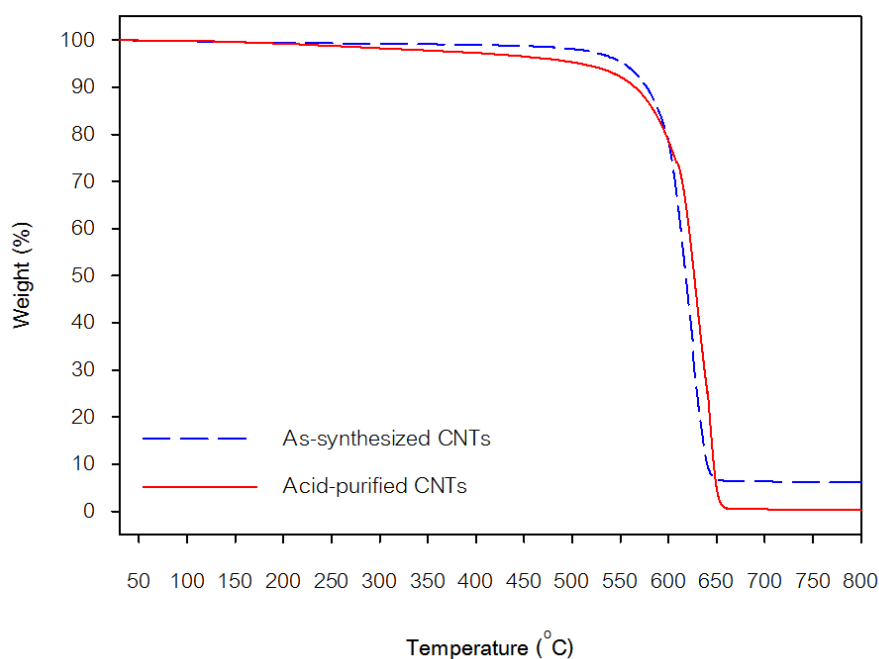
Figure 4.8 TGA profile for as-synthesized and purified CNTs

4.3 Acid functionalization of carbon nanotubes

FTIR was employed to characterize the functional groups sited on CNTs. **Figure 4.9** shows the FTIR spectra of the as-synthesized CNT and the acid-functionalized CNTs.
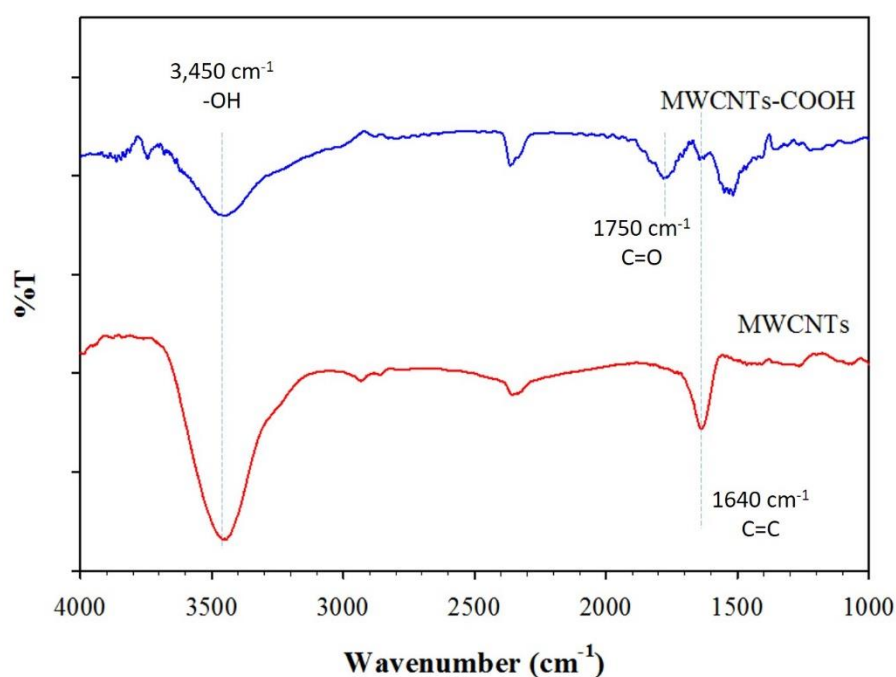
Figure 4.9 FTIR spectra of as-synthesized and acid-functionalized CNTs.

FTIR spectra from the both samples showed a CNT backbone (C=C) peak at around 1640 cm^{-1}. Broad peak around 3450 cm^{-1} in both spectra corresponded to –O–H groups of adsorbed water. Most of the –O–H was assumed to come from water adsorbed in the specimen rather than surface functional groups. Because the remaining trace of water in the KBr pellet could not be totally eliminated even heating in oven before the measurement had been done. A C=O stretching vibration of carbonyl and carboxyl groups can be seen around 1750 cm^{-1} for the acid-functionalized CNTs, indicating the formation of carboxylic groups due to the oxidation of some carbon atoms on the surface of CNTs. Chen and co-workers suggested that the band at around 1540 cm^{-1} observed in the acid-functionalized CNTs is also related to carboxyl groups (Chen et al., 2005). The results indicated that the CNTs were successfully functionalized by sulfuric and nitric acid mixture (Buang et al., 2012, Turgunov et al., 2014).

Theoretically, the oxygen-containing functional groups attached on the surface of CNTs help decrease the aggregation of CNT bundles, which was in good agreement with SEM results, hence the availability of adsorption sites will increase (Pan and Xing, 2008). Moreover, the COOH polar groups attached onto the CNTs surface enhance the adsorption efficiency between the polar organic molecules and the COOH on the CNTs due to the dipole-dipole interactions (Sin et al., 2006). The sensors are believed to give better responses toward volatile organic molecules.
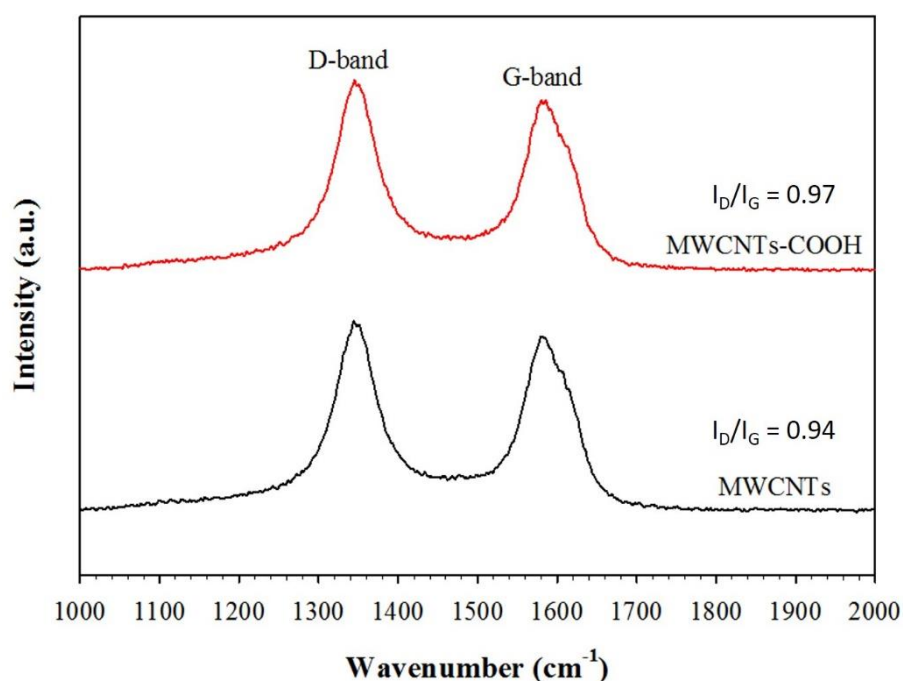
Figure 4.10 Raman spectra of as-synthesized and acid-functionalized CNTs.

Raman spectroscopy was used to examine the graphitic structure and structural defects in the CNT materials. **Figure 4.10** shows the Raman spectra from 1000-2000 cm^{-1} of the as-synthesized CNTs via FCCVD and the acid-functionalized CNTs. The Raman spectra contain two domains in the range. The first band located at 1345 cm^{-1} is denoted as D band; the presence of imperfection or disorder in carbon structure. The second band at 1580 cm^{-1} (G band) is assigned to the in-plane vibration of C=C bond with a shoulder at around 1600 cm^{-1}. D band and G band of the spectra confirmed that the synthesized CNTs were structured with multiple layers. The intensity ratio of D- to G-band (I_D/I_G) reflects both purity and the defect density of CNTs.

The spectra of the acid-functionalized CNTs exhibited higher intensity of D-band due to the breaking of sidewall C-C bonds (Zhang and Zhang, 2015) and introduction of the oxygenated functional groups onto the sidewall and the end wall of the nanotubes (Dhall et al., 2013). The I_D/I_G increased from 0.94 to 0.97 after acid functionalization. The crystallite size (L_a) could be determined by the **Equation 4.1** (Cançado et al., 2006).

$$L_a(nm) = (2.4 \times 10^{-10})\lambda_l^4 \left(\frac{I_D}{I_G}\right)^{-1} \qquad (4.1)$$

where λ_l is the wavelength of excitation laser in nanometer units. The equation gives the crystallite size from the integrated intensity ratio I_D/I_G by using any laser line in the visible range.

The calculated crystallite size (L_a) of the acid functionalized CNTs is found to decrease to 17.27 nm as compared to17.82 nm for the as-synthesized CNT. The nanotube defects introduced by the acid treatment lead to the decrease of crystallite size (L_a). The electrical resistivity increases with decreasing structural perfection (Issi and Nysten, 1998).
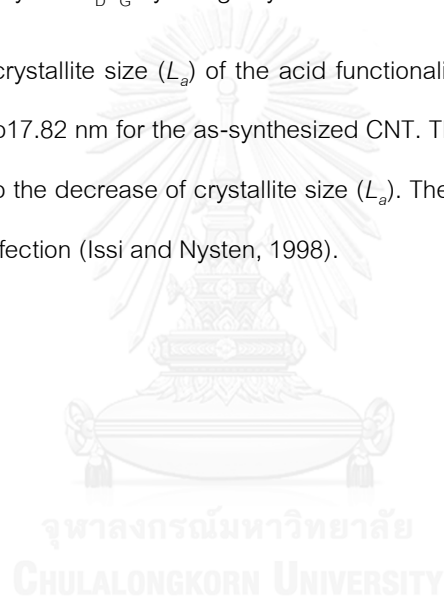
4.4 CNT buckypaper

CNT buckypaper were successfully prepared via vacuum filtration of MWCNT dispersions using Triton X-100 as a surfactant through a PVDF filtration. SEM images of CNT buckypaper and acid-functionalized CNT buckypaper are shown in **Figure 4.11 (a) and (b)**. Acid-functionalized CNTs showed much cleaner and more uniformly distributed surface than that of as-synthesized one, demonstrating that acid treatment helped remove residue and amorphous carbon.
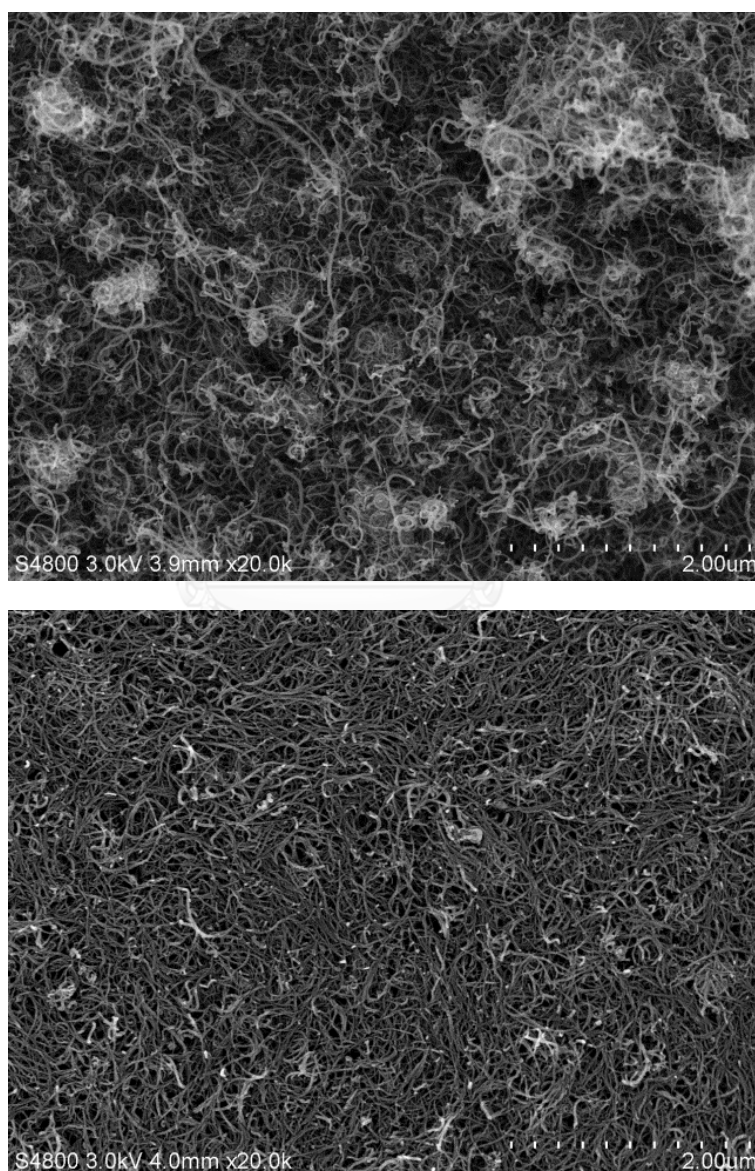
Figure 4.11 SEM images of a) non-modified CNT buckypaper and b) acid-functionalized CNT buckypaper

It can be obviously seen that the acid-functionalized CNTs have a shorter length, slightly smaller diameter. The acid-functionalized CNTs were found to be stable with significantly less aggregation in solution resulting in better CNT distribution in the buckypaper (Jiang et al., 2015). Past research reported that defects on the CNTs induced by acid treatment tend to break carbon-carbon bonds while promoting bonding with carboxyl groups. The treatment leads to a decrease in weight and thickness of CNTs (Saito et al., 2002).

Figure 4.12 shows the SEM images of CNT buckypapers. The buckypaper tend to form a porous network of randomly orientated MWCNTs. It is observed that CNTs mainly lie parallel to the membrane surface resulted from tube self-assembly by Van der Waals force during filtration (Ji et al., 2012). The CNTs were spread and evenly distributed over the network surface, indicating good dispersion of CNTs in the suspension. The **Inset** shows the cross sectional view. The thickness of the buckypaper was about 90-100 μm and weighed 44 mg, and the density of the buckypaper was about 0.82 g/cm^3.
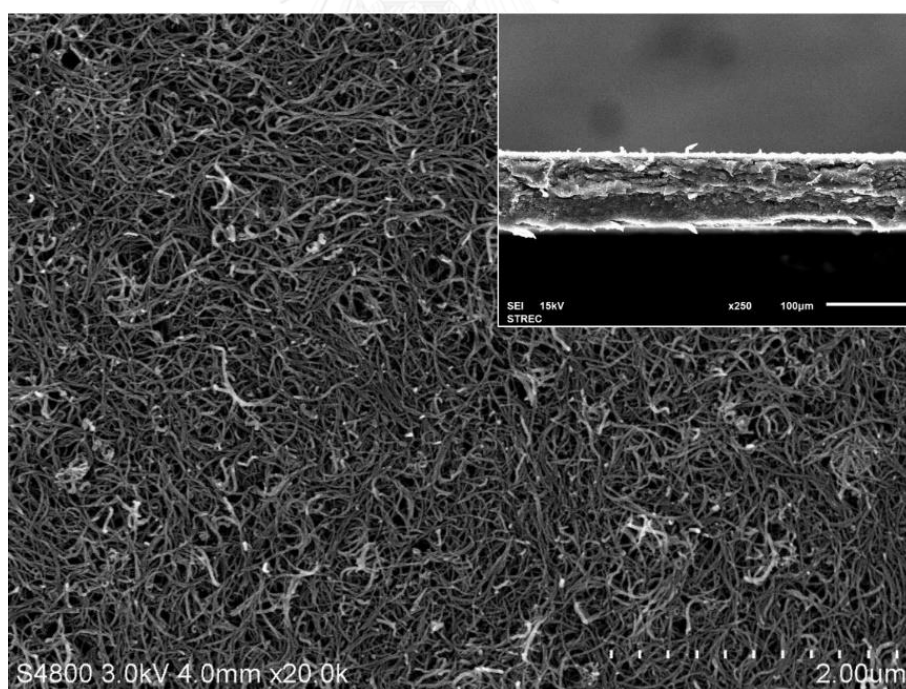
Figure 4.12 SEM image of the acid-functionalized CNT buckypaper **Inset**: Cross sectional view.

The thermal stability of CNT buckypapers were investigated by TGA. The TGA profiles of the non-modified CNT buckypaper and the acid-functionalized CNT buckypaper are shown in **Figure 4.13**. The profiles of both buckypapers were similar and showed two main weight losses at around 300°C and 600°C. The first loss accounted for 10% was due to the decomposition of the residual surfactant and the second loss accounted for 85-90% was due to the decomposition of carbon nanotubes. It can be seen that the CNT buckypapers lost some thermal stability compared to the as-synthesized CNT powder (dotted line in the figure). However, the both CNT buckypapers can withstand temperatures up to 500°C.
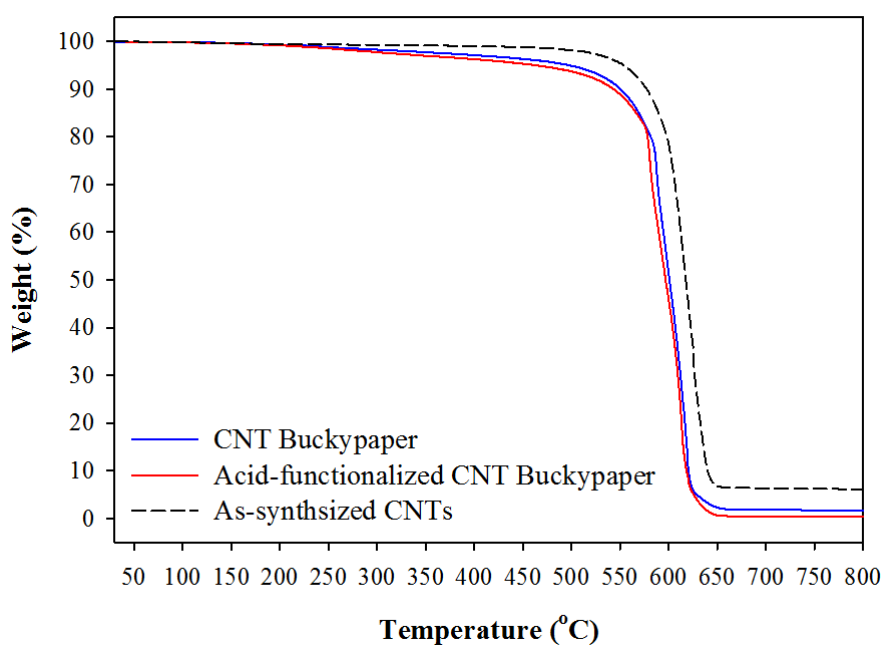
Figure 4.13 TGA profiles for non-modified CNT buckypaper and acid-functionalized CNT buckypaper.

Chapter 5

Methodology: Adsorption and gas sensing studies

This chapter consists of two main parts: Adsorption and Gas sensing studies. The adsorption study includes adsorption isotherms and the adsorption behaviors of chlorinated phenolic compounds on the acid functionalized CNTs adsorbent. For the gas sensing study, the sensing capability of the synthesized CNTs for three chlorinated phenolic compounds procedure were described.

5.1 Adsorption isotherms

Equilibrium isotherms were used to determine the adsorption capacity of acid-functionalized CNTs subject to the exposure to three different phenolic compounds, namely phenol, 2-chlorophenol and 2,4-dichlorophenol. Five mg of the CNTs were placed in a 50 ml glass sampling bottle. Each phenolic compound was injected into the sampling bottles with various controlled amounts to make initial concentration in the range of 1 to 250 ppm (**Figure 5.1**). The adsorption experiments were carried out at 25°C for 72 hours to ensure adsorption equilibrium.
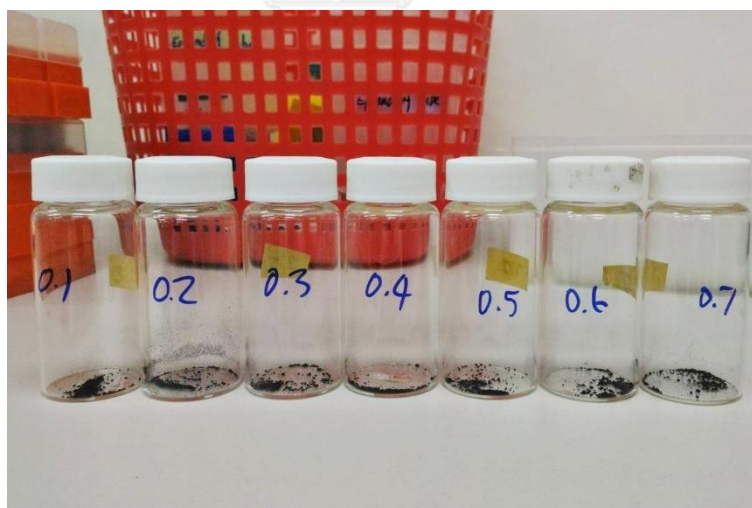
Figure 5.1 CNTs in seven different concentrations of gaseous CPs

The equilibrium adsorbed CNTs were analyzed by thermal gravimetric technique on (TG/DTA, SII Exstar 6000, Japan) to determine the equilibrium adsorption capacity (q_e). The equilibrated gas samples were taken from the sampling bottles and then analyzed by gas chromatography (GC, K07380, Thermo Scientific, USA) coupled with mass spectrometry (MS, Trace DSQ II, Thermo Scientific, USA).

The experiment procedure is illustrated in **Figure 5.2**. Chromatographic analysis was achieved on a TG-5MS capillary column (30 m length, 0.25 mm ID, and 0.25 µm nominal film thickness). Helium was used as the carrier gas at a flow rate of 1 ml/min. The injection temperature was set at 280°C. The temperature of transferring line between GC and MS was maintained at 250°C. The temperature program was set as follows: Injection temperature was initially held at 70°C for 1 min, then ramped to 110°C with a rate of 20°C/min, followed by another ramp to 200°C with 25°C/min heating rate and held for 2 min. The ion source temperature was set at 200°C. The detector of MS was operated in full scan electron ionization mode. The data were obtained in range of m/z 50─400.
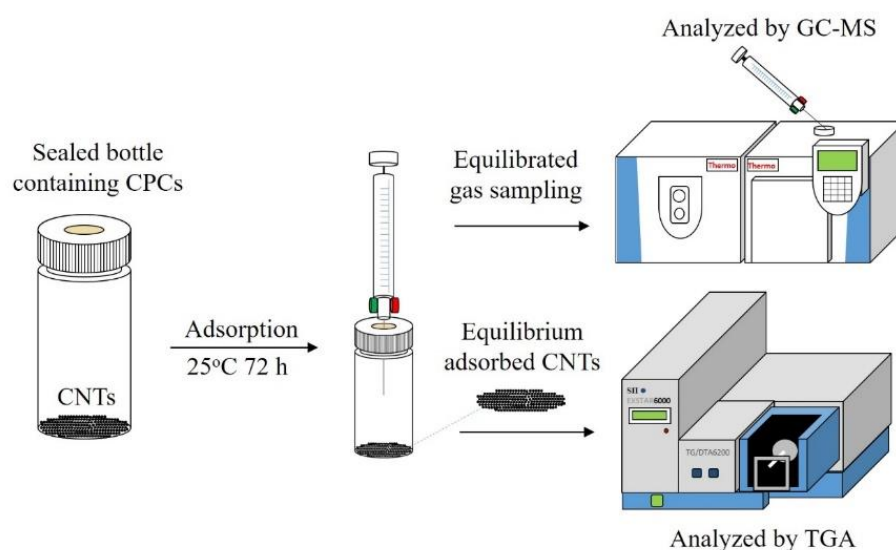
Figure 5.2 Schematic diagram of adsorption isotherm experiment

Three adsorption isotherm models, namely the Langmuir, Freundlich and Redlich-Peterson (R-P) isotherms, were used to fit the experimental data in this work. The adsorption capacities of were estimated from the results fitted by linear equations. In order to determine the best fit isotherm model, the correlation coefficient (r^2) were used to evaluate data.

The Langmuir adsorption isotherm is the most common model used to quantify the amount of adsorbate on an adsorbent as a function of partial pressure (or concentration) at a given temperature. The Langmuir isotherm and its linearized form are expressed as Equation 1 and 2, respectively

$$q_e = \frac{q_m b C_e}{1 + b C_e} \qquad (5.1)$$

$$\frac{1}{q_e} = \frac{1}{bq_m}\frac{1}{C_e} + \frac{1}{q_m} \qquad (5.2)$$

where q_e is the amount of adsorbed adsorbate per unit weight of the adsorbent at equilibrium (mg/g$_{adsorbent}$), C_e is the equilibrium concentration in the gas phase (mg/l), b is a constant (L/mg), and q_m is the maximum adsorption capacity (mg/g$_{adsorbent}$). The constants are determined from the slope and interception of the linear plot of $1/q_e$ versus $1/C_e$.

The Freundlich adsorption isotherm gives an empirical expression representing the isothermal variation of adsorption of a quantity of gas adsorbed by unit mass of solid adsorbent under a constant pressure. It can be expressed through Equation 3 and 4:

$$q_e = K_f C_e^{1/n} \qquad (5.3)$$

The linear form of the Freundlich isotherm can be written as

$$\ln q_e = \ln K_f + \frac{1}{n}\ln C_e \qquad (5.4)$$

where K_f is an indicator of adsorption capacity (mg l$^{1/n}$ /mg$^{1/n}$ g), and n is the intensity of adsorption of the adsorbents. Both values are evaluated from the slope and interception of the plot of ln q_e versus ln C_e.

The Redlich–Peterson isotherm combines elements from both the Langmuir and Freundlich equations incorporating three parameters. The mechanism of adsorption is a hybrid and does not follow ideal monolayer adsorption. It is expressed by parameters, q_{mon}, $\boldsymbol{\alpha}$, and b_{RP}, as shown in Equation 5.

$$q_e = \frac{q_{mon}b_{RP}C_e}{1+b_{RP}C_e^{\alpha}} \qquad (5.5)$$

Rearrangement into its linear form gives (Equation 6)

$$\frac{C_e}{q_e} = \frac{1}{b_{RP}q_{mon}} + \left(\frac{1}{q_{mon}}\right)C_e^{\alpha} \qquad (5.6)$$

The C_e^{α} values were first calculated with Microsoft Excel and then the linear regression line was plotted. The linear plot with the optimum correlation coefficient (r^2) by trial-and-error determination of $\boldsymbol{\alpha}$ values.

5.2 Adsorption behaviors

The adsorption behaviors of phenol, 2-chlorophenol and 2,4-dichlorophenol on the acid-functionalized CNTs were studied by thermal gravimetric analysis. Five mg of the CNTs were placed in a sealed bottle containing saturated pollutant vapor. The adsorption process was kept at constant temperature for 72 h to reach equilibrium. The saturated sorbents were then characterized by thermogravimetric (TG) and differential thermogravimetric (DTG) analyses (TG/DTA, SII Exstar 6000, Japan) (**Figure 5.3**). The sample was heated up from room temperature to 500°C with different heating rates (i.e., 1, 3, 5 and 7°C/min) under N_2 atmosphere. The DTG desorption profiles provided the peak temperatures at each heating rate which were used to calculate the activation energy for desorption (E_d) of the CPCs on the adsorbents.
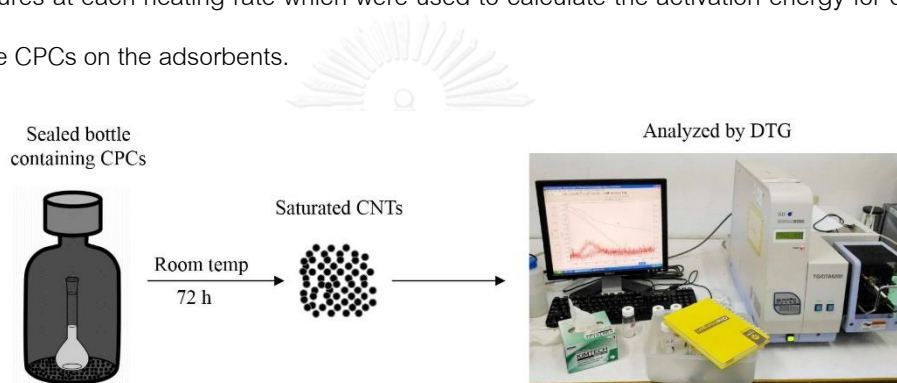
Figure 5.3 Schematic diagram of adsorption behavior study

In general, desorption processes follow a first-order kinetics with respect to the adsorbed species, as expressed in the equation $d\theta/dt = k_d\theta$, where the parameter θ is the surface coverage and k_d is the desorption rate constant. According to the Arrhenius equation, $k_d = A \exp(E_d/RT)$, k_d is a function of temperature. When the temperature profile is a linear function of time and heating rate, the first-order equation may be integrated as described in Equation 7.

$$\int_{\theta_0}^{\theta_t} -\frac{d\theta}{\theta} = \frac{A}{B}\int_{T_0}^{T_t} exp\left(-\frac{E_d}{RT}\right) dT \qquad (5.7)$$

Equation 7 may be integrated and expressed as a linear function in Equation 8. E_d was obtained from the slope of the plot of $2\ln T_m$ - ln B versus $1000/T_m$.

$$2\ln T_m - \ln B = \frac{E_d}{RT_m} + \frac{E_d}{AR} \qquad (5.8)$$

where A is the pre-exponential factor, B is the heating rate ($^{\circ}$C/min), and θ_0 and θ_t are the surface coverage at time t = 0 and t, respectively. R is the gas constant (kJ/mol K), T is the temperature (K), and E_d is the activation energy for desorption (kJ/mol). The maximum desorption temperatures (T_m) were obtained from the thermogram at different heating rates and used to determine the activation energy for desorption (E_d) for each adsorbate.

5.3 Gas sensing study

5.3.1 Gaseous chlorinated phenol preparation

The saturator unit consisted of a series of three saturators submerged in the water inside the refrigeration unit. N_2 gas was used as carrier and diluting gas (**Figure 5.4**). The first saturator contained target chemicals and was connected to the second saturator filled with glass beads for helping gas dispersion. The third saturator was a blank saturator used for mixing the evaporated CPs and N_2. The different concentrations of CPs were prepared by adjusting the N_2 flow rate and water temperature to control the amount of phenolic compounds and then measured by GC-MS as described earlier. The calibration curve of the CPs are shown in **Figure A1**. When the concentration of CPs became stable, the gas was filled into a 3-Liter Tedlar bag for gas sensing application.
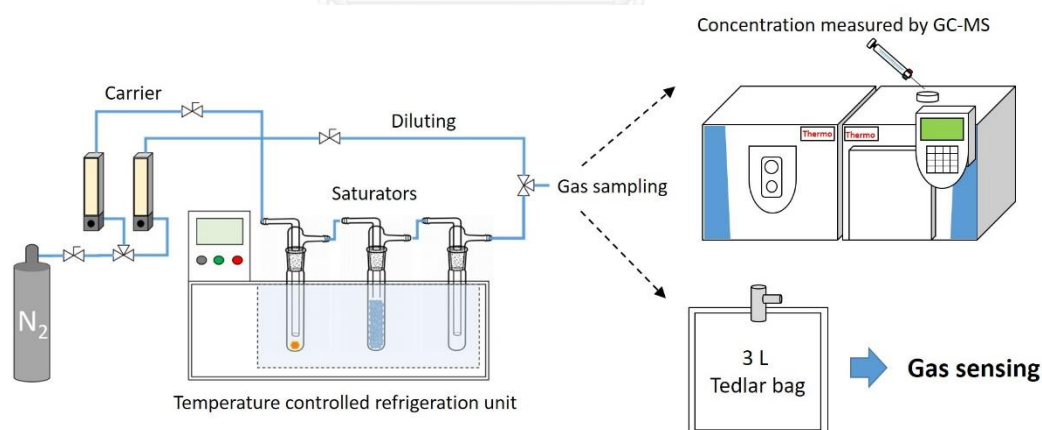
Figure 5.4 Schematic diagram of gas saturator unit

5.3.2 Gas sensing system setup

An airtight glass chamber (0.1 L in volume) **(Figure 5.5)** was equipped with electrical feedthrough. The four-point probe **(Figure 5.6)** was mounted on the top of the sample to make electrical contacts and the wires were connected to a Keithley's Series 2400 SourceMeter Source Measure Unit (SMU) used to supply voltage and monitor the values of resistance **(Figure 5.7)**. High-purity air was used as the background and purge gas. The flow rate of the gases were controlled by a PC-540 multi-channel flow controller (MFC) readout power supply (PROTEC Instruments, U.S.A.) equipped with 2×500 sccm (standard cubic centrimeter per minute) mass flow controllers (Sierra Instruments). The SMU was connected to the computer via the USB interface and the data were acquired using National Instrument LabVIEW version 2013 program.
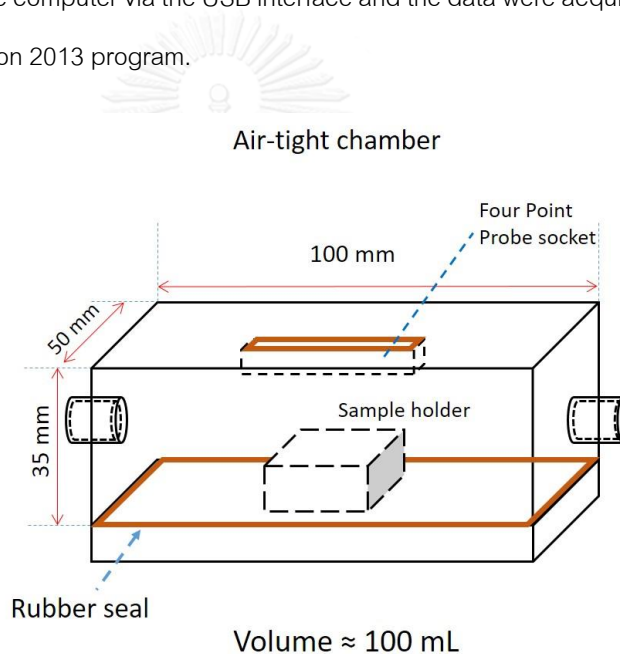
Figure 5.5 Airtight glass chamber
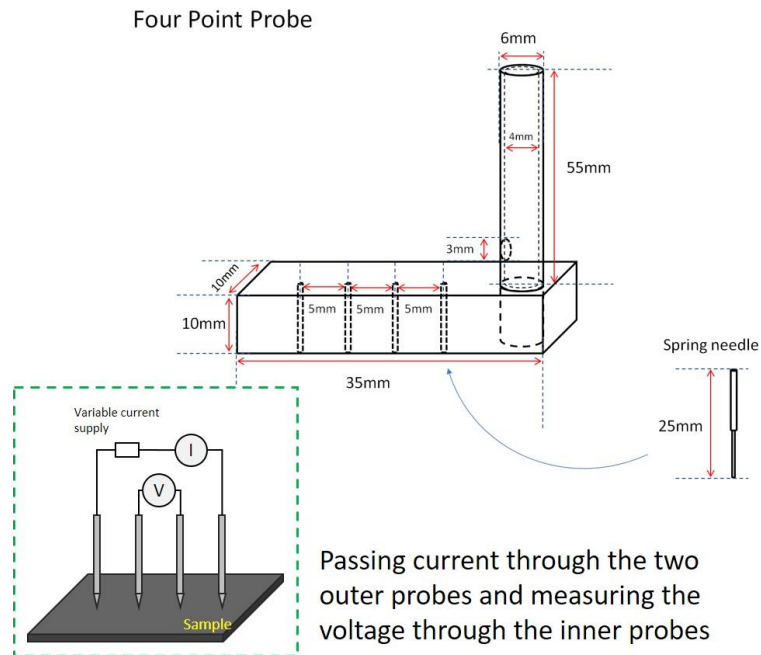
Four Point Probe

Figure 5.6 Four-point probe system
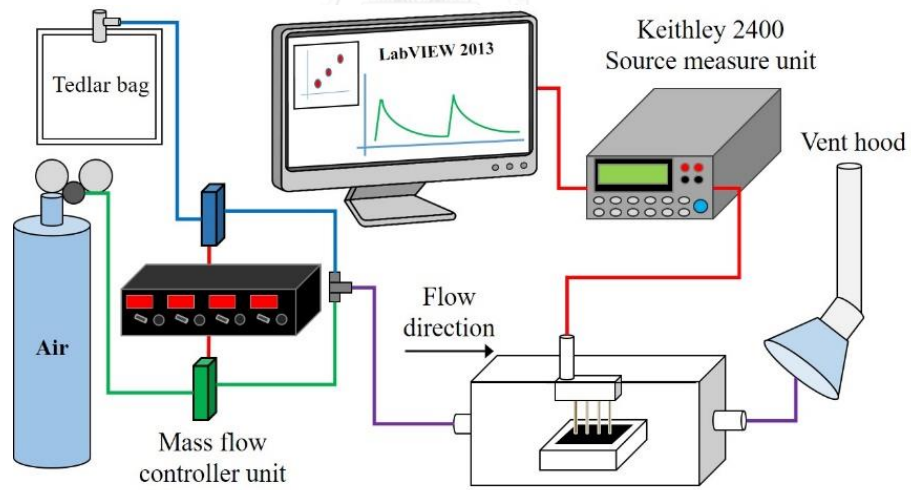
Figure 5.7 Schematic diagram of the gas sensing system

5.3.3 Gaseous chlorinated phenol sensing on acid-functionalized CNT buckypaper

A four-point probe measurement device was adopted for monitoring the change of resistivity of the CNT buckypaper while exposing to air contaminated with a pre-determined concentration of target gas in an air-tight glass chamber. Three types of gas (i.e., phenol, 2-chlorophenol and 2,4-dichlorophenol) were tested in the experiment. The target gases with desired concentrations were prepared in the gas saturator unit (**Figure 5.4**) and were transferred into a 3-Liter Tedlar bag.

Acid functionalized CNT buckypaper was placed in the gas sensing glass chamber (**Figure 5.5**). The four-point probe was mounted on the top of the buckypaper sample to make electrical contacts and the wires were connected to the SMU for monitoring the resistance values of the buckypaper. The input current was set at 50 mA. High-purity air was used as the background gas a flow rate of 300 sccm. When the resistance of CNTs gave constant results (**Figure A2**), the background gas was switched off and the target gas (phenol or 2-chlorophenol or 2,4-dichlorophrnol) in a Tedlar bag with pre-defined concentrations was fed into the chamber at a constant flow rate of 300 sccm for 1 minute. Then air was fed through the chamber to flush the target gas out from the chamber. All measurements were taken at room temperature with three replicates and the resistance of CNTs was recorded at every 1 second.

The sensor sensitivity (S) is calculated by using **Equation 5.9** (Varghese et al., 2001).

$$S\ (\%) = \frac{R_{gas} - R_{air}}{R_{air}} \times 100\% \qquad (5.9)$$

where R_{gas} is the resistance (Ω) in the presence of a test gas, and R_{air} is the resistance (Ω) in the presence of air.

Chapter 6

Results and discussion: Adsorption and gas sensing studies

The adsorption capacity of the synthesized CNTs were determined by adsorption isotherm experiment and fitted by three isotherm models. The effect of acid functionalization and the influence of chlorine functional groups in CPs on acid-functionalized CNTs adsorptivity were studied in adsorption behavior experiment. The sensing capability of the acid-functionalized CNT buckypaper for gaseous CPs was evaluated, and the results were reported and discussed in this chapter.

6.1 Adsorption isotherms

The equilibrium adsorbed amounts of gaseous phenol (P), 2-chlorophenol (2-CP) and 2,4-dichlorophenol (2,4-DCP) at equilibrium concentrations on acid-functionalized CNTs are shown in Figure 6.1.
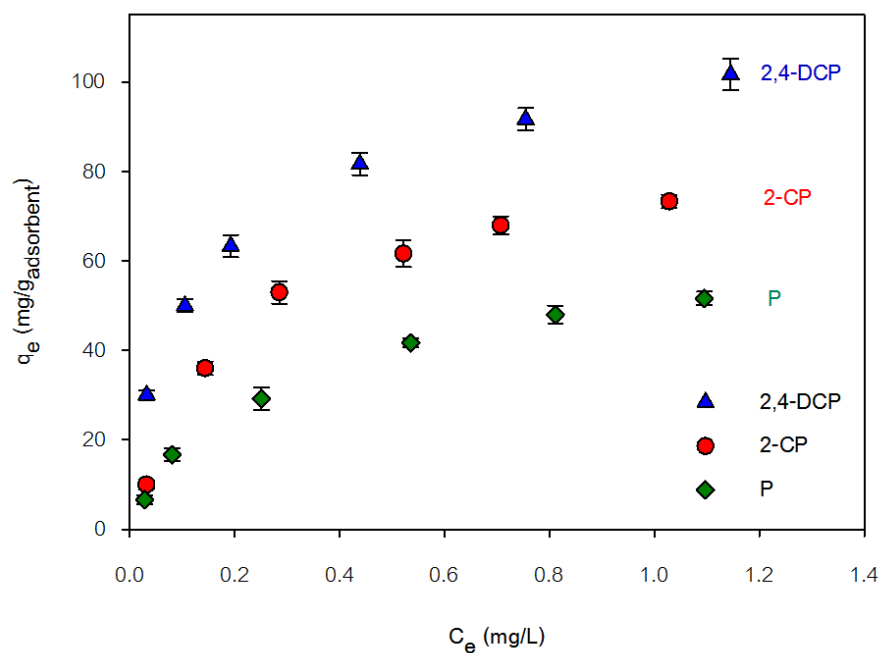
Figure 6.1 Adsorption equilibriums of gaseous CPs on acid-functionalized CNTs.

The adsorption capacity of different CPs onto the acid-functionalized CNT buckypaper varies with the number of chlorine atoms in the compounds. The results showed that chlorophenols were adsorbed better than phenol. The adsorption capacities can be ranked in descending order as 2,4-

DCP > 2-CP > P. The strong electronegativity of chlorine atoms decreases the electron density of benzene ring. The decrease in electron density of benzene ring is believed to enhance the π-π electron-donor-acceptor interaction between chlorophenols and the surface of CNTs (Ding et al., 2016).

The three adsorption isotherm models (Langmuir, Freundlich and Redlich-Peterson isotherms) were used to fit the experimental data in this work and the plots fitted by Langmuir, Freundlich and Redlich-Peterson models are shown in **Figure 6.2 (a)-(c)**, and the results are summarized in **Table 6.1**.

(c)
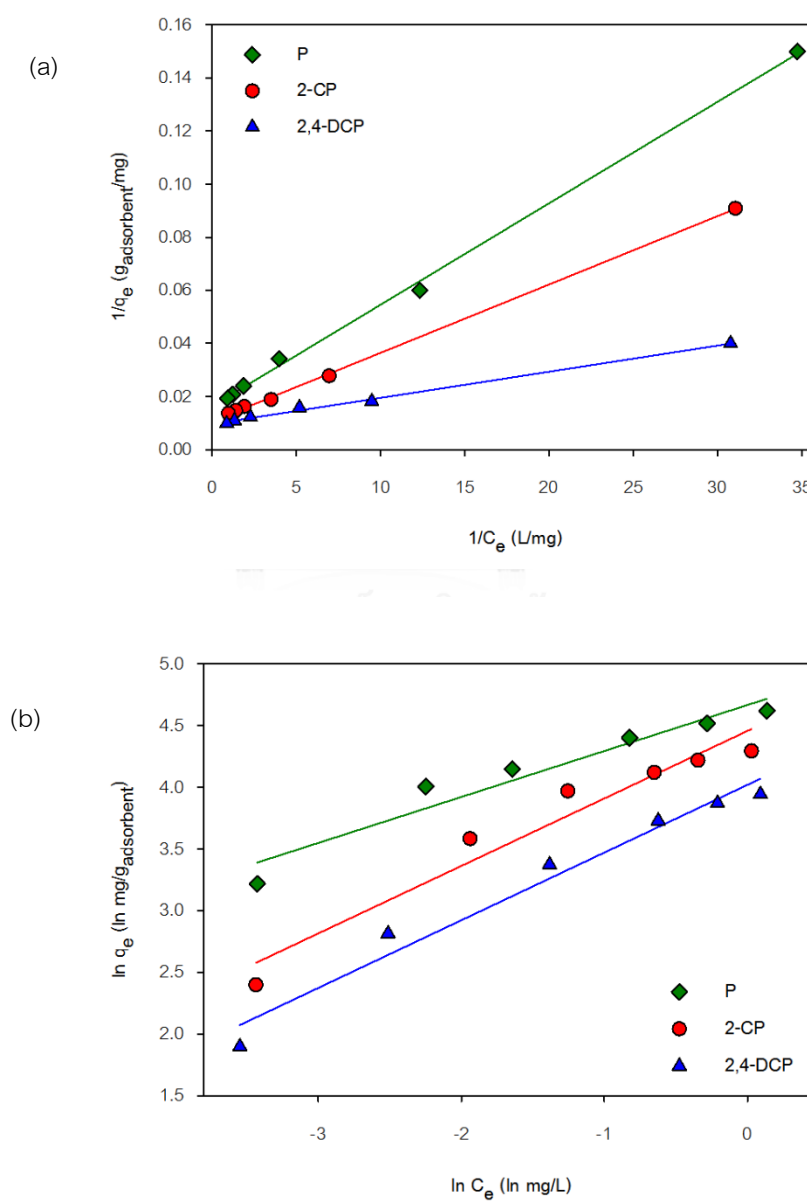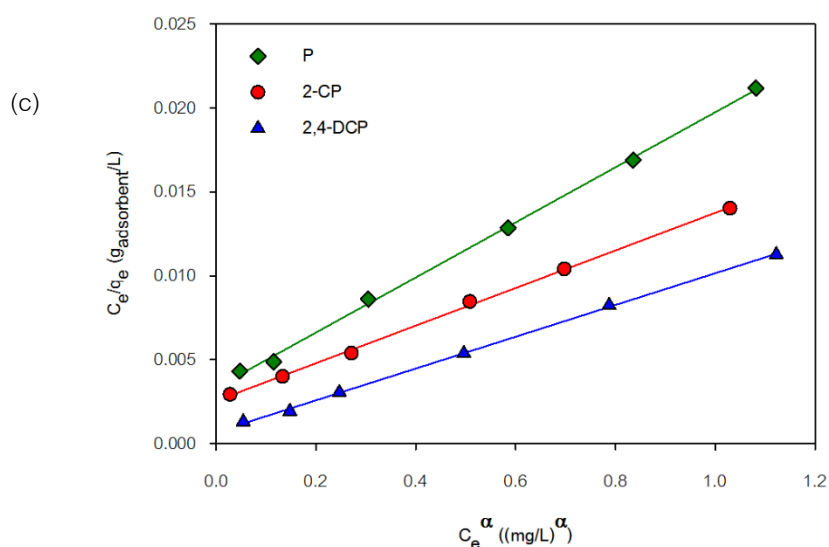
Figure 6.2 Adsorption data fitted with Langmuir (a), Freundlich (b), and Redlich-Peterson

models (c)

The Redlich-Peterson isotherm equation provided the best fit in the adsorptions of phenol, 2-chlorophenol and 2,4-dichlorophenol with α values of 0.86, 1.04 and 0.85, respectively. As α values approached 1, the adsorption tended to followed monolayer adsorption of Langmuir. However, the results from Redlich-Peterson model could imply that another adsorption mode, multilayer adsorption, might occurred at higher concentration range. The correlation coefficients for the Freundlich isotherm are significantly less than those of the Langmuir and the Redlich-Peterson isotherms. The results showed that adsorption equilibrium data were fitted best with the Langmuir isotherm as the r^2 value were relatively high. The fitted data showed that the r^2 values for the Langmuir isotherm model are greater than 0.996, with maximum adsorption capacity calculated from Langmuir equation of 61.35, 93.46 and 104.17 mg/g for phenol, 2-chlorophenol and 2,4-dichlorophenol, respectively. It is clearly observed that the equilibrium adsorption capacity of CPs on the adsorbent increased with increasing number of chlorine atoms. The higher adsorption affinity between CPs and the CNTs contributes the higher adsorption capacity.

Table 6.1 Isotherm parameters for CPCs adsorption fitted on the Langmuir, Freundlich and Redlich-Peterson models

Chemical	Langmuir			Freundlich			Redlich-Peterson			
	q_m (mg/g)	b (L/mg)	r^2	$1/n$	k_f ((mg/g)(L/mg)$^{1/n}$)	r^2	α	b_{RP}	q_{mon}	r^2
Phenol	61.35	0.233	0.9984	0.373	55.72	0.9704	0.86	0.201	60.97	0.9988
2-chlorophenol	93.46	0.243	0.9995	0.548	86.34	0.9448	1.04	0.223	89.29	0.9989
2,4-dichlorophenol	104.17	0.104	0.9964	0.549	106.46	0.9365	0.85	0.074	105.26	0.9994

The adsorption capacity of the acid-functionalized CNT in the present study was compared to the previous research in the **Table 6.2**. The results were in good agreement with other works, even though in aqueous phase, that the adsorption capacity increased with increasing of chlorine atoms in the compounds. In addition, the acid-functionalized CNTs in this study showed higher adsorption capacity than previous works with pristine CNTs and CNTs-COOH.

Table 6.2 The adsorption capacity of the materials

Material	Phase	Chemical	Adsorption capacity (mg/g)	References
MWCNTs	Aqueous	P	64.6	(Dehghani et al., 2016)
SWCNTs	Aqueous	2-CP 2,4-DCP	24.9 59.9	(Ding et al., 2016)
MWCNTs-COOH	Aqueous	P 3-CP	14.12 51.49	(Tóth et al., 2012)
MWCNTs-COOH	Aqueous	2,4-DCP	24.15	(Kragulj et al., 2015)
MWCNTs/SiO$_2$	Gaseous	P 2-CP 2,4-DCP	3.12 13.83 44.25	(Tulaphol et al., 2016)
MWCNTs-COOH	Gaseous	P 2-CP 2,4-DCP	61.35 93.46 104.17	This work

6.2 Adsorption behaviors

6.2.1 Effect of acid functionalization on CP adsorption

Surface functionalization was expected to enhance the adsorptivity of the adsorbent. In order to prove the hypothesis, 2-chlorophenol (2-CP) was selected as a target pollutant in this experiment. The 2-CP vapor was adsorbed by the non-modified and the acid-functionalized CNTs. The activation energy for desorption of 2-CP were studied by TG/DTG method. The desorption profiles from DTG measurement of 2-chlorophenol adsorbed on CNTs under N_2 atmosphere are shown in **Figure 6.3 (a)-(b)**.
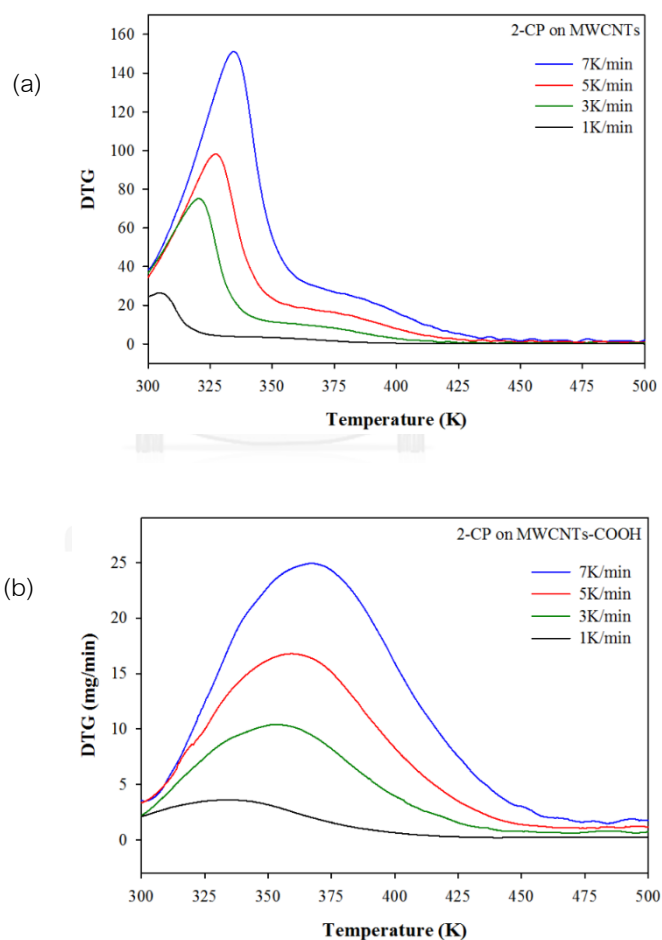
Figure 6.3 DTG desorption profiles for 2-CP on non-modified CNTs **(a)** and acid-functionalized CNTs **(b)**.

It can be seen from the DTG desorption profiles that the peak of desorbed chlorophenol on the acid-functionalized CNTs occurred at higher temperature than the non-modified CNTs. The peak temperature (T_m) for each heating rate was calculated to determine the activation energy for desorption (E_d) of each material. The E_d were found to be 52.3 kJ/mol for the non-modified CNTs and 62.5 kJ/mol for the acid-functionalized CNTs. The adsorption behaviors of chlorophenol on both materials were higher than 40 kJ/mol which were classified as chemisorpion (Guo et al., 2014). These results suggested that carboxyl group on CNTs could enhance the bonding energy between CNTs material and the 2-chlorophenol.

6.2.2 Adsorption behaviors of CPCs on acid-functionalized CNTs

The activation energy for desorption of the three different target CPCs were studied on acid-functionalized CNTs by TG/DTG method. The differential thermogravimetric measurements at different heating rates of three CPCs are shown in **Figure 6.4 (a)-(c)**.

(a)

(b)
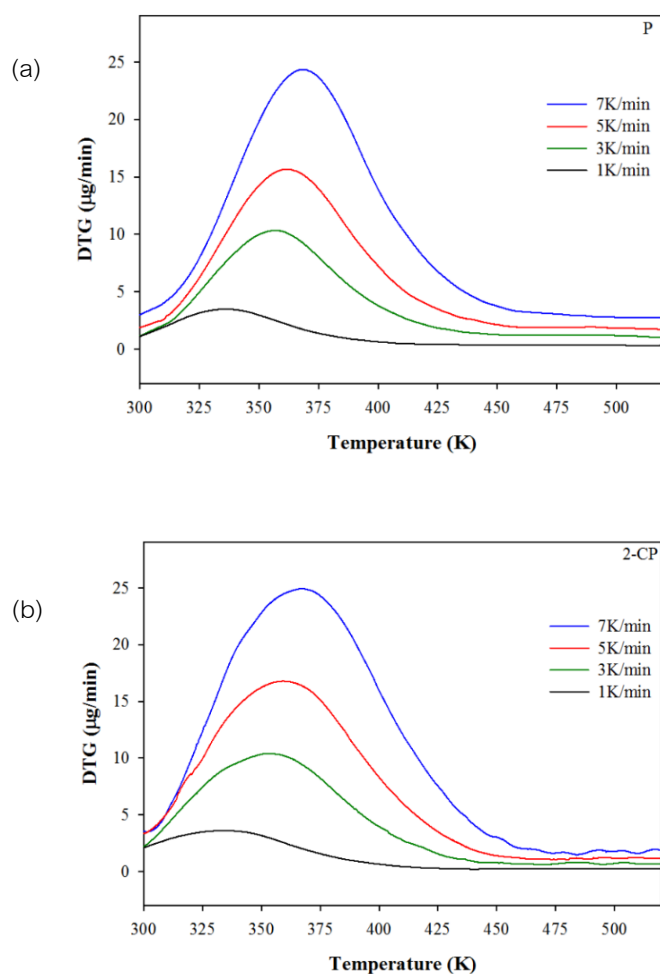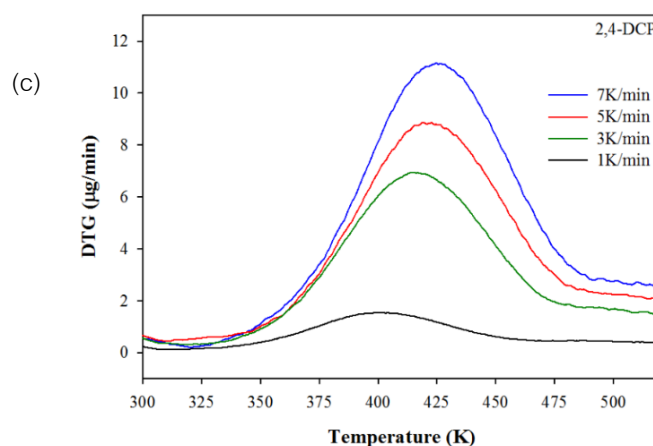
Figure 6.4 DTG desorption profiles for **(a)** P, **(b)** 2-CP and **(c)** 2,4-DCP
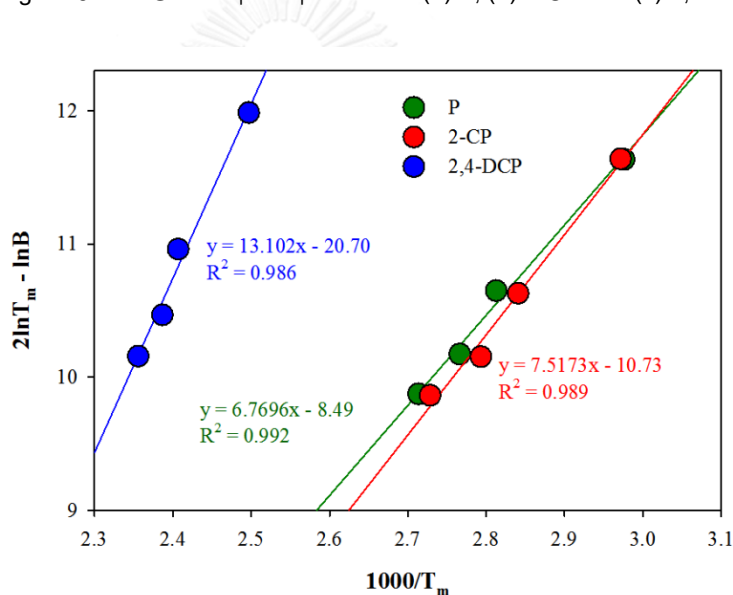
Figure 6.5 Plots of $2\ln T_m$-lnB versus $1000/T_m$

All phenolic compounds showed a similar pattern where the desorption peaks occurred at a higher temperature as the heating rate increased. **Figure 6.5** shows the plotted peak temperature (T_m) values against the heating rate. 2,4-dichlorophenol possessed the steepest slope, followed by 2-chlorophenol and then phenol. The T_m for each heating rate was calculated based on **Equation 8** to determine the activation energy for desorption (E_d) of each compound. The E_d value of each pollutant was found to be 56.3, 62.5 and 108.9 kJ/mol for phenol, 2-chlorophenol and 2,4-dichlorophenol, respectively. The strong activation energy (E_d values) indicated that the adsorption for all three tested

CPCs on the MWCNT surfaces were chemisorption type, where the energy involved in the adsorption is typically greater than 40 kJ/mol (Guo et al., 2014).

The results also revealed that the E_d value increased with the presence of chlorine atoms in the pollutants. Chlorine atoms have a strong ability to withdraw electron and cause electrons on the chloro-substituted benzene rings to be depleted. Therefore, they work as π-electron acceptors that interact powerfully with the π-electron-rich of the graphene surface sites of CNTs. Consequently, the adsorption of chloroaromatic compounds becomes much stronger. The number of substituted groups (nitro and chloro) could have significant effect on the adsorption, indicating that the more groups substitution will have higher adsorption affinity (Ding et al., 2016).

6.3 Gas sensing study

A p-type semiconductor is a material that have a majority of positives charge carriers. Under oxygen ambient, when p-type gas sensor absorbs oxygen ions, the electrons from valence band are excited and positive holes are generated on the surface. Consequently, a quantity of charge carriers on the surface increase and results in a decrease of the sensor resistance. Conversely, when a p-type gas sensor is under the target gas ambient (reducing gas), the negative charges are introduced into the material and recombine with the positive holes. As a result, the positive (holes) charge-carrier concentration reduces, and leads to an increase of the sensor resistance. The interaction between the MWCNT gas sensor and the reducing gas (electron donor) is likely to be a charge-transfer interaction. The interaction energy is in between a purely adsorptive process (<40 kJ/mol) and a true covalent bond (approximately 300 kJ/mol) (Kolesar and Wiseman, 1989).

6.3.1 Effect of acid functionalization on CP gas sensing

The sensitivity of 100 ppm gaseous chlorophenol on two different buckypapers is shown in **Figure 6.6**. Both buckypapers performed rapid detection when chlorophenol gas was introduced into the chamber. The acid-functionalized CNT buckypaper showed substantially more sensitive than the non-modified one. The carboxylate group on the surface of acid-functionalized CNT could enhance the electron transfer rate (Jacobs et al., 2011), resulting in significantly higher resistance change when exposed to chlorophenol gas. The signal change was about three times higher while the recovery time was slightly longer than that of non-modified CNT buckypaper due to the stronger bonding energy.

These results are in good agreement with the results of adsorption behavior test discussed in previous section.
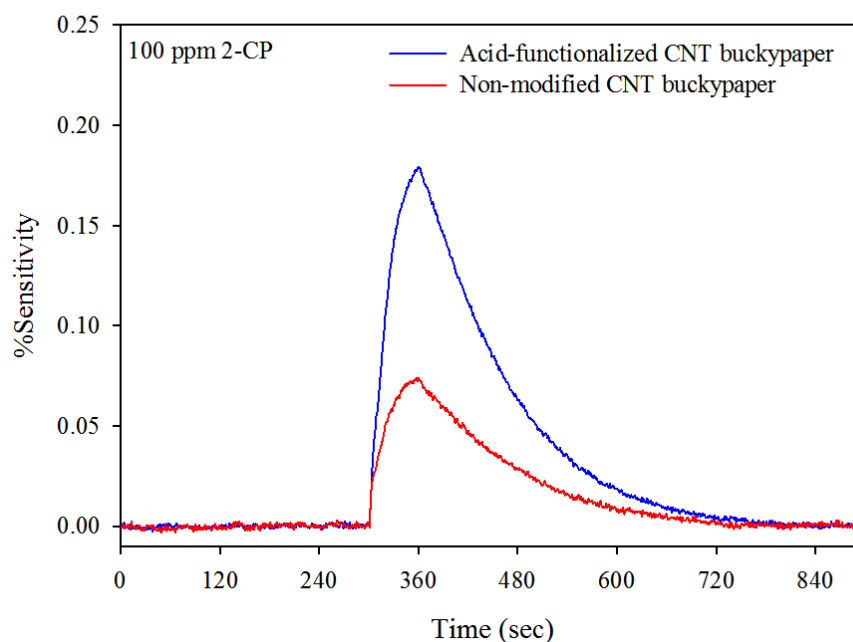
Figure 6.6. The sensitivity of 100 ppm 2-chlorophenol

6.3.2 CPC Gas sensing on acid-functionalized CNT buckypaper

The performance of acid-functionalized CNT buckypaper gas sensor on the detection of phenol, 2-chlorophenol and 2,4-dichlorophenol are shown in **Figure 6.7 (a)-(c)**. The gas sensor revealed good sensitivity and fast response to all three gaseous CPCs. Upon gas exposure, the resistance of the CNT buckypaper was observed to increase rapidly. The response time of the buckypaper was approximately 30 seconds. As the CPCs gas feed was terminated, the increased resistance returned to its original value in 300~420 s for all CPCs. The recovery time was slow because of the high bonding energy between CNTs and CPCs. However, some researchers found that the recovery time can be decreased by increasing carrier gas flow (Jung et al., 2014), heating (Kong et al., 2000), and using ultraviolet (UV) light (Li et al., 2003).
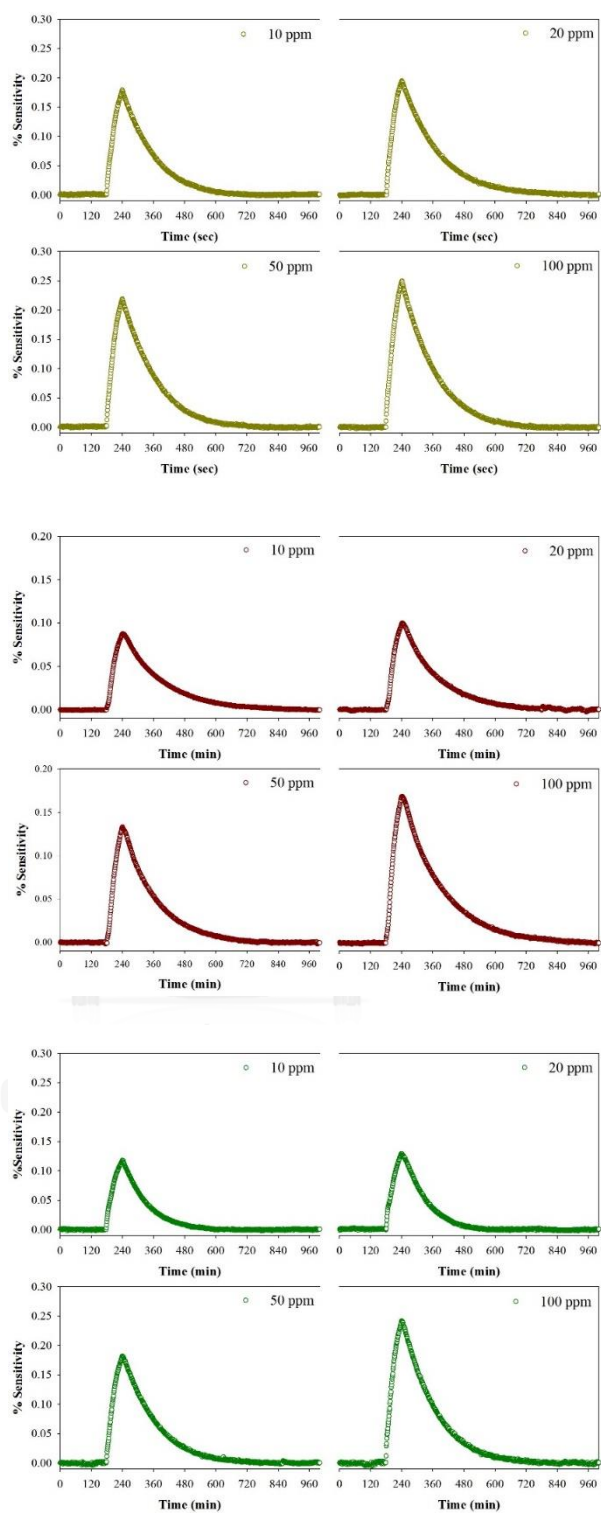
Figure 6.7 Effect of gas concentration on the resistance of acid-functionalized CNT

buckypaper (a) phenol (b) 2-chlorophenol and (c) 2,4-dichlorophenol.

From the sensor response, the resistance of the acid-functionalized CNT buckypaper increased when it was exposed to the CPC gases. It can be concluded that CPC gaseous molecules act as electron donors to the CNT gas sensor. A p-type semiconducting CNTs have positive (holes) majority charge carriers. The CPC gases donated electrons to the CNT buckypaper causes a reduction in the number of holes in active layer. The decrease in charge carrier density then led to an increase the distance between valence band and Fermi level. Therefore, the resistance of the device increased (Afrin and Shah, 2015).
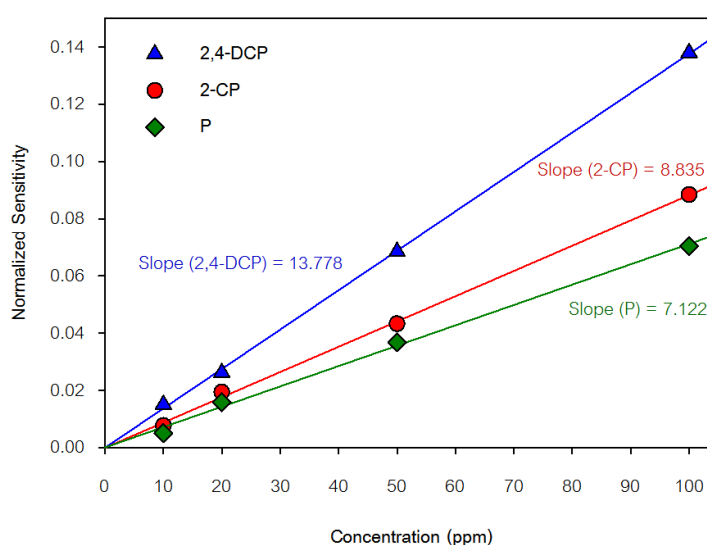
Figure 6.8 Sensitivity comparison of three CPCs on acid-functionalized CNT gas sensor.

The sensitivity of the CNT buckypaper is defined as the slope of the dose-response curve ($\Delta y/\Delta x$), representing sensing response versus the measured concentration curve. Ideally, one would like to have the sensitivity to be constant over the dynamic range of the sensor. This would imply a linear dose-response curve. The sensitivity of CNT buckypaper was investigated by exposing it to the three CPCs with a tested concentration range between 10 and 100 ppm in synthetic air. The calculated slope of the curves can be used as an index of sensor sensitivity. The dose-response curves of each CPC are shown in Figure **A3**. The comparison between these three compounds was made to observe the sensitivity and selectivity for each compound (**Figure 6.8**). It can be seen that the acid-functionalized MWCNT gas sensor responses were linear with respect to analyte concentration ($r^2 >$ 0.99), suggesting a first-order interaction kinetics between the analyte and CNTs. From the slope of the lines, it is clear that the sensitivity of acid-functionalized CNT buckypaper on 2,4-dichlorophenol

was higher than 2-chlorophenol and phenol gases. The sensitivity values obtained were 13.778×10^{-4}, 8.835×10^{-4} and 7.122×10^{-4} for 2,4-dichlorophenol, 2-chlorophenol and phenol, respectively. It is noteworthy that the sensitivity of gas sensor to the target gases increased with an increasing of the number of chlorine atoms, which corresponded with the results in adsorption behavior study. The limit of detection (LOD) for phenol, 2-chlorophenol and chlorophenol could be estimated by the signal-to-noise (S/N) method. The magnitude of noise was measured manually from the baseline noise of the plot (**Figure A4**). Generally, an S/N ratio of three is accepted to estimate the LOD of the sensor. The LOD of the acid-functionalized CNT gas sensor for phenol, 2-chlorophenol and chlorophenol were estimated to be 476, 384 and 246 ppb, respectively.

In order to evaluate the stability and repeatability of the acid-functionalized MWCNT gas sensor, the sensor was exposed to 4 consecutive pulses of 100 ppm 2-chlorophenol. The exposure duration was 2 min/pulse and then purging with air for 10 min, repeatedly. **Figure 6.9** shows 4 reversible cycles of the response curve of the acid-functionalized gas sensor exposed to 2-chlorophenol. The sensor showed insignificant change in response recovery time and the sensitivity. The sensor responded rapidly in few seconds upon the exposure of the target gas. After the target gas was turned off, the resistance of the gas sensor recovered to the initial value in around 8~9 minutes. The deviations of sensitivity and the recovery time was 1.7% and 3.9%, respectively.
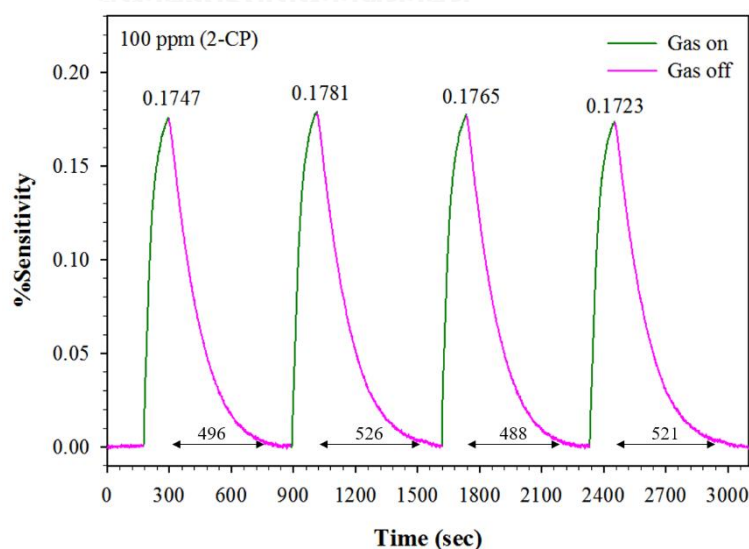
Figure 6.9 Stability and repeatability of acid-functionalized CNT gas sensor with 4 consecutive pulses of 2-chlorophenol (2 min/pulse).

In addition, the gas sensor was further tested with 8 consecutive pulses of 100 ppm 2-chlorophenol with 1 min exposure duration for each pulse (**Figure 6.10**). The sensor showed good stability after 8 loops of gas sensing. The sensitivity at 1 min were in range of approximately 0.1679 to 0.1686 accounted for the deviations of 0.22%. It can be seen that the sensor performed good repeatability.
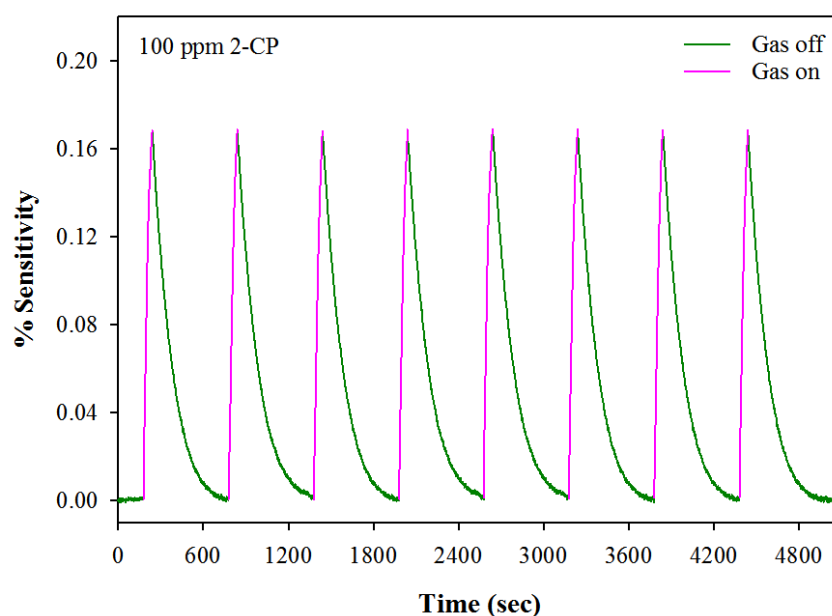
Figure 6.10 Stability and repeatability of acid-functionalized CNT gas sensor with 8 consecutive pulses of 2-chlorophenol (1 min/pulse).

6.3.3 Validation of gas sensor

The CNT gas sensor was validated with 2-chlorophenol with various concentrations in a range of 1-118 ppm to investigate the accuracy of the gas sensor. The target gas samples with different concentrations were prepared by the gas saturator unit and then prepared gas concentrations were confirmed with gas chromatography-mass spectrometry (GC-MS). **Figure 6.11** shows the linearly adjusted dose-response curve of 2-chlorophenol and the experimental data. The results showed that the sensor could detect 2-CP gas concentration as low as 1 ppm. However, the accuracy and precision were very low because it nearly reached the limit of detection of the sensor. Furthermore, the accuracy and precision of the sensor increased when the concentration of 2-CP were in the range of 24-118 ppm. The sensor performed acceptably precise detection with the deviations of less than 3%.
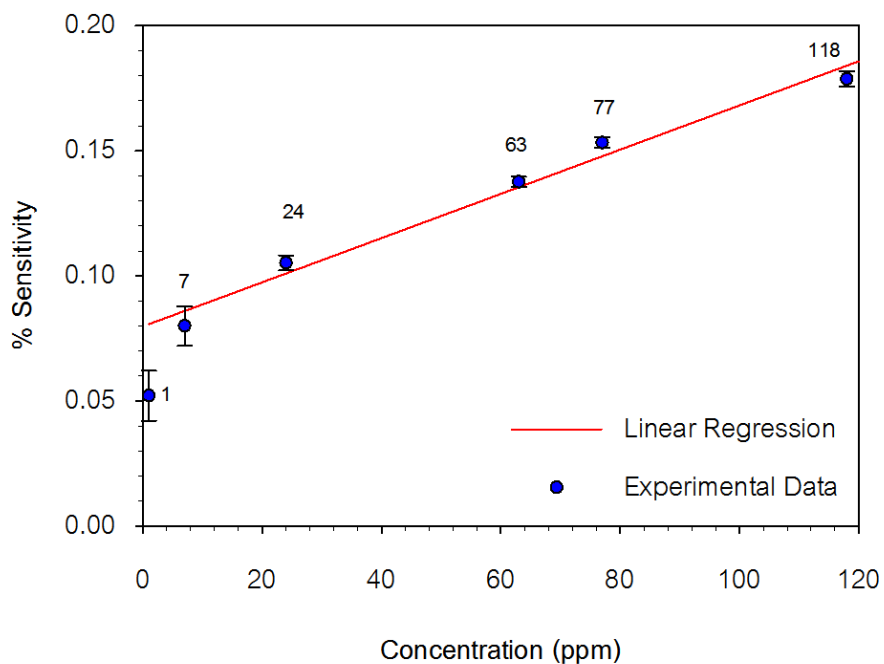
Figure 6.11 Sensor validation with different 2-CP concentrations

6.3.4 Study of selectivity

To investigate the selectivity of the gas sensor, the CNT buckypaper gas sensor was tested with various gas species besides chlorophenols such as ethanol, methanol, acetone and toluene at 100 ppm. **Figure 6.12** displays the sensitivity of acid-functionalized CNT gas sensor to each kind of gases.
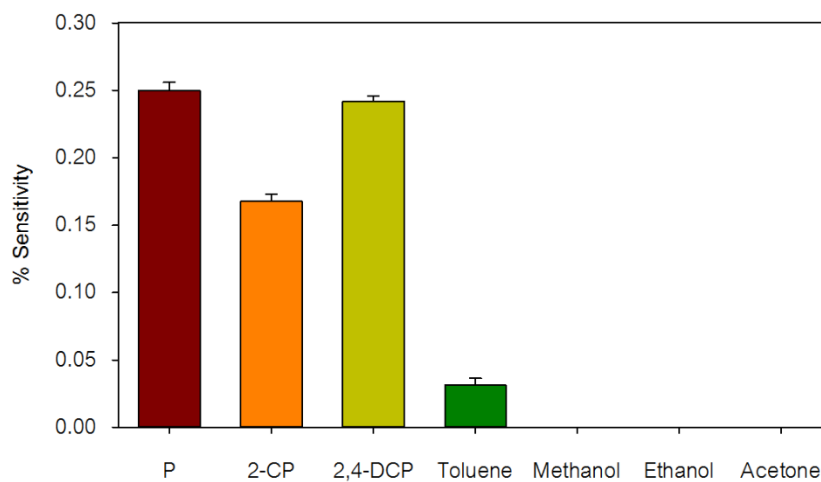
Figure 6.12 Selectivity of the gas sensor to various gases at 100 ppm

The results showed that the acid-functionalized CNT gas sensor could not detect three kinds of gases i.e. methanol, ethanol and acetone at 100 ppm concentration. However, small detection of toluene were observed. This may be due to the π-π stacking from benzene ring in toluene structure enhanced the electron transfer between toluene and the gas sensor, and consequently gave better sensitivity than other three gases.
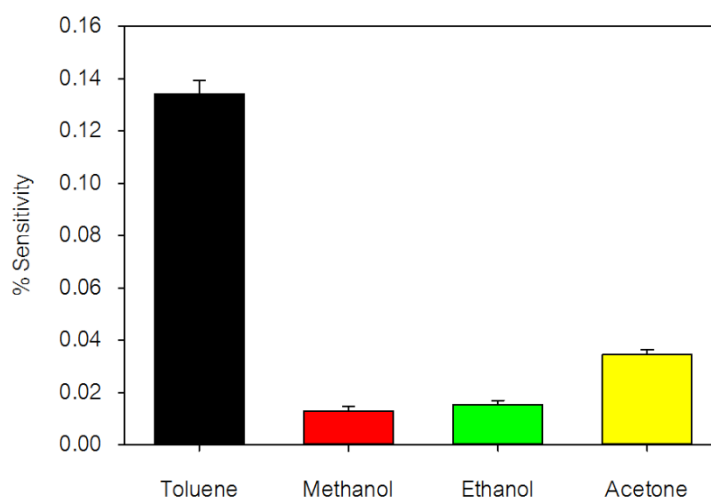
Figure 6.13 Selectivity of the gas sensor to various gases at 500 ppm

Furthermore, when the concentrations of toluene, methanol, ethanol and acetone were increased to 500 ppm, the sensor was able to detect all four kinds of gases. The sensitivity to toluene was obviously higher than the other three gases due to its aromatic structures. The results implied that the adsorption and sensing performance affected greatly by the π-π electron stacking of benzene rings in the target compounds and the CNTs.

Chapter 7

Conclusions and recommendations

7.1 Conclusions

MWCNTs were successfully synthesized via FCCVD method using ferrocene catalyst. The high density growth of the carbon nanotubes indicated the high catalytic activity of the iron catalyst. The synthesized MWCNTs were purified by acid treatment and thermal oxidation to remove amorphous carbon and residual metal catalyst particles. The purified CNTs were then functionalized with a mixture of sulfuric and nitric acid to attach carbonyl functional group (C=O) on to the surface of nanotubes. The adsorption isotherms results showed that the adsorption capacity of the adsorbent to the phenolic compounds were affected by the number of chlorine atoms in the target pollutants. The adsorption experimental data were fitted best with Langmuir model, suggesting monolayer adsorption of CPCs on the CNT surface. Maximum adsorption capacity calculated from Langmuir equation were 61.35, 93.46 and 104.17 mg/g for phenol, 2-chlorophenol and 2,4-dichlorophenol, respectively. Acid functionalization of the CNTs was found to enhance the adsorption bonding energy between CNTs and chlorophenol. Adsorption behaviors of three CPCs adsorbed on the CNTs were classified as chemisorption. Afterwards, CNT buckypaper were prepared by vacuum filtration and utilized as gas sensor. The CNT buckypaper responded quickly (several seconds) upon the exposure of the target gases and the sensitivity was directly proportional to the degree of chlorination in the target CPCs. The CNT buckypaper gas sensor showed good sensitivity to all gaseous CPCs through the concentration range of 10-100 ppm. After 4 consecutive cycles test, the CNT buckypaper still gave unchanged responses indicating satisfied stability and repeatability. The results suggest that the acid-functionalized CNT buckypaper is a promising material for a simple detection of CPCs in air.

7.2 Recommendations

Mixed gaseous CPCs should be studied for better understanding on the selectivity of the gas sensor. Different response patterns are expected from the different gas mixture. More modification and functionalization techniques should be assessed to improve the selectivity of the sensor. The current experiments were carried out under the controlled condition (e.g. $25^{o}C$, 40-50 %Rh). Different operating parameters should be studied. The sensing chamber might be equipped with UV lamp or heating system in order to shorten the recovery time of the gas sensor. The four-point probe material might be a limitation for very low concentration gas sensing. Switching the other kind of metals (e.g. Cu or Ag) which have higher electrical conductivity is expected to increase the signal to noise ratio.

REFERENCES

AFRIN, R. & SHAH, N. A. 2015. Room temperature gas sensors based on carboxyl and thiol functionalized carbon nanotubes buckypapers. *Diamond and Related Materials,* 60, 42-49.

AKBARI, E., AFROOZEH, A., TAN, M. L. P., ARORA, V. K. & GHADIRY, M. 2016. Analytical assessment of carbon allotropes for gas sensor applications. *Measurement: Journal of the International Measurement Confederation,* 92, 295-302.

ANDO, Y. & IIJIMA, S. 1993. Preparation of Carbon Nanotubes by Arc-Discharge Evaporation. *Japanese Journal of Applied Physics,* 32, L107.

ARCAND, Y., HAWARI, J. & GUIOT, S. R. 1995. Solubility of pentachlorophenol in aqueous solutions: The pH effect. *Water Research,* 29, 131-136.

AREPALLI, S. 2004. Laser Ablation Process for Single-Walled Carbon Nanotube Production. *Journal of Nanoscience and Nanotechnology,* 4, 317-325.

AYUDE, M. A., OKADA, E., GONZÁLEZ, J. F., HAURE, P. M. & MURIALDO, S. E. 2009. Bacillus subtilis as a bioindicator for estimating pentachlorophenol toxicity and concentration. *Journal of Industrial Microbiology & Biotechnology,* 36, 765-768.

BISWAS, A., WANG, T. & BIRIS, A. S. 2010. Single metal nanoparticle spectroscopy: optical characterization of individual nanosystems for biomedical applications. *Nanoscale,* 2, 1560-1572.

BUANG, N. A., FADIL, F., MAJID, Z. A. & SHAHIR, S. 2012. Characteristic of mild acid functionalized multiwalled carbon nanotubes towards high dispersion with low structural defects. *Digest Journal of Nanomaterials and Biostructures,* 7, 33-39.

BUMBRAH, G. S. & SHARMA, R. M. 2015. Raman spectroscopy – Basic principle, instrumentation and selected applications for the characterization of drugs of abuse. *Egyptian Journal of Forensic Sciences*.

CANÇADO, L. G., TAKAI, K., ENOKI, T., ENDO, M., KIM, Y. A., MIZUSAKI, H., JORIO, A., COELHO, L. N., MAGALHÃES-PANIAGO, R. & PIMENTA, M. A. 2006. General

equation for the determination of the crystallite size La of nanographite by Raman spectroscopy. *Applied Physics Letters,* 88, 163106.

CANTALINI, C., VALENTINI, L., ARMENTANO, I., LOZZI, L., KENNY, J. M. & SANTUCCI, S. 2003. Sensitivity to NO2 and cross-sensitivity analysis to NH3, ethanol and humidity of carbon nanotubes thin film prepared by PECVD. *Sensors and Actuators B: Chemical,* 95, 195-202.

CASSELL, A. M., RAYMAKERS, J. A., KONG, J. & DAI, H. 1999. Large Scale CVD Synthesis of Single-Walled Carbon Nanotubes. *Journal of Physical Chemistry B,* 103, 6484-6492.

CHANG, F.-W., KUO, M.-S., TSAY, M.-T. & HSIEH, M.-C. 2004. Effect of calcination temperature on catalyst reducibility and hydrogenation reactivity in rice husk ash–alumina supported nickel systems. *Journal of Chemical Technology & Biotechnology,* 79, 691-699.

CHEN, P.-C., ISHIKAWA, F. N., CHANG, H.-K., RYU, K. & ZHOU, C. 2009. A nanoelectronic nose: a hybrid nanowire/carbon nanotube sensor array with integrated micromachined hotplates for sensitive gas discrimination. *Nanotechnology,* 20, 125503.

CHEN, X.-H., CHEN, C.-S., XIAO, H.-N., CHEN, X.-H., LI, W.-H. & XU, L.-S. 2005. Lipophilic functionalization of multi-walled carbon nanotubes with stearic acid. *Carbon,* 43, 1800-1803.

CHOPRA, S., MCGUIRE, K., GOTHARD, N., RAO, A. M. & PHAM, A. 2003. Selective gas detection using a carbon nanotube sensor. *Applied Physics Letters,* 83, 2280-2282.

CONSALES, M., CRESCITELLI, A., PENZA, M., AVERSA, P., VENERI, P. D., GIORDANO, M. & CUSANO, A. 2009. SWCNT nano-composite optical sensors for VOC and gas trace detection. *Sensors and Actuators B: Chemical,* 138, 351-361.

CONSALES, M., CUTOLO, A., PENZA, M., AVERSA, P., CASSANO, G., GIORDANO, M. & CUSANO, A. 2007. Carbon Nanotubes Coated Acoustic and Optical VOCs

Sensors: Towards the Tailoring of the Sensing Performances. *IEEE Transactions on Nanotechnology,* 6, 601-612.

CUI, S., YANG, L., WANG, J. & WANG, X. 2016. Fabrication of a sensitive gas sensor based on PPy/TiO2 nanocomposites films by layer-by-layer self-assembly and its application in food storage. *Sensors and Actuators B: Chemical,* 233, 337-346.

DAI, H. 2001. Nanotube Growth and Characterization. *In:* DRESSELHAUS, M. S., DRESSELHAUS, G. & AVOURIS, P. (eds.) *Carbon Nanotubes: Synthesis, Structure, Properties, and Applications.* Berlin, Heidelberg: Springer Berlin Heidelberg.

DAS, R., ALI, M. E., HAMID, S. B. A., RAMAKRISHNA, S. & CHOWDHURY, Z. Z. 2014. Carbon nanotube membranes for water purification: A bright future in water desalination. *Desalination,* 336, 97-109.

DE VARGAS-SANSALVADOR, I. M. P., FAY, C., PHELAN, T., FERNÁNDEZ-RAMOS, M. D., CAPITÁN-VALLVEY, L. F., DIAMOND, D. & BENITO-LOPEZ, F. 2011. A new light emitting diode–light emitting diode portable carbon dioxide gas sensor based on an interchangeable membrane system for industrial applications. *Analytica Chimica Acta,* 699, 216-222.

DEHGHANI, M. H., MOSTOFI, M., ALIMOHAMMADI, M., MCKAY, G., YETILMEZSOY, K., ALBADARIN, A. B., HEIBATI, B., ALGHOUTI, M., MUBARAK, N. M. & SAHU, J. N. 2016. High-performance removal of toxic phenol by single-walled and multi-walled carbon nanotubes: Kinetics, adsorption, mechanism and optimization studies. *Journal of Industrial and Engineering Chemistry,* 35, 63-74.

DEMENTEV, N., OSSWALD, S., GOGOTSI, Y. & BORGUET, E. 2009. Purification of carbon nanotubes by dynamic oxidation in air. *Journal of Materials Chemistry,* 19, 7904-7908.

DEN, W., LIU, H. C., CHAN, S. F., KIN, K. T. & HUANG, C. 2006. Adsorption of phthalate esters with multiwalled carbon nanotubes and its applications. *Journal of Environmental Engineering and Management,* 16, 8.

DHALL, S., JAGGI, N. & NATHAWAT, R. 2013. Functionalized multiwalled carbon nanotubes based hydrogen gas sensor. *Sensors and Actuators A: Physical,* 201, 321-327.

DING, F., LARSSON, P., LARSSON, J. A., AHUJA, R., DUAN, H., ROSÉN, A. & BOLTON, K. 2008. The Importance of Strong Carbon−Metal Adhesion for Catalytic Nucleation of Single-Walled Carbon Nanotubes. *Nano Letters,* 8, 463-468.

DING, H., LI, X., WANG, J., ZHANG, X. & CHEN, C. 2016. Adsorption of chlorophenols from aqueous solutions by pristine and surface functionalized single-walled carbon nanotubes. *Journal of Environmental Sciences,* 43, 187-198.

DONG, K.-Y., CHOI, J., LEE, Y. D., KANG, B. H., YU, Y.-Y., CHOI, H. H. & JU, B.-K. 2013. Detection of a CO and NH3 gas mixture using carboxylic acid-functionalized single-walled carbon nanotubes. *Nanoscale Research Letters,* 8, 1-6.

DONG, L., JIAO, J., PAN, C. & TUGGLE, D. W. 2004. Effects of catalysts on the internal structures of carbon nanotubes and corresponding electron field-emission properties. *Applied Physics A,* 78, 9-14.

DUBE, I., JIMÉNEZ, D., FEDOROV, G., BOYD, A., GAYDUCHENKO, I., PARANJAPE, M. & BARBARA, P. 2015. Understanding the electrical response and sensing mechanism of carbon-nanotube-based gas sensors. *Carbon,* 87, 330-337.

DUPUIS, A.-C. 2005. The catalyst in the CCVD of carbon nanotubes—a review. *Progress in Materials Science,* 50, 929-961.

EDER, D. 2010. Carbon Nanotube−Inorganic Hybrids. *Chemical Reviews,* 110, 1348-1385.

EISENREICH, S. J., LOONEY, B. B. & THORNTON, J. D. 1981. Airborne organic contaminants in the Great Lakes ecosystem. *Environmental Science & Technology,* 15, 30-38.

ESWARAMOORTHY, M., SEN, R. & RAO, C. N. R. 1999. A study of micropores in single-walled carbon nanotubes by the adsorption of gases and vapors. *Chemical Physics Letters,* 304, 207-210.

FAN, S., CHAPLINE, M. G., FRANKLIN, N. R., TOMBLER, T. W., CASSELL, A. M. & DAI, H. 1999. Self-Oriented Regular Arrays of Carbon Nanotubes and Their Field Emission Properties. *Science,* 283, 512-514.

FATEMI, S. M. & FOROUTAN, M. 2015. Study of dispersion of carbon nanotubes by Triton X-100 surfactant using molecular dynamics simulation. *Journal of the Iranian Chemical Society,* 12, 1905-1913.

FEJES, D. & HERNÁDI, K. 2010. A Review of the Properties and CVD Synthesis of Coiled Carbon Nanotubes. *Materials,* 3, 2618.

FINE, G. F., CAVANAGH, L. M., AFONJA, A. & BINIONS, R. 2010. Metal oxide semi-conductor gas sensors in environmental monitoring. *Sensors,* 10, 5469-5502.

FUTABA, D. N., HATA, K., YAMADA, T., HIRAOKA, T., HAYAMIZU, Y., KAKUDATE, Y., TANAIKE, O., HATORI, H., YUMURA, M. & IIJIMA, S. 2006. Shape-engineerable and highly densely packed single-walled carbon nanotubes and their application as super-capacitor electrodes. *Nat Mater,* 5, 987-994.

GARDNER, J. W., WEI, G., VINCENT, T., VOLANS, K., TREMLETT, P., WOTHERSPOON, T. & DYER, D. C. 2015. A Gas sensor system for Harsh environment applications. *Procedia Engineering,* 120, 275-278.

GERASIMOV, G. Y. 2007. Gas-phase radiation-chemical formation of dioxins from chlorinated phenols. *High Energy Chemistry,* 41, 20-24.

GHADDAB, B., SANCHEZ, J. B., MAVON, C., PAILLET, M., PARRET, R., ZAHAB, A. A., BANTIGNIES, J. L., FLAUD, V., BECHE, E. & BERGER, F. 2012. Detection of O3 and NH3 using hybrid tin dioxide/carbon nanotubes sensors: Influence of materials and processing on sensor's sensitivity. *Sensors and Actuators B: Chemical,* 170, 67-74.

GILANI, N., TOWFIGHI, J., RASHIDI, A., MOHAMMADI, T., OMIDKHAH, M. R. & SADEGHIAN, A. 2013. Investigation of H2S separation from H2S/CH4 mixtures using functionalized and non-functionalized vertically aligned carbon nanotube membranes. *Applied Surface Science,* 270, 115-123.

GOMEZ, M. J., BRUNEAU, C., SOYER, N. & BRAULT, A. 1988. Thermal degradation of chlorophenoxy acid herbicides. *Journal of Agricultural and Food Chemistry,* 36, 649-653.

GUO, Y., LI, Y., WANG, J., ZHU, T. & YE, M. 2014. Effects of activated carbon properties on chlorobenzene adsorption and adsorption product analysis. *Chemical Engineering Journal,* 236, 506-512.

HOLT, J. K., PARK, H. G., WANG, Y., STADERMANN, M., ARTYUKHIN, A. B., GRIGOROPOULOS, C. P., NOY, A. & BAKAJIN, O. 2006. Fast Mass Transport Through Sub-2-Nanometer Carbon Nanotubes. *Science,* 312, 1034-1037.

IIJIMA, S. 1991. HELICAL MICROTUBULES OF GRAPHITIC CARBON. *Nature,* 354, 56-58.

ISSI, J. P. & NYSTEN, B. 1998. *Electrical and thermal transport in carbon fibers,* New York, Marcel Dekker Inc.

JACOBS, C. B., VICKREY, T. L. & VENTON, B. J. 2011. Functional groups modulate the sensitivity and electron transfer kinetics of neurochemicals at carbon nanotube modified microelectrodes. *The Analyst,* 136, 3557-3565.

JANATA, J. & JOSOWICZ, M. 2003. Conducting polymers in electronic chemical sensors. *Nat Mater,* 2, 19-24.

JAVEY, A. & KONG, J. 2009. *Carbon Nanotube Electronics*, Springer US.

JI, Y., SOONG, C. J. & LIN, Y. J. 2012. An investigation of nanotube-integrated buckysheets' properties with molecular dynamics modeling and analysis. *International Journal of Engineering Inventions,* 1, 31-37.

JIANG, H., ZHANG, D. & WANG, R. 2009. Silicon-doped carbon nanotubes: a potential resource for the detection of chlorophenols/chlorophenoxy radicals. *Nanotechnology,* 20, 145501.

JIANG, X., SHAO, Z., LI, J., LIU, W., ZHU, D. & LIU, D. 2015. Dispersion characteristics of multi-walled carbon nanotubes with gallic acid. *Journal of Nanoscience and Nanotechnology,* 15, 9874-9878.

JIJUN, Z., ALPER, B., JIE, H. & JIAN PING, L. 2002. Gas molecule adsorption in carbon nanotubes and nanotube bundles. *Nanotechnology,* 13, 195.

JUNG, D., HAN, M. & LEE, G. S. 2014. Gas sensor using a multi-walled carbon nanotube sheet to detect hydrogen molecules. *Sensors and Actuators A: Physical,* 211, 51-54.

KANOUN, O., MÜLLER, C., BENCHIROUF, A., SANLI, A., DINH, T., AL-HAMRY, A., BU, L., GERLACH, C. & BOUHAMED, A. 2014. Flexible Carbon Nanotube Films for High Performance Strain Sensors. *Sensors,* 14, 10042.

KARMAOUI, M., LEONARDI, S. G., LATINO, M., TOBALDI, D. M., DONATO, N., PULLAR, R. C., SEABRA, M. P., LABRINCHA, J. A. & NERI, G. 2016. Pt-decorated In2O3 nanoparticles and their ability as a highly sensitive (<10 ppb) acetone sensor for biomedical applications. *Sensors and Actuators B: Chemical,* 230, 697-705.

KAROUSIS, N., TAGMATARCHIS, N. & TASIS, D. 2010. Current Progress on the Chemical Modification of Carbon Nanotubes. *Chemical Reviews,* 110, 5366-5397.

KEANE, M. A. 2005. A review of catalytic approaches to waste minimization: case study—liquid-phase catalytic treatment of chlorophenols. *Journal of Chemical Technology & Biotechnology,* 80, 1211-1222.

KHAVARIAN, M., CHAI, S.-P., TAN, S. H. & MOHAMED, A. R. 2009. Floating catalyst CVD synthesis of carbon nanotubes using iron (iii) chloride: influences of the growth parameters. *Nano,* 04, 359-366.

KıLıÇ, M. & ÇıNAR, Z. 2008. Hydroxyl radical reactions with 4-chlorophenol as a model for heterogeneous photocatalysis. *Journal of Molecular Structure: THEOCHEM,* 851, 263-270.

KISHI, T., SUZUKI, S., TAKAGI, M., KAWAKAMI, T. & ONODERA, S. 2009. Influence of experimental conditions on the formation of PCDD/Fs during the thermal reactions of 2,4,6-trichlorophenol. *Chemosphere,* 76, 205-211.

KOLESAR, E. S. & WISEMAN, J. M. 1989. Interdigitated gate electrode field effect transistor for the selective detection of nitrogen dioxide and diisopropyl methylphosphonate. *Analytical Chemistry,* 61, 2355-2361.

KONG, J., FRANKLIN, N. R., ZHOU, C., CHAPLINE, M. G., PENG, S., CHO, K. & DAI, H. 2000. Nanotube molecular wires as chemical sensors. *Science,* 287, 622-625.

KRAGULJ, M., TRICKOVIC, J., KUKOVECZ, A., JOVIC, B., MOLNAR, J., RONCEVIC, S., KONYA, Z. & DALMACIJA, B. 2015. Adsorption of chlorinated phenols on multiwalled carbon nanotubes. *RSC Advances,* 5, 24920-24929.

KRATSCHMER, W., LAMB, L. D., FOSTIROPOULOS, K. & HUFFMAN, D. R. 1990. Solid C60: a new form of carbon. *Nature,* 347, 354-358.

KUKOVITSKY, E. F., L'VOV, S. G., SAINOV, N. A. & SHUSTOV, V. A. 2003. CVD growth of carbon nanotube films on nickel substrates. *Applied Surface Science,* 215, 201-208.

KULJANISHVILI, I., DIKIN, D. A., ROZHOK, S., MAYLE, S. & CHANDRASEKHAR, V. 2009. Controllable Patterning and CVD Growth of Isolated Carbon Nanotubes with Direct Parallel Writing of Catalyst Using Dip-Pen Nanolithography. *Small,* 5, 2523-2527.

KUMAR, A., BRUNET, J., VARENNE, C., NDIAYE, A. & PAULY, A. 2015. Eurosensors 2015Room Temperature Measurements of Aromatic Hydrocarbons by QCM-based Gas Sensors: Intercomparison between Phthalocyanines and Phthalocyanine/CNTs Hybrid Material. *Procedia Engineering,* 120, 594-597.

LEE, C. J., SON, K. H., PARK, J., YOO, J. E., HUH, Y. & LEE, J. Y. 2001. Low temperature growth of vertically aligned carbon nanotubes by thermal chemical vapor deposition. *Chemical Physics Letters,* 338, 113-117.

LI, J., LU, Y., YE, Q., CINKE, M., HAN, J. & MEYYAPPAN, M. 2003. Carbon nanotube sensors for gas and organic vapor detection. *Nano Letters,* 3, 929-933.

LI, Y., HODAK, M., LU, W. & BERNHOLC, J. 2016. Mechanisms of NH3 and NO2 detection in carbon-nanotube-based sensors: An ab initio investigation. *Carbon,* 101, 177-183.

LI, Y., YU, T., PUI, T., CHEN, P., ZHENG, L. & LIAO, K. 2011. Fabrication of transparent and conductive carbon nanotube/polyvinyl butyral films by a facile solution surface dip coating method. *Nanoscale,* 3, 2469-2471.

LIM, S. Y., NORANI, M. M. & SURIATI, S. 2012. Effect of parameters on carbon nanotubes grown by floating catalyst chemical vapor deposition. *AIP Conference Proceedings,* 1502, 242-254.

LIN, D. & XING, B. 2008. Adsorption of Phenolic Compounds by Carbon Nanotubes: Role of Aromaticity and Substitution of Hydroxyl Groups. *Environmental Science & Technology,* 42, 7254-7259.

LIU, J., RINZLER, A. G., DAI, H., HAFNER, J. H., BRADLEY, R. K., BOUL, P. J., LU, A., IVERSON, T., SHELIMOV, K., HUFFMAN, C. B., RODRIGUEZ-MACIAS, F., SHON, Y.-S., LEE, T. R., COLBERT, D. T. & SMALLEY, R. E. 1998. Fullerene Pipes. *Science,* 280, 1253-1256.

LIU, X., CHENG, S., LIU, H., HU, S., ZHANG, D. & NING, H. 2012. A Survey on Gas Sensing Technology. *Sensors (Basel, Switzerland),* 12, 9635-9665.

LOKHNAUTH, J. K. & SNOW, N. H. 2005. Determination of Parabens in Pharmaceutical Formulations by Solid-Phase Microextraction-Ion Mobility Spectrometry. *Analytical Chemistry,* 77, 5938-5946.

LONG, R. Q. & YANG, R. T. 2001. Carbon Nanotubes as Superior Sorbent for Dioxin Removal. *Journal of the American Chemical Society,* 123, 2058-2059.

LORENC-GRABOWSKA, E. 2016. Effect of micropore size distribution on phenol adsorption on steam activated carbons. *Adsorption,* 22, 599-607.

LU, Y., LI, J., HAN, J., NG, H. T., BINDER, C., PARTRIDGE, C. & MEYYAPPAN, M. 2004. Room temperature methane detection using palladium loaded single-walled carbon nanotube sensors. *Chemical Physics Letters,* 391, 344-348.

LU, Y., MEYYAPPAN, M. & LI, J. 2011. A carbon-nanotube-based sensor array for formaldehyde detection. *Nanotechnology,* 22, 055502.

LU, Y., PARTRIDGE, C., MEYYAPPAN, M. & LI, J. 2006. A carbon nanotube sensor array for sensitive gas discrimination using principal component analysis. *Journal of Electroanalytical Chemistry,* 593, 105-110.

LUCCI, M., REALE, A., DI CARLO, A., ORLANDUCCI, S., TAMBURRI, E., TERRANOVA, M. L., DAVOLI, I., DI NATALE, C., D'AMICO, A. & PAOLESSE, R. 2006.

Optimization of a NOx gas sensor based on single walled carbon nanotubes. *Sensors and Actuators B: Chemical,* 118, 226-231.

LUO, C., ZUO, X., WANG, L., WANG, E., SONG, S., WANG, J., WANG, J., FAN, C. & CAO, Y. 2008. Flexible Carbon Nanotube⁃Polymer Composite Films with High Conductivity and Superhydrophobicity Made by Solution Process. *Nano Letters,* 8, 4454-4458.

MACKAY, D., SHIU, W. Y., MA, K. C. & LEE, S. C. 2006. *Handbook of Physical-Chemical Properties and Environmental Fate for Organic Chemicals, Second Edition*, CRC Press.

MANUKYAN, K. V., AVETISYAN, A. G., SHUCK, C. E., CHATILYAN, H. A., ROUVIMOV, S., KHARATYAN, S. L. & MUKASYAN, A. S. 2015. Nickel Oxide Reduction by Hydrogen: Kinetics and Structural Transformations. *Journal of Physical Chemistry C,* 119, 16131-16138.

MEITL, M. A., ZHOU, Y. X., GAUR, A., JEON, S., USREY, M. L., STRANO, M. S. & ROGERS, J. A. 2004. Solution casting and transfer printing single-walled carbon nanotube films. *Nano Letters,* 4, 1643-1647.

MEMON, M. O., HAILLOT, S. & LAFDI, K. 2011. Carbon nanofiber based buckypaper used as a thermal interface material. *Carbon,* 49, 3820-3828.

MILLIGAN, M. S. & ALTWICKER, E. R. 1996. Chlorophenol reactions on fly ash. 1. adsorption/desorption equilibria and conversion to polychlorinated dibenzo-p-dioxins. *Environmental Science & Technology,* 30, 225-229.

MUNA, G. W., QUAISEROVÁ-MOCKO, V. & SWAIN, G. M. 2005. Chlorinated Phenol Analysis Using Off-Line Solid-Phase Extraction and Capillary Electrophoresis Coupled with Amperometric Detection and a Boron-Doped Diamond Microelectrode. *Analytical Chemistry,* 77, 6542-6548.

NEGASH, N., ALEMU, H. & TESSEMA, M. 2014. Determination of phenol and chlorophenols at single-wall carbon nanotubes/poly(3,4-ethylenedioxythiophene) modified glassy carbon electrode using flow injection amperometry. *ISRN Analytical Chemistry,* 2014, 10.

NERI, G. 2015. First Fifty Years of Chemoresistive Gas Sensors. *Chemosensors,* 3, 1.

NOVAK, J. P., SNOW, E. S., HOUSER, E. J., PARK, D., STEPNOWSKI, J. L. & MCGILL, R. A. 2003. Nerve agent detection using networks of single-walled carbon nanotubes. *Applied Physics Letters,* 83, 4026-4028.

ÖBERG, T., WARMAN, K. & BERGSTRÖM, J. 1989. Proceedings of the Eight International Symposium Production of chlorinated aromatics in the post-combustion zone and boiler. *Chemosphere,* 19, 317-322.

OKAMOTO, Y. & TOMONARI, M. 1999. Formation pathways from 2,4,5-trichlorophenol (TCP) to polychlorinated dibenzo-p-dioxins (PCDDs): an ab initio study. *Journal of Physical Chemistry A,* 103, 7686-7691.

PAN, B. & XING, B. 2008. Adsorption mechanisms of organic chemicals on carbon nanotubes. *Environmental Science & Technology,* 42, 9005-9013.

PARK, Y., DONG, K.-Y., LEE, J., CHOI, J., BAE, G.-N. & JU, B.-K. 2009. Development of an ozone gas sensor using single-walled carbon nanotubes. *Sensors and Actuators B: Chemical,* 140, 407-411.

PAVESE, M., MUSSO, S., BIANCO, S., GIORCELLI, M. & PUGNO, N. 2008. An analysis of carbon nanotube structure wettability before and after oxidation treatment. *Journal of Physics: Condensed Matter,* 20, 474206.

PENG, X., LI, Y., LUAN, Z., DI, Z., WANG, H., TIAN, B. & JIA, Z. 2003. Adsorption of 1,2-dichlorobenzene from water to carbon nanotubes. *Chemical Physics Letters,* 376, 154-158.

PLÜMACHER, J. & RENNER, I. 1993. Determination of volatile chlorinated hydrocarbons and trichloroacetic acid in conifer needles by headspace gas-chromatography. *Fresenius' Journal of Analytical Chemistry,* 347, 129-135.

PROCACCINI, C., BOZZELLI, J. W., LONGWELL, J. P., SAROFIM, A. F. & SMITH, K. A. 2003. Formation of Chlorinated Aromatics by Reactions of Cl•, Cl2, and HCl with Benzene in the Cool-Down Zone of a Combustor. *Environmental Science & Technology,* 37, 1684-1689.

QI, P., VERMESH, O., GRECU, M., JAVEY, A., WANG, Q., DAI, H., PENG, S. & CHO, K. J. 2003. Toward Large Arrays of Multiplex Functionalized Carbon Nanotube Sensors for Highly Sensitive and Selective Molecular Detection. *Nano Letters,* 3, 347-351.

QI, X., QIN, C., ZHONG, W., AU, C., YE, X. & DU, Y. 2010. Large-Scale Synthesis of Carbon Nanomaterials by Catalytic Chemical Vapor Deposition: A Review of the Effects of Synthesis Parameters and Magnetic Properties. *Materials,* 3, 4142.

RAHDAR, A., ALIAHMAD, M. & AZIZI, Y. 2015. NiO Nanoparticles: Synthesis and Characterization. *Journal of Nanostructures,* 5, 145-151.

RANDENIYA, L. K., MARTIN, P. J. & BENDAVID, A. 2012. Detection of hydrogen using multi-walled carbon-nanotube yarns coated with nanocrystalline Pd and Pd/Pt layered structures. *Carbon,* 50, 1786-1792.

RAO, A. M., JACQUES, D., HADDON, R. C., ZHU, W., BOWER, C. & JIN, S. 2000. In situ-grown carbon nanotube array with excellent field emission characteristics. *Applied Physics Letters,* 76, 3813-3815.

REDLICH, O. & PETERSON, D. L. 1959. A Useful Adsorption Isotherm. *Journal of Physical Chemistry,* 63, 1024-1024.

REGE, S. U. & YANG, R. T. 2000. Corrected Horváth-Kawazoe equations for pore-size distribution. *AIChE Journal,* 46, 734-750.

RYABTSEV, S. V., SHAPOSHNICK, A. V., LUKIN, A. N. & DOMASHEVSKAYA, E. P. 1999. Application of semiconductor gas sensors for medical diagnostics. *Sensors and Actuators B: Chemical,* 59, 26-29.

RYU, J.-Y. 2008. Formation of chlorinated phenols, dibenzo-p-dioxins, dibenzofurans, benzenes, benzoquinnones and perchloroethylenes from phenols in oxidative and copper (II) chloride-catalyzed thermal process. *Chemosphere,* 71, 1100-1109.

SAITO, T., MATSUSHIGE, K. & TANAKA, K. 2002. Chemical treatment and modification of multi-walled carbon nanotubes. *Physica B: Condensed Matter,* 323, 280-283.

SCHINDLER, A., BRILL, J., FRUEHAUF, N., NOVAK, J. P. & YANIV, Z. 2007. Solution-deposited carbon nanotube layers for flexible display applications. *Physica E: Low-dimensional Systems and Nanostructures,* 37, 119-123.

SCHUERLE, S., TIWARI, M. K., SHOU, K., POULIKAKOS, D. & NELSON, B. J. 2011. Fabricating devices with dielectrophoretically assembled, suspended single walled carbon nanotubes for improved nanoelectronic device characterization. *Microelectronic Engineering,* 88, 2740-2743.

SIN, M. L. Y., CHOW, G. C. T., FUNG, C. K. M., LI, W. J., LEONG, P., WONG, K. W. & LEE, T. Ultra-low-power alcohol vapor sensors based on multi-walled carbon nanotube. 2006 1st IEEE International Conference on Nano/Micro Engineered and Molecular Systems, 18-21 Jan. 2006 2006. 1198-1202.

SLOBODIAN, P., RIHA, P., LENGALOVA, A., SVOBODA, P. & SAHA, P. 2011. Multi-wall carbon nanotube networks as potential resistive gas sensors for organic vapor detection. *Carbon,* 49, 2499-2507.

SOMEYA, T., SMALL, J., KIM, P., NUCKOLLS, C. & YARDLEY, J. T. 2003. Alcohol Vapor Sensors Based on Single-Walled Carbon Nanotube Field Effect Transistors. *Nano Letters,* 3, 877-881.

SREEKUMAR, T. V., LIU, T., KUMAR, S., ERICSON, L. M., HAUGE, R. H. & SMALLEY, R. E. 2003. Single-Wall Carbon Nanotube Films. *Chemistry of Materials,* 15, 175-178.

SUMANASEKERA, G. U., PRADHAN, B. K., ROMERO, H. E., ADU, K. W. & EKLUND, P. C. 2002. Giant Thermopower Effects from Molecular Physisorption on Carbon Nanotubes. *Physical Review Letters,* 89, 166801.

SZE, S. M. 1988. *VLSI Technology, 2nd edition*, McGraw-Hill.

TEO, K. B. K., CHHOWALLA, M., AMARATUNGA, G. A. J., MILNE, W. I., PIRIO, G., LEGAGNEUX, P., WYCZISK, F., PRIBAT, D. & HASKO, D. G. 2002. Field emission from dense, sparse, and patterned arrays of carbon nanofibers. *Applied Physics Letters,* 80, 2011-2013.

THOSTENSON, E. T., REN, Z. & CHOU, T.-W. 2001. Advances in the science and technology of carbon nanotubes and their composites: a review. *Composites Science and Technology,* 61, 1899-1912.

TITUS, E., ALI, N., CABRAL, G., GRACIO, J., BABU, P. R. & JACKSON, M. J. 2006. Chemically functionalized carbon nanotubes and their characterization using

thermogravimetric analysis, Fourier transform infrared, and Raman spectroscopy. *Journal of Materials Engineering and Performance,* 15, 182-186.

TÓTH, A., TÖR**Ő**CSIK, A., TOMBÁCZ, E. & LÁSZLÓ, K. 2012. Competitive adsorption of phenol and 3-chlorophenol on purified MWCNTs. *Journal of Colloid and Interface Science,* 387, 244-249.

TÓTH, A., TÖR**Ő**CSIK, A., TOMBÁCZ, E., OLÁH, E., HEGGEN, M., LI, C., KLUMPP, E., GEISSLER, E. & LÁSZLÓ, K. 2011. Interaction of phenol and dopamine with commercial MWCNTs. *Journal of Colloid and Interface Science,* 364, 469-475.

TULAPHOL, S., BUNSAN, S., KANCHANATIP, E., MIAO, H.-Y., GRISDANURAK, N. & DEN, W. 2016. Influence of chlorine substitution on adsorption of gaseous chlorinated phenolics on multi-walled carbon nanotubes embedded in SiO2. *International Journal of Environmental Science and Technology,* 13, 1465-1474.

TURGUNOV, M. A., OH, J. O. & YOON, S. H. 2014. Surface modification of multiwall carbon nanotubes by sulfuric acid and nitric acid. *Advanced Science and Technology Letters,* 64, 22-25.

VARGHESE, O. K., KICHAMBRE, P. D., GONG, D., ONG, K. G., DICKEY, E. C. & GRIMES, C. A. 2001. Gas sensing characteristics of multi-wall carbon nanotubes. *Sensors and Actuators B: Chemical,* 81, 32-41.

WHITE, J. 2012. Computational Fluid Dynamics Modelling and Experimental Study on a Single Silica Gel Type B. *Modelling and Simulation in Engineering,* 2012, 9.

WU, F.-C., LIU, B.-L., WU, K.-T. & TSENG, R.-L. 2010a. A new linear form analysis of Redlich–Peterson isotherm equation for the adsorptions of dyes. *Chemical Engineering Journal,* 162, 21-27.

WU, J., PAUDEL, K. S., STRASINGER, C., HAMMELL, D., STINCHCOMB, A. L., HINDS, B. J. & DRESSELHAUS, M. 2010b. Programmable transdermal drug delivery of nicotine using carbon nanotube membranes. *Proceedings of the National Academy of Sciences of the United States of America,* 107, 11698-11702.

WU, Z., CHEN, Z., DU, X., LOGAN, J. M., SIPPEL, J., NIKOLOU, M., KAMARAS, K., REYNOLDS, J. R., TANNER, D. B., HEBARD, A. F. & RINZLER, A. G. 2004. Transparent, Conductive Carbon Nanotube Films. *Science,* 305, 1273.

XIE, H., SHENG, C., CHEN, X., WANG, X., LI, Z. & ZHOU, J. 2012. Multi-wall carbon nanotube gas sensors modified with amino-group to detect low concentration of formaldehyde. *Sensors and Actuators B: Chemical,* 168, 34-38.

XU, M., SUN, Z., CHEN, Q. & TAY, B. K. 2009. Effect of chemical oxidation on the gas sensing properties of multi-walled carbon nanotubes. *International Journal of Nanotechnology,* 6, 735-744.

YANG, H. Y., HAN, Z. J., YU, S. F., PEY, K. L., OSTRIKOV, K. & KARNIK, R. 2013. Carbon nanotube membranes with ultrahigh specific adsorption capacity for water desalination and purification. *Nat Commun,* 4.

YANG, K. & XING, B. 2007. Desorption of polycyclic aromatic hydrocarbons from carbon nanomaterials in water. *Environmental Pollution,* 145, 529-537.

YANG, K., ZHU, L. & XING, B. 2006. Adsorption of Polycyclic Aromatic Hydrocarbons by Carbon Nanomaterials. *Environmental Science & Technology,* 40, 1855-1861.

YUCA, N., KARATEPE, N. & YAKUPHANOǦLU, F. 2011. Thermal and Electrical Properties of Carbon Nanotubes Purified by Acid Digestion. *International Journal of Chemical, Molecular, Nuclear, Materials and Metallurgical Engineering,* 5, 602-608.

YUN, J.-H., KIM, J. D., PARK, Y. C., SONG, J.-W., SHIN, D.-H. & HAN, C.-S. 2009. Highly sensitive carbon nanotube-embedding gas sensors operating at atmospheric pressure. *Nanotechnology,* 20, 055503.

ZHANG, K. & ZHANG, Q. 2015. Raman signatures of broken C–C bonds in single-walled carbon nanotubes upon [2 + 1] cycloaddition. *Journal of Physical Chemistry C,* 119, 18753-18761.

ZHANG, S., SHAO, T., KOSE, H. S. & KARANFIL, T. 2010. Adsorption of Aromatic Compounds by Carbonaceous Adsorbents: A Comparative Study on Granular Activated Carbon, Activated Carbon Fiber, and Carbon Nanotubes. *Environmental Science & Technology,* 44, 6377-6383.

ZHANG, T., MUBEEN, S., V. MYUNG, N. & A. DESHUSSES, M. 2008. Recent progress in carbon nanotube-based gas sensors. *Nanotechnology,* 19, 332001.

APPENDIX

Chemicals and materials for Chapter 3

The chemicals and materials used in this study include:

Silicon wafer (P-type <100>) from Sumitomo Sitix Corp., Japan.

Durapore membrane filter (PVDF, 0.45 µm) from Merck Millipore, Ireland.

Nickel (II) chloride ($NiCl_2 \cdot 6H_2O$) from Showa Chemical, Japan

Ferrocene ($Fe(C_5H_5)_2$, 98%) from Acros Organics, Germany.

Methanol (CH_3OH, 99.8) from Sigma Aldrich, Germany.

Acetone (CH_3COH_3, $\geq$99.5%) from J.T. Baker, U.S.A.

Ethanol (C_2H_5OH, 99.8%) from Sigma Aldrich, Germany.

Triton^{TM} X-100 from Sigma Aldrich, U.S.A.

Hydrochloric acid (HCl, $\geq$37%) from Sigma Aldrich, Austria.

Nitric acid (HNO_3, >65%) from Sigma Aldrich, Germany.

Sulfuric acid (H_2SO_4, 95%) from Sigma Aldrich, Germany.

Thionyl chloride ($SOCl_2$, 99%) from Merck, Germany

Ehtylenediamine ($NH_2CH_2CH_2NH_2$, 100%) from J.T. Baker, U.S.A.

These chemicals were of analytical reagent grade or better and were used as received without any further purification.

Chemicals for Chapter 5

Three chlorinated phenolic compounds were used to study the adsorption on the acid-functionalized carbon nanotubes. The chemicals used in the experiment are listed as follows:
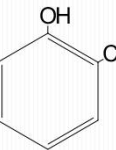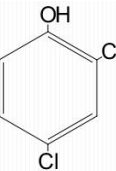
Phenol (purity ≥99%) from Sigma Aldrich, U.S.A.

2-chlorophenol (purity >98%) from Lancaster, England.

2,4-dichlorophenol (purity 99%) from Alfa Aesar, Great Britain.

Dichloromethane (purity ≥99.5%) from Macron Fine Chemicals, U.S.A.

All chemicals were of analytical reagent grade and were used without further purification. The chemical properties are shown in Table A1.

Table A1 Properties of the chemicals for Chapter 5

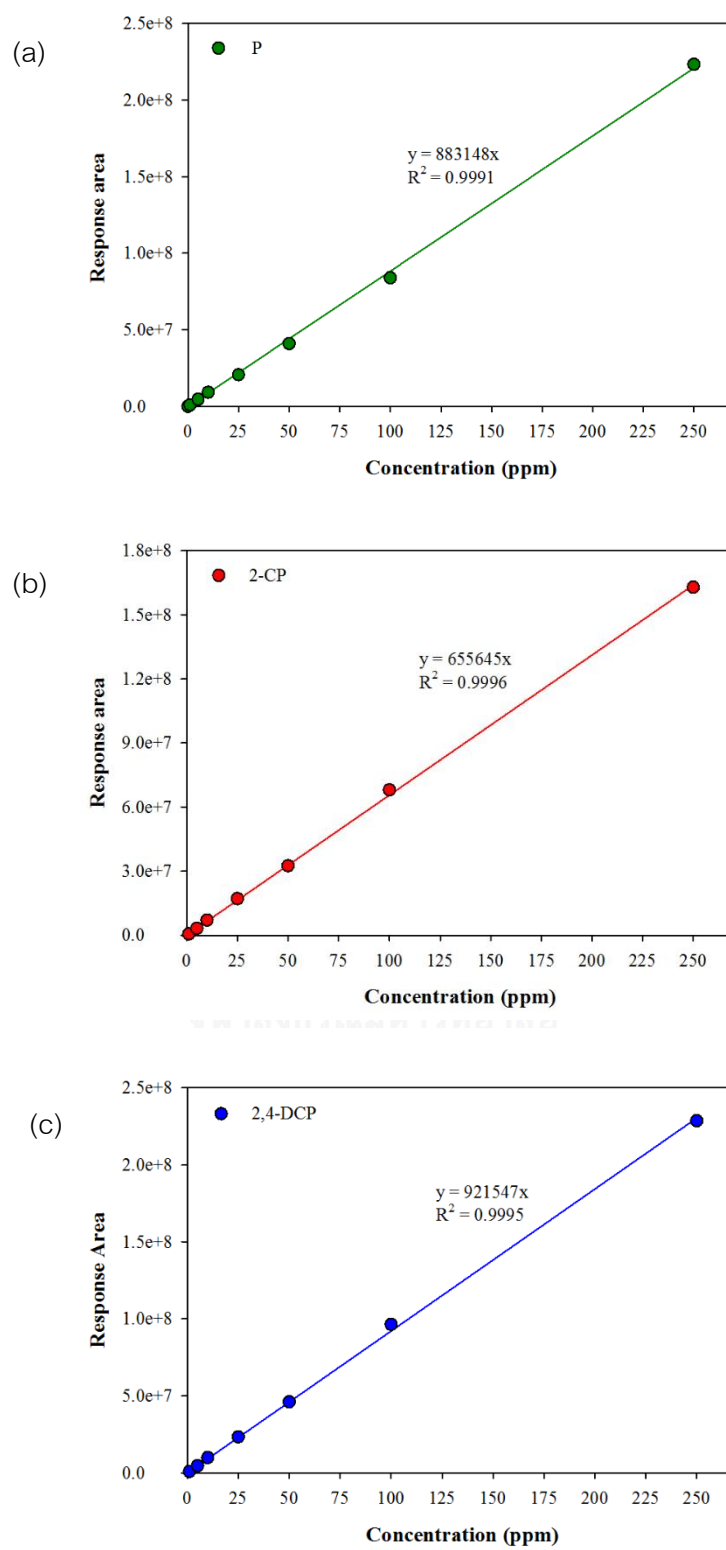| Chemical name	Chemical Structure	Molecular formula	Molecular weight (g/mol)
Phenol		C_6H_5OH	94.11
2-chlorophenol		C_6H_4ClOH	128.56
2,4-dichlorophenol		$C_6H_4Cl_2O$	163.00
Dichloromethane		CH_2Cl_2	84.93

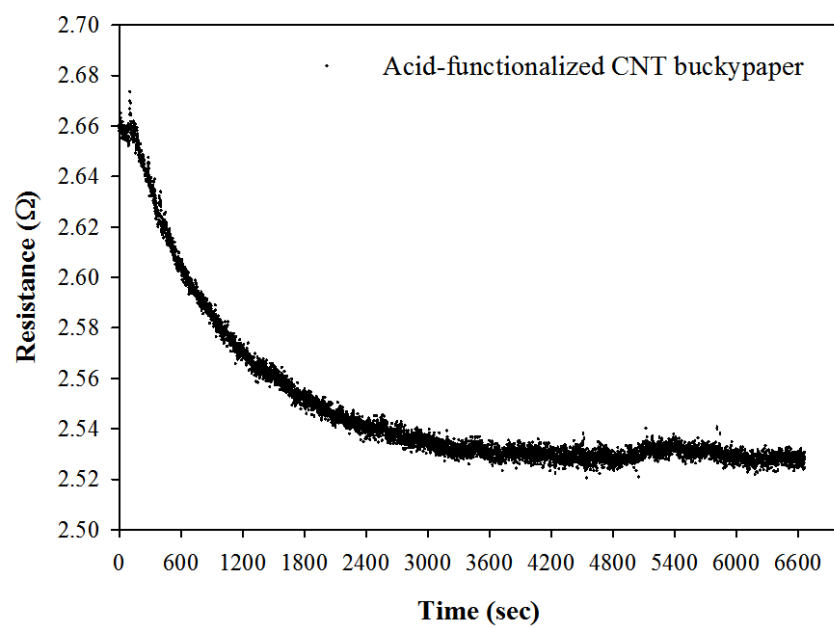**Figure A1** The calibration curves for phenol **(a)**, 2-chlorophenol **(b)** and 2,4-dichlorophenol **(c)**
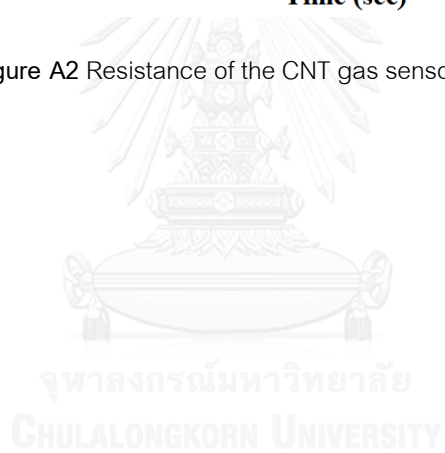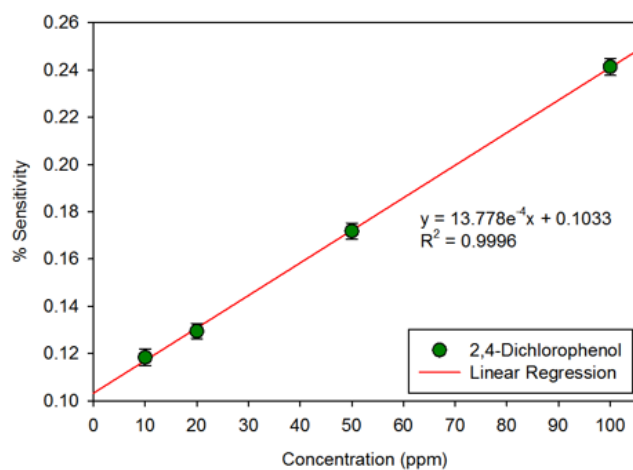
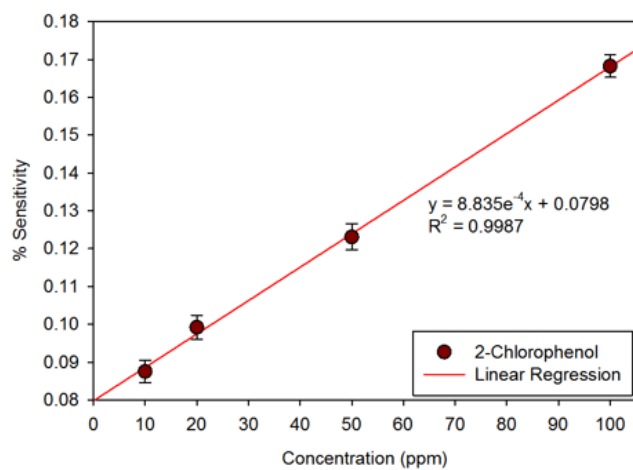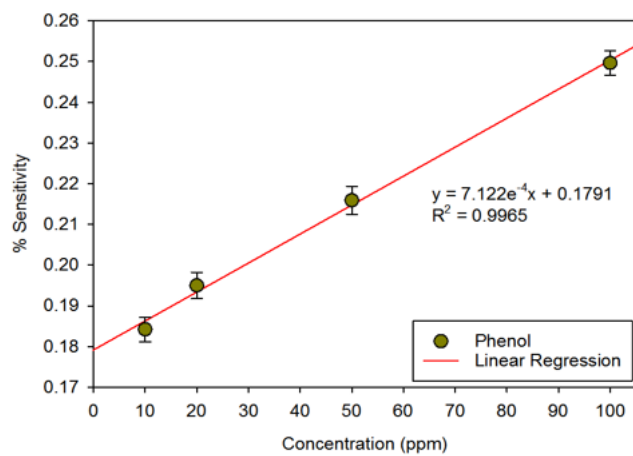Figure A2 Resistance of the CNT gas sensor in background gas

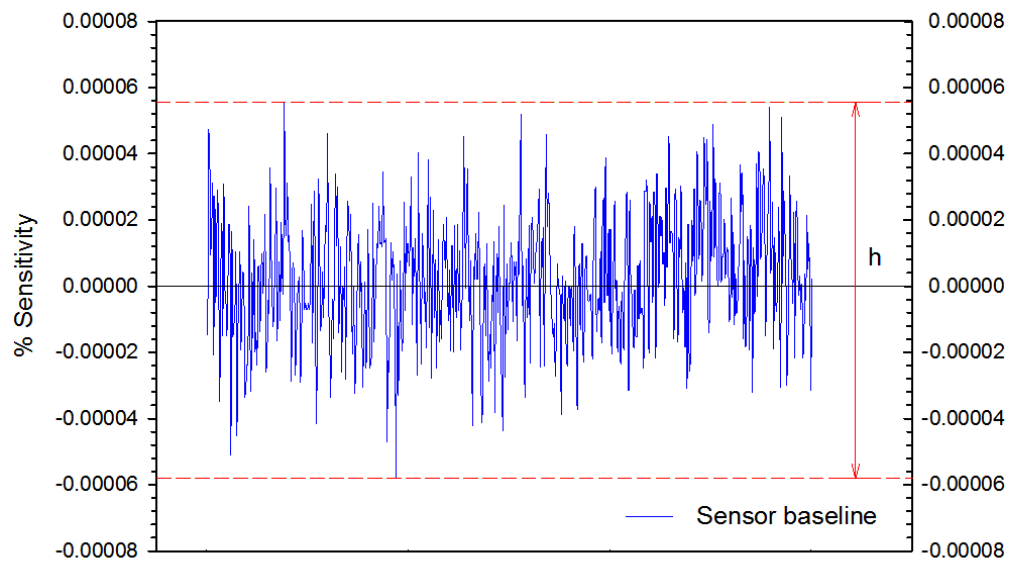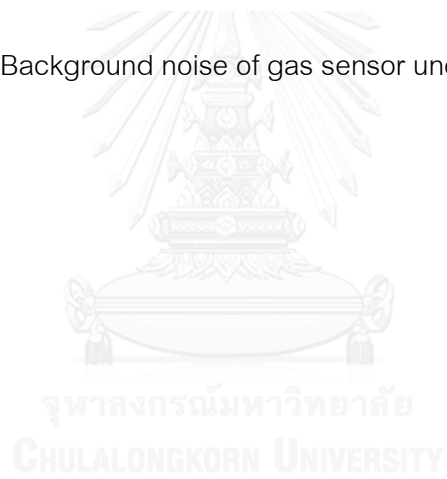**Figure A3** Dose-response curves for P, 2-CP and 2,4-DCP

Figure A4 Background noise of gas sensor under air atmosphere

VITA

Ekkachai Kanchanatip, the author was born on 11th April, 1986 in Bangkok, Thailand. He attended his elementary education at Udomsuksa School. He also attended his Junior and High-school education at Bodindecha (Sing Singhaseni) 2 School and graduated in 2004. He graduated from Thammasat University (Bangkok, Thailand) in 2008 with a Bachelor of Engineering degree in Chemical Engineering. After graduation, he continued his studies at Thammasat University and completed his Master of Enginieering in Energy and Environmental Technology Management in 2010 under the supervision of Associate Professor Nurak Grisdanurak. The thesis was on "Characterization of C60 Modified V-TiO2 Prepared by Chelation Method for Degradation of Paraquat". In October 2010, He started his Ph.D. studies in Environmental Management at Chulalongkorn University (Bangkok, Thailand) under the supervision of Associate Professor Nurak Grisdanurak. During his Ph.D. studies, he had an opportunity to work with Professor Philip T. Cheng at Aqua Molecular Genetics Laboratory, Department of Tropical Agriculture and International Cooperation, National Pingtung University of Science and Technology (Pingtung, Taiwan) in 2012 for 9 months on the topic "Activated Bactericidal Effect of Metal-C60-TiO2/Magnetic Support on Fish Pathogens under Visible Light". In 2013, he decided to change his thesis topic and moved to Tunghai University, (Taichung, Taiwan) to start over his thesis on Carbon Nanotubes Synthesis, Sorption and Sensing with the co-advisor, Professor Walter Den, at Air Pollution Control and Nanomaterial Laboratory, Department of Environmental Science and Engineering since June 2013.

Publications

Kanchanatip, E., Su, B. R., Tulaphol, S., Den, W., Grisdanurak, N. and Kuo, C. C. (2016) Fouling characterization and control for harvesting microalgae Arthrospira (Spirulina) maxima using a submerged, disc-type ultrafiltration membrane, Bioresource Technology, 209, 23-30.

Kanchanatip, E., Grisdanurak, N., Yeh, N. and Cheng, T. C. (2014) Photocatalytic bactericidal efficiency of Ag doped TiO2/Fe3O4 on fish pathogens under visible light, International Journal of Photoenergy, 2014, Article ID 903612, 8 pages.

Kanchanatip, E., Grisdanurak, N., Thongruang, R. and Neramittagapong, A. (2011) Degradation of paraquat under visible light over fullerene modified V-TiO2, Reaction Kinetics Mechanisms and Catalysis, 103, 227-237.